IN VIVO QUANTIFICATION OF HEMOGLOBIN IN SKIN

INTEGRATING SPHERE-BASED SPECTRALLY CONSTRAINED TOTAL DIFFUSE REFLECTANCE FOR IN VIVO QUANTIFICATION OF HEMOGLOBIN IN SKIN

By DIANA L. GLENNIE, B. SC., M. SC.

A Thesis Submitted to the School of Graduate Studies in Partial Fulfillment of the Requirements for the Degree Doctor of Philosophy

McMaster University © Copyright by Diana L. Glennie, November 2014

McMaster University DOCTOR OF PHILOSOPHY (2014) Hamilton, Ontario (Medical Physics)

TITLE: Integrating sphere-based spectrally constrained total diffuse reflectance for in vivo quantification of hemoglobin in skin

AUTHOR: Diana L. Glennie, B.Sc., M. Sc. (McMaster University)

SUPERVISOR: Professor Thomas J. Farrell

NUMBER OF PAGES: xi, 139

Abstract

The ability to monitor changes in skin redness through the hemoglobin concentration in skin has the potential to personalize patient care by providing a quantitative objective way of monitoring patient response to interventions such as radiation therapy and plastic surgery. Currently available commercial systems for monitoring skin redness rely on total diffuse reflectance spectroscopy and can only accurately measure hemoglobin changes relative to a baseline measurement when all other skin chromophores, such as melanin, remain constant. This work investigates the application of a spectrally-constrained diffusion theory model for analyzing total diffuse reflectance spectra obtained with an integrating sphere-based system. A low cost integrating sphere-based system was designed, constructed, and characterized to yield accurate total diffuse reflectance spectra. The system was first used with an absorbance-based erythema index to investigate the time to maximal effect of epinephrine – a vasoconstrictor used in plastic surgery. A spectrally-constrained diffusion theory model was developed to improve the interpretation of the reflectance spectra obtained with the integrating sphere-based system. Correction factors necessary to apply the developed model to the obtained spectra were determined through Monte Carlo simulations, and then confirmed with tissue-simulating liquid phantoms. The model was tested for sensitivity and specificity, as well as how it responded to variations in the experimental parameters. The system and model were then used to monitor radiation-induced erythema in head and neck intensity modulated radiation therapy patients. Analysis of the results enabled earlier detection of erythema by 1-19 days compared to visual assessment. The work completed in this thesis illustrates a cost-effective, user-friendly diffuse reflectance spectroscopy system which has potential applications in a number of clinical settings.

Acknowledgements

I cannot begin without first thanking my incomparable husband, Dr. Gabriel Devenyi. It is not an exaggeration to say that I would not have persevered to the end of this thesis if it weren't for his continual love and support. In addition to acting as a scientific peer during the experimental and analytical processes, his words of reassurance and motivation were exactly what I needed when presented with a difficult problem or frustrating situation.

I would like to express the deepest appreciation to my supervisor, Dr. Tom Farrell, and committee members, Dr. Joe Hayward, Dr. Orest Ostapiak, and Dr. Mike Patterson. Without their guidance and support, this work and my achievements would not have been possible. Although not on my committee, I would be remiss if I did not also thank Dr. Kevin Diamond for his constant presence in the lab and his willingness to help whenever I had questions (and for all of the coffees!). I would also like to thank Dr. Qiyin Fang for the many academic opportunities he helped me earn, including a Mitacs internship at Christie Digital.

I genuinely believe that, while the focus of graduate school should be on academic achievement, successful individuals develop other aspects of themselves during the process. I would like to thank my fellow members of the Graduate Students Association (GSA) and the Graduate Student Life team in Graduate Studies for providing me with such opportunities throughout my long stint at McMaster. Thank you, again, to my supervisor for giving me an opportunity to teach during my final year of studies.

To my family, friends, and colleagues who stood by me and provided support and stress-relief, especially during the final months... thank you. I love you, Mom & Dad. To Dan, Jill, Judi, Nancy, and Rayna; words cannot express my gratitude.

Contents

List of Figures

Declaration of Academic Achievement

The work presented here is the result of research performed by myself during the years 2009–2014. Results that have substantial contributions from other authors are clearly prefaced and the contributions of those authors are indicated.

Chapter 1

Introduction

1.1 Motivation

The ability to measure changes in the hemoglobin concentration in skin has the potential to enable more personalized patient care which, in turn, could lead to an increase in treatment success rates and a decrease in per-patient costs. For example, in radiation therapy, a common side effect is a skin-reddening reaction known as erythema, or radiation dermatitis.[1] Depending on the severity of the reaction, erythema can be quite painful and may even prevent the completion of the radiation treatment schedule, thereby reducing the overall treatment efficacy.[2] Although it is a deterministic effect, there is a varying threshold dose and a patient-dependent rate of increase in severity[3] that makes erythema impossible to reliably predict in advance for an individual patient.[4] Instead, patient responses are monitored by the therapy team over the course of treatment. Currently, the most prevalent method for monitoring erythema is by visual assessment (VA).[1, 5, 6] VA uses a pre-determined scale to classify the current condition of the skin. If there are too few divisions on the scale (four or less), there is not a sufficient amount of information regarding the patient's progress from the erythema stage to the next stage of moist desquamation. If there are more than four divisions on the scale, it is difficult to eliminate, or even minimize, the inter- and intra-observer variation, making the results imprecise. The implementation of a quantitative objective method for measuring skin redness could allow the treatment team to better manage the reaction, thereby potentially improving the treatment's success rate and the patient's quality of life.

Another application of a quantitative system for monitoring the hemoglobin concentration in skin is in the field of plastic surgery. Prior to incision, lidocaine (an anesthetic) and epinephrine (a hormone used for vasodilation) are commonly used to numb the surgical region and reduce bleeding during surgery. The commonly cited time to maximal effect of epinephrine is 7-10 minutes, but this time interval was determined in a porcine model[7] in 1987 using laser Doppler flowmetry[8] and was never confirmed with human trials or more advanced methods, possibly due to the associated difficulty and cost of the experiments.

Diffuse reflectance spectroscopy (DRS) with visible light (400-750 nm) is a good candidate for monitoring changes in the hemoglobin concentration in skin because the majority of these wavelengths of light do not penetrate deeper than the dermal layer.[9] As well, hemoglobin preferentially absorbs green light ($\sim$ 550 nm) and there

are no major chromophores in the skin that absorb strongly in the red region ($\sim$ 650 nm).[10] The combined measurement and analysis techniques of DRS are many and varied,[11] but they can be categorized by whether the reflectance spectra are spatially resolved (at one or more radial positions from the source) or not.

DRS without spatial-resolution can be performed either with an integrating sphere or focusing optics, or with a bifurcated or random mixed fiber bundle.[12] In both instances, the measured reflectance is interpreted as an analogue for the total diffuse reflectance but is not necessarily equal to it. For this reason, the majority of the analysis methods focus on using approximations to infer the hemoglobin concentration from the uncalibrated reflectance spectrum. Possibly the most popular approach is to relate changes in the area under the log-inverse-reflectance (LIR) spectrum to changes in the hemoglobin concentration. This approach was first proposed by Dawson et al. in 1980.[13] Dawson drew on work from chemistry in which the concentration of a chromophore could be determined from the transmitted light intensity through a sample cuvette using the Beer-Lambert law. He noted that when more hemoglobin was present, the area under the LIR curve increased, and he proposed an erythema index that was equal to the area under the curve (approximated by a polynomial) that represented the hemoglobin concentration in arbitrary units. Similar techniques have used the ratio between strategically chosen wavelengths (usually one green and one red) to act as a measure of the area under the LIR curve.[14–16] More recently, several researchers have shown a direct relationship between this area and the constituent chromophore concentrations.[17, 18] However, due to the required assumptions and approximations made during this analysis, such as an unknown pathlength correction factor, the concentrations are still expressed in arbitrary concentration units and are incorrect should any of the non-hemoglobin concentrations change (e.g. melanin). A final method of analyzing this type of DRS measurement is by direct comparison with Monte Carlo simulations,[19, 20] but as it is computationally expensive and requires the obtained spectra to be highly characterized for modeling purposes, it is rarely used.

Presently available commercial systems that employ spatially-resolved DRS to determine the optical properties of human skin are limited to a fixed geometry fiber optic bundle, although video detection is possible. For a typical setup, several detection fibers are placed at one or more distances from the source fiber. The collected reflectance spectrum can either be fit with a model derived from diffusion theory or with the results

of Monte Carlo simulations.[21] In either approach, the chromophore concentrations would act as fitting parameters. While both are capable of accounting for the layered structure of skin, the diffusion theory model fitting approach is less computationally expensive, and so is used most often.[22–25]

Recent advances in technology have made hyperspectral imaging (HSI) an option for detecting changes to the hemoglobin concentration in human skin.[26, 27] An advantage to this technique is that it provides a spatial map of the hemoglobin concentration across the image instead of a "single" measurement location. However, as the technology is still relatively new, it is prohibitively expensive, and so is rarely used, especially outside of research institutions.

1.2 Light-tissue interactions

The propagation of light in tissue can be described by three main interactions:[28]

1. Reflection (and refraction)
2. Absorption
3. Scattering

Reflection and refraction occur at the boundary between two materials with different indices of refraction, such as between air and tissue. The light that is reflected at the boundary obeys the law of specular reflection which states that the angle of reflection of a ray of light is equal to the angle of incidence.[29] Light that is transmitted past the boundary refracts toward or away from the normal as described by Snell's law,

$$n_1 \sin\theta_1 = n_2 \sin\theta_2 \tag{1.1}$$

where n_1 and n_2 are the indices of refraction of the two materials, θ_1 is the angle of incidence, and θ_2 is the angle of refraction.

The amount of light that undergoes either of these two processes can be predicted using Fresnel's equations which require the relative index of refraction (n_2/n_1) and the angle of incidence (θ_1) for input parameters.[30] There is a wavelength dependence in all indices of refraction that is negligible for small wavelength ranges.[29, 31]

While inside a material, light can either be absorbed or scattered. The probabilities of these two occurrences are based on the optical properties of the material. When an

absorption event occurs, the light energy is transferred to a bound electron, elevating it to an excited state.[32] Atoms or molecules with excited electronic states can "discharge" this energy either through radiative processes such as fluorescence or phosphorescence or, more commonly, through non-radiative processes like vibrational relaxation. The probability of absorption occurring within an infinitesimal distance ds is $\mu_a ds$, where $\mu_a[mm^{-1}]$ is known as the absorption coefficient. In the case of (elastic) scattering, the exact process depends on the size of the particles with which the light interacts. When the particles are much smaller than the wavelength of light, Rayleigh scattering applies, which favors the scattering of shorter wavelengths in the forward or backward directions.[33] When the particles are comparable in size to the wavelength of light, Mie scattering best describes the interaction. Mie scattering is only weakly wavelength dependent and is forward-directed.[32] The probability of scattering occurring within an infinitesimal distance ds is $\mu_s ds$, where $\mu_s[mm^{-1}]$ is known as the scattering coefficient.

Elastic scattering is isotropic in nature. However, in a medium with many small, suspended particles, another direction may dominate when Mie and Rayleigh scattering apply. This can be accounted for with an anisotropy factor (g) that is equal to the average cosine of the scattering angle. An anisotropy factor of 0 represents isotropic scattering while a factor of 1 represents forward scattering. To account for this directionality when modeling light transport in tissue, a reduced scattering coefficient is commonly defined as $\mu_s' = (1-g)\mu_s$ such that its inverse is the average distance between isotropic scattering events that would produce the same results as the anisotropic scattering.[34]

Another helpful quantity is the total reduced attenuation coefficient, $\mu_t' = \mu_a + \mu_s'$ which, when multiplied by an infinitesimal distance, represents the probability of any photon interaction occurring across that space. Its inverse is specially termed the "reduced mean free path" (mfp') and represents the average distance between interactions.[35]

1.3 Modeling of light transport in turbid material

1.3.1 Radiation transport equation and diffusion theory

The radiation transport equation (RTE), also known as the Boltzmann equation, describes the transfer of neutral particles (in this case, energy modeled as discrete

photons) within an infinitesimal volume as a function of time.[36] It is often expressed as a change in the time- and space-resolved energy radiance, $L(\mathbf{r}, \mathbf{\Omega}, t)$ with respect to time. This quantity can be determined by investigating the mechanism by which the energy radiance can be gained and lost from the volume in question. When considering the steady-state condition, there is no net change in the energy radiance and the gain terms are equal to the loss terms.
The gain mechanisms are:

1. Any photon sources within the volume, $S(\mathbf{r}, \mathbf{\Omega})$
2. Photons already within the volume that scatter into the direction of interest, $\int_{4\pi} L(\mathbf{r}, \mathbf{\Omega})\mu_s(\mathbf{r}, \mathbf{\Omega}' \rightarrow \mathbf{\Omega})d\mathbf{\Omega}'$
3. Photons that enter into the volume along the direction of interest

Loss mechanisms include:

1. Photons that are absorbed within the volume, $\mu_a L(\mathbf{r}, \mathbf{\Omega})$
2. Photons that scatter out of the volume, $\mu_s L(\mathbf{r}, \mathbf{\Omega})$
3. Photons that exit the volume

A single convection term can be used to account for the photons entering and exiting the volume, $-\mathbf{\Omega} \cdot \nabla L(\mathbf{r}, \mathbf{\Omega})$. The combination of all of the terms results in the following equation for the steady-state RTE,[35]

$$\mathbf{\Omega} \cdot \nabla L(\mathbf{r}, \mathbf{\Omega}) + (\mu_a + \mu_s)L(\mathbf{r}, \mathbf{\Omega}) - \int_{4\pi} L(\mathbf{r}, \mathbf{\Omega})\mu_s(\mathbf{r}, \mathbf{\Omega}' \rightarrow \mathbf{\Omega})d\mathbf{\Omega}' - S(\mathbf{r}, \mathbf{\Omega}) = 0 \quad (1.2)$$

Solutions to the above equation may be found via intense numerical methods, but they are extremely computationally expensive to achieve. For this reason, a simpler approach is often employed in which approximations are made that simplify the RTE into a solution-friendly form. In the case of light transport in tissue, the diffusion approximation simplifies the above equation into a single differential equation. Diffusion theory requires: 1) that more scattering events occur than absorption events ($\mu_a < 0.1\mu_s'$), 2) that the radiance is, at most, linearly anisotropic, and 3) that the location of interest is sufficiently far from any boundaries (greater than 1 mfp).[32, 37] Under these conditions, the RTE can be reduced into the following diffusion equation,

$$\nabla^2 \cdot E(\mathbf{r}) - \frac{\mu_a}{D} E(\mathbf{r}) = S(\mathbf{r}) \tag{1.3}$$

where $E(\mathbf{r})$ is the energy fluence rate (the integral of the energy radiance over all angles), D is the diffusion constant, $(3\mu_t')^{-1}$, and $S(\mathbf{r})$ is the source term.

The diffusion equation can be solved analytically by applying a set of boundary conditions. In the case of tissue optics, the most common sets of boundary conditions, such as the extrapolated boundary condition, attempt to satisfy the Robin boundary condition through various approximations with image sources and extended boundaries.[38]

1.3.2 Monte Carlo simulations

Monte Carlo (MC) simulations offer a method of solving the steady-state RTE that is slightly less computationally expensive than traditional numerical methods. It is also useful for confirming solutions for approximations such as diffusion theory. Millions of photons are "launched" and their propagation through the medium is determined by the random sampling of probability distributions that represent the absorption and scattering conditions of the medium. The basic principles of MC simulations have been thoroughly covered by Prahl *et al.*[39] and Wang *et al.*,[40] so only two important variations are outlined here.

If a single simulation must be run several times with different sets of optical properties, it is useful to adapt the code into what has been termed mono (or "white") MC.[41, 42] Under this simulation, photons are tracked through a homogeneous scattering, non-absorbing medium. There is no survival weighting in mono MC, so the photons' weights are never modified in the tissue and they are only killed when they scatter too many times (via Russian roulette) or migrate too far from the region of interest. The total distance traveled by each photon (the pathlength, s) in the medium is tracked. When photons are finally scored, their weight is added to a bin for the corresponding total pathlength. The effect of absorption can be introduced after the simulation is complete by multiplying each bin by $\exp(-\mu_a s)$ and summing over all the bins.

When multiple processors are available on a computer, parallelization is an option for increasing the speed of the MC simulation. In parallel computing, single calculations are performed by each available processor in a computer and the results are collated at

the end. Parallelization is only possible if all the calculations are independent of one another (i.e. the order doesn't matter). Since MC is based on stochastic processes, each photon can be treated separately. For example, in a computer with four processors, it is possible to track four photons simultaneously, record their progress, and collect their results once terminated. This yields a MC simulation that would run four times faster than the original serial code.

1.4 In vivo measurements of tissue optical properties with diffuse reflectance

For the purposes of monitoring patient response, *ex vivo* methods of DRS for determining tissue optical properties are obviously not appropriate. Therefore, this section will focus solely on *in vivo* methods, specifically those that require steady-state conditions.

1.4.1 Total diffuse reflectance

The total diffuse reflectance represents the fraction of incident light fluence remitted from the tissue across the entire surface (i.e. it is spatially integrated) at a single wavelength. It can be modeled with the diffusion approximation and is dependent only on the reduced albedo and the relative index of refraction.[43] The index of refraction for skin has been accurately measured, and a value of 1.4 is typically used for incident light within the visible spectrum.[41] With this information, the albedo of the tissue can be determined from the measured total diffuse reflectance. For a single total diffuse reflectance measurement, there is no way to determine the individual contributions from scattering and absorption. However, if the scattering and mean pathlength are assumed constant, a second measurement in which the absorption coefficient is known or can be approximated, will allow for the determination of the first absorption coefficient. This technique relies on the relationship between the total diffuse reflectance and the exponential of the product of the absorption coefficient and the pathlength,

$$R_d \propto \exp(\mu_a l) \tag{1.4}$$

The total diffuse reflectance is generally measured either with an integrating sphere

(see Section 1.5) or with an optical system, off-set from the normal to avoid collecting any specular reflectance.

1.4.2 Spatially-resolved diffuse reflectance

The spatially-resolved diffuse reflectance is the fraction of the incident light remitted at a set of radial distances from the incident light source. It can be collected in one of two ways: either with an imaging system[44] or by detection fibers positioned at known distances from the source fiber.[43] In a fiber optic array, the source and detection fibers are usually bundled together in a single probe to maintain accurate and consistent positioning of the fibers. Several detection fiber probes are used at greater distances to improve the signal-to-noise ratio (see Figure 1.1). The signals from the detection fibers are then processed by a spectrometer. When the reflectance is captured with an imaging system, such as a digital camera, the radially-dependent reflectance curve can be constructed by binning pixel intensities at equal radial distances. This method provides more data points for the subsequent analysis. Unless a hyperspectral camera is used, only the optical properties at a single wavelength (that of the incident laser source) can be determined.

Both the absorption and reduced scattering coefficients can be determined from this collected data. One analysis method is to compare the spatially resolved diffuse reflectance spectrum to one produced by a single mono Monte Carlo simulation. In addition to applying the effect of absorption post-simulation (see Section 1.3.2), it is also possible to scale the results for different scattering coefficients from a single reference scattering coefficient as follows,[41]

$$R(\rho) = \left(\frac{\mu_s'}{\mu_{sref}'}\right)^2 R_{ref}\left(\rho\frac{\mu_s'}{\mu_{sref}'}\right) \tag{1.5}$$

where the ratio of the new reduced scattering coefficient to the reference reduced scattering coefficient acts as a scaling factor. A fitting algorithm will adjust the optical properties and generate a reflectance curve from the MC data until the resulting chi-squared statistic between the measured data and the calculated data is minimized.

The data can also be fitted with a nonlinear equation for the spatially-resolved reflectance derived from diffusion theory. The absorption and reduced scattering coefficients would act as input parameters for the equation and those that resulted in the best fit (via a given fitting algorithm) would be the approximate values. When deriving

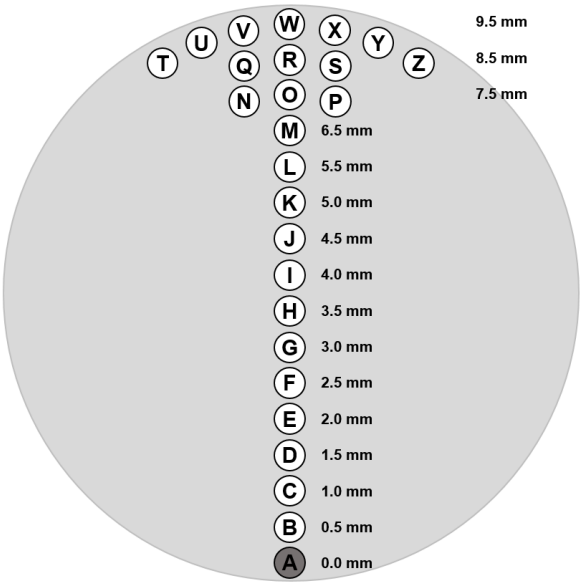

Figure 1.1: A diagram representing the configuration of the optical fibers in a spatially-resolved diffuse reflectance probe. Light enters through fiber "A" (dark grey) and is detected by additional fibers placed at set distances away (white). More fibers are placed at further distances to strengthen the signal.

this equation, the selection of the boundary conditions is integral in recovering reliable results. Farrell *et al.*[45] used an extrapolated boundary condition and an negative image source to yield a fluence rate of zero at a new (extrapolated) boundary located above the actual tissue-air interface. The height of the image source and the boundary are dependent on the tissue optical properties. Using this set of approximations and boundary conditions, the recovered values for the absorption and reduced scattering coefficients agreed with the true values within 10%.

1.4.3 Spectrally-constrained diffuse reflectance

The most common method employs a single source-detector pair instead of a spatially-resolved array of detector fibers. In this approach, a broad spectrum light source is used instead of a single wavelength light source, and the collected signal is resolved into a reflectance measurement at each wavelength. However, this reflectance spectrum is not sufficient to determine the tissue optical properties. Generally, a forward model of the diffusion theory is derived and fit to the obtained reflectance spectrum. Such a model requires both the absorption and reduced scattering coefficient spectra, which

can be approximated.

The absorption coefficient is estimated to be the sum of the individual chromophore concentrations c_i, multiplied by their respective extinction coefficient spectra $\varepsilon_i(\lambda)$, as follows,

$$\mu_a(\lambda) = \sum_i c_i \varepsilon_i(\lambda) \tag{1.6}$$

The extinction coefficient is the absorption coefficient per molar (mol/L) for the medium. These spectra for the majority of chromophores found in human skin (see Section 1.6) have been well characterized and the chromophore concentrations are included as fitting parameters in the forward model. It is important to include only those chromophores that contribute significantly to the overall absorption within the wavelength range of interest.[43] Including insignificant chromophores will add too many variables to the fitting equation while omitting significant chromophores will yield inaccurate results.

The reduced scattering coefficient for human skin has been well-characterized and follows a wavelength-dependent power law,[31]

$$\mu_s'(\lambda) = a\lambda^{-b} \tag{1.7}$$

As a result, the scaling factor a, and the exponential b can be included as fitting parameters in the forward model. This spectrally constrained approach has been used by Yohan et al.[46] where it was used to track ionizing radiation-induced erythema through the hemoglobin fitting parameters.

1.4.4 Commercially available systems

Currently available commercial systems that measure diffuse reflectance are primarily used in dermatological applications. As such, their focus is on measuring the skin color which is directly related to the concentrations of the chromophores found in skin, specifically oxy- and deoxy-hemoglobin, and melanin.

Two such systems are the DSM II Skin ColorMeter (Cortex Technology, Hadsun, Denmark) and the Mexameter®MX 18 (Courage+Khazaka electronic GmbH, Cologne, Germany). The DSM II Skin ColoMeter employs a plastic probe with focusing optics to shine a white LED onto the skin surface. The reflected light is then focused back

onto multispectral detectors within the probe. The detector processes the reflected signal into one of the many color systems (RBG, CMYK, or L*a*b*) or a proprietary erythema index. The Mexameter uses three wavelengths (568 nm, 660 nm, and 870 nm) emitted by a 16 LED array onto the skin within a probe head that is placed on the skin surface. The requirement of direct contact between the skin and the probe suggests that this may be a fiber-based device although that is not explicitly stated. The red and near-infrared (NIR) wavelengths are used to determine a melanin index, and the green and red wavelengths are used to determine the erythema index.[47] Both systems rely on calibration measurements performed on black and white reflectance standards (provided).

The prices for either system could not be determined from the company websites, but a recent competitor, the Derma Spectrometer (MIC Global, London, United Kingdom) (no longer for sale) was priced at $6000 in early 2014.

1.5 Integrating sphere theory

An integrating sphere is a light delivery and/or collection device. As its name suggests, it is made from a hollow sphere with several "ports" cut out of the surface through which light can enter or exit. A typical sphere is shown in Figure 1.2. The inner surface of the sphere is covered with a highly diffuse reflective coating to create what is known as a Lambertian surface. When used as a light delivery device, the light emitted from the irradiation port is uniformly distributed and is isotropic in direction. When used as a measurement device, it is capable of capturing all of the light emitted from the sample area directly below the measurement port. Together, these illumination and measurement qualities make integrating spheres ideal for measuring the total diffuse reflectance (spectrum).

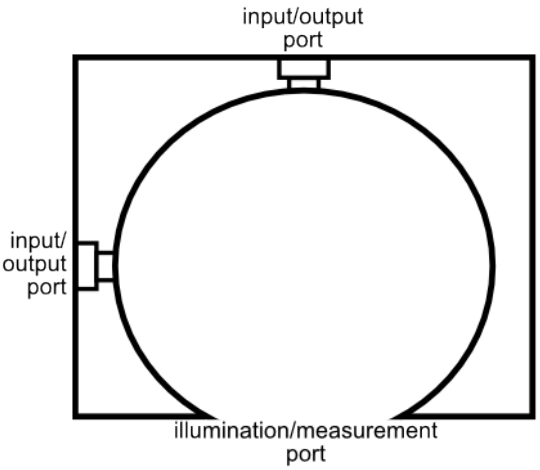

Figure 1.2: A diagram displaying a common geometry for an integrating sphere. There are two ports for delivering and collecting the light and one port for measuring the reflectance from a sample.

1.5.1 Relative reflectance and sphere throughput

The total diffuse reflectance is a relative (as opposed to absolute) reflectance measurement. As such, it requires a characterized reflectance sample known as a reference standard. Measurements performed with the sample of interest are compared to measurements performed with the reference standard. To ensure accurate reflectance measurements, it is important to maintain a consistent throughput, or efficiency within the sphere between the sample and the standard measurements.[48]

The throughput or efficiency of an integrating sphere is the best way of characterizing its performance. It can either be empirically determined or approximated by the following equation,

$$\tau = f_d \frac{\rho_w}{1 - \bar{\rho}_w} \tag{1.8}$$

where f_d is the exchange factor – equal to the ratio of the total surface area of all the ports to the surface area of the sphere, ρ_w is the actual reflectance of the sphere wall material, and $\bar{\rho}_w$ is the average sphere wall reflectance accounting for the reflectances at each of the ports.

When the integrating sphere is sufficiently large, a change in the reflectance at one of the ports has a proportionately small effect on the sphere's throughput. Unfortunately, large spheres are not only expensive, but often impractical. For smaller spheres,

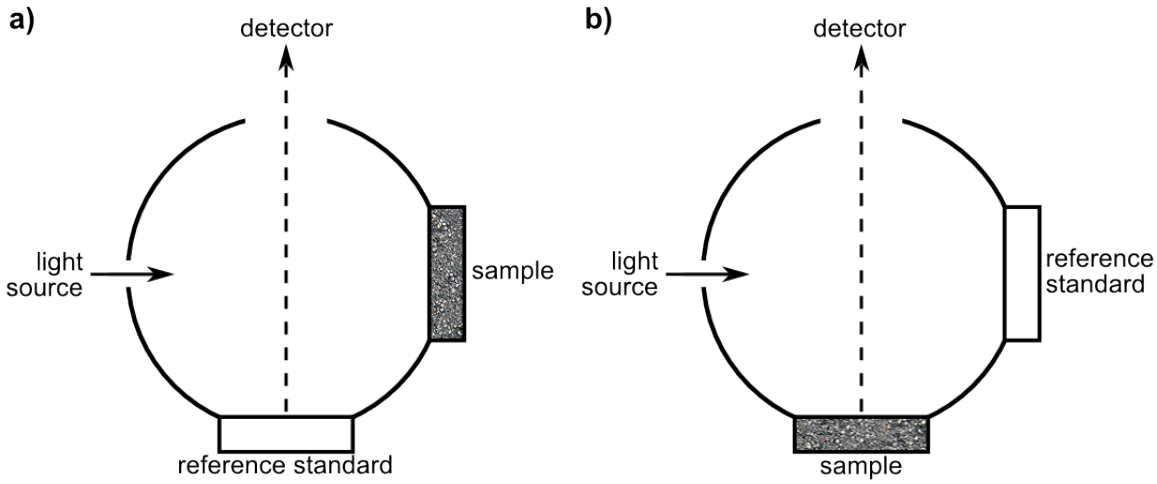

Figure 1.3: To ensure a constant throughput in the sphere between sample and reference measurements, a dummy port can be added to sufficiently large spheres that will eliminate the SBSE.

changes in the sphere throughput between the sample and the reference standard cause what are known as Single Beam Substitution Errors (SBSE) in the total diffuse reflectance measurement.

If the sphere is sufficiently large to allow for an additional "dummy" port, a second measurement can be performed to account for SBSE, as shown in Figure 1.3.[49] The geometry for the first measurement positions the sample directly opposite the light source and the reference standard at the dummy port. This is the primary reflectance measurement. The geometry for the second measurement positions the reference standard directly opposite the light source and the sample at the dummy port. This represents the background correction factor. Under this experimental design, the sphere throughputs and average reflectances are equal for the two measurements.

If the sphere is too small to permit a second port, the SBSE must be corrected mathematically or empirically. Of these two options, the empirical approach is preferred as a mathematical solution would be extremely complex and only accurate if precise values for parameters such as port fractions and reflectances were provided. For a given sphere, reflectance measurements are performed on a set of characterized reflectance standards covering the range of reflectances expected from the unknown samples. By comparing the observed reflectances to the expected ones, a correction factor equation or a lookup table can be produced. This process is described in detail in Chapter 2.

1.5.2 Integrating sphere design

When constructing an integrating sphere, there are several major design parameters that must be optimized to minimize measurement error. The first is the sphere size, which cannot be determined until the total surface area of all of the ports has been calculated. Ports intended for coupling with optical fibers will have a fixed surface area while the area of the detection/illumination port(s) will depend on the use of the sphere. Once the total surface area of the ports has been determined, the sphere size can be calculated based on the rule of thumb that the resulting exchange factor be less than 5%.[50] Spheres that exceed this ratio no longer display some of the desired characteristics such as the isotropy of the light within the sphere.

The next consideration is the material of the sphere wall or the sphere's internal coating. Spheres can be created from a highly reflective material such as Spectralon®, or they can be produced with another material and subsequently coated on the inside with a highly reflective paint, such as barium sulfate. In either case, it is extremely important that the interior surface of the sphere have as high a reflectance as possible, ideally greater than 94%. This material should also be matte or diffuse in nature in order to produce the desired scattering that creates the isotropic illumination.

The final consideration for the integrating sphere is the geometry of the ports. Usually light from the input port is not directly incident on the output port. To accomplish this, the numerical aperture of the optical fibers connected to the ports and the overall sphere geometry should be considered. If physical positioning of the ports cannot accomplish this task, wall projections into the center of the sphere, known as baffles, can be added. Baffles are not ideal for smaller spheres as they introduce inhomogeneities to the smooth inner surface of the sphere that affect the isotropic characteristic. Once this requirement has been satisfied, the illumination geometry can be decided. The two most popular setups are: (1) diffuse-direct (d/0°), where incident light is first incident on the sphere wall and the detection port is directly opposite the output port, and (2) direct-diffuse (0°/d), where the incident light is first incident on the detection port and the output port is focused on a portion of the inner sphere wall.[51]

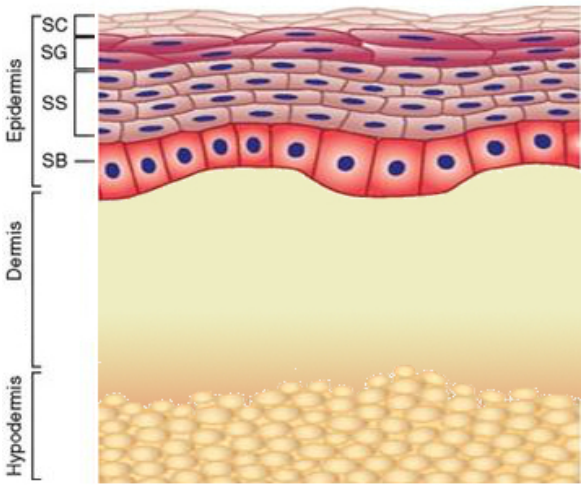

Figure 1.4: The three main layers of skin: The epidermis, the dermis, and the subcutaneous layers. Cells of the epidermis begin at the stratum basale (SB) and migrate through the stratum spinosum (SS) and stratum gradulosum (SG) to the stratum corneum (SC). Modified with permission: ©David J. Wong (`http://www.stembook.org`), CC-BY-SA-3.0.[54]

1.6 Human skin

1.6.1 Skin Anatomy

Human skin consists of three main layers: the epidermis, the dermis, and the subcutaneous layer.[52] The epidermis is the top-most layer of skin. Keratinocytes (skin cells) are produced at the deepest section of the epidermis in the stratum basale (or basal layer) and migrate toward the surface, through the statum spinosum and the stratum granulosum to the stratum corneum, losing their internal structures and organelles during the process (see Figure 1.4). Once the cells reach the skin surface, they are no longer alive and can be shed easily. The basal cells undergo mitosis at an average rate of 10% per day[1] and the migration of cells toward the surface occurs at a steady equilibrium rate. A completely new dermal layer is formed every 4 weeks. Also found in the epidermis are melanocytes, the melanin-producing cells which are majorly responsible for skin color. The average epidermal thickness is 0.1 mm.[53]

The second layer of skin is the dermis. It contains mostly collagen and elastin fibers but is also the location of capillaries and some nerves. The average dermal thickness is approximately 1.5 mm but can vary widely depending on the site.

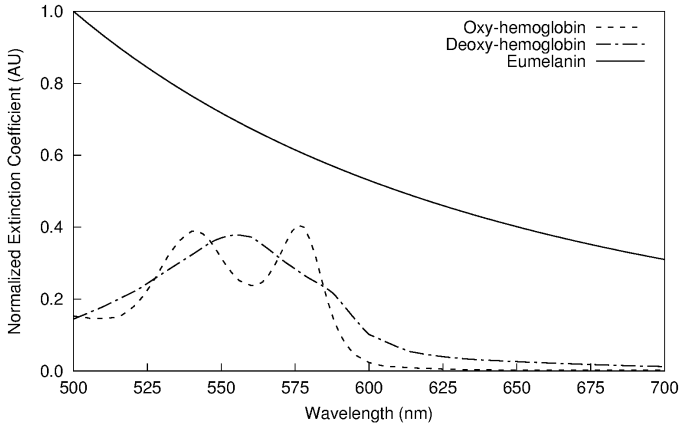

Figure 1.5: The extinction coefficients of the major chromphores found in skin within the visible light spectrum: Oxy- and deoxy-hemoglobin and melanin. Data shown are from Prahl & Jacques (2001).[10]

Below the skin is the subcutaneous layer, also known as the hypodermis or subcutis. The thickness of this layer varies greatly because this is the layer that contains subcutaneous fat. This is also the location of the majority of superficial veins which can occasionally be visible at the surface. A representative thickness for this layer is 5 mm.

Light in the visible spectrum (400-750 nm) is only able to penetrate the first two layers of skin.[55] For 500 nm light (green/blue), the average penetration depth in human skin is 0.6 mm while for 700 nm light (red/near-infrared), the average depth is 1.2 mm.[9] Diffusely reflected light must first travel into and then out of the skin, therefore the majority of the reflected light signal is due to scattering and absorption events within the epidermis and dermis. Within these layers, the dominant chromophores are: oxy- and deoxy-hemoglobin, and melanin. The relative extinction coefficient spectra for these three chromophores are shown in Figure 1.5. While water accounts for roughly 70% (w/w) of human tissue,[56] its absorption below 700 nm is negligible. Similarly, beta-carotene (in the epidermis) and bilirubin (in the dermis) do not contribute significantly at wavelengths above 450 nm. Also, they are only found in relatively small concentrations in healthy human skin. Although its contribution is small, there is a significant amount of absorption by the structural components of skin.[57]

1.6.2 Skin Physiology

Changes to the vasculature within the dermal and subcutaneous layers impacts the blood flow that, in turn, changes the physical appearance at the surface. When the blood vessels narrow, less blood is present in the dermal layer of the skin. This process is known as vasoconstriction and results in a perceived blanching of the skin. When the blood vessels expand in a process known as vasodilation, more blood is present in the skin, which appears redder to the human eye.

As illustrated in Figure 1.5, both oxy- and deoxy-hemoglobin have low absorption in the red region of the visible spectrum, but have significant absorption within the green/yellow region. Therefore, when vasodilation occurs, the skin does not appear redder due to an increase in reflected red light, rather it is because of a decrease in the other colours in the reflected spectrum. Similarly, when vasoconstriction occurs, more green and yellow light are scattered back out of the tissue, contributing to a whiter appearance given that white light is a collection of all of the colors within the visible spectrum. Regarding the ratio of the two major hemoglobin chromophores during these two processes, McNaulty *et al.* determined that the tissue oxygen saturation (StO_2) is related to blood flow.[58] Therefore, more oxy-hemoglobin is present during vasodilation and less is present during vasoconstriction.

Vasoconstriction and vasodilation are normal thermal regulatory responses of the human body.[59] When the body begins to overheat, blood vessels near the surface expand to release heat. When the body temperature drops, blood vessels in the skin constrict to maintain more blood flow in the core. While this is the most commonly observed cause of these two processes, both can be induced by other means. For example, the anesthetic lidocaine acts as a vasodilator and epinephrine, a hormone, behaves as a vasoconstrictor. They are often used together in a subcutaneous injection to simultaneously numb the region of interest while keeping it blanched for better viewing and minimal bleeding during surgery. As the name suggests, the needle is inserted into the subcutaneous tissue below the dermis and acts on the blood vessels that span both layers. The actual area of skin impacted depends on the volumes and concentrations of the two injected drugs. Depending on the local vasculature, the effect can last up to several hours.

Vasodilation is also the most common response to inflammation because the increased blood flow supplies the affected tissue with more oxygen and white blood

cells, which are useful when infection occurs. During radiation therapy, radiation dermatitis/erythema occurs because some of the healthy cells in the basal layer are prevented from dividing.[60] This disrupts the steady rate of progression of cells toward the skin surface, causing an inflammatory response.[61] Erythema is also promoted by an increase in skin dryness due to the destruction of sweat and oil (sebaceous) glands. Although all patients respond differently and are prescribed different treatment plans, the general trend is for erythema to appear around the second week of treatment and last for approximately two to four weeks following treatment. For head and neck intensity modulated radiation therapy (IMRT), clinical experience predicts that the maximum skin response will occur during the fifth week of treatment (J. Wright, personal communication, Aug. 28, 2014.).

1.7 Thesis proposal

Currently available commercial systems for monitoring erythema rely on total diffuse reflectance spectroscopy.[47] As a result, they can only provide measurements in the form of a skin redness scale (or "erythema index"). Such an index is only capable of detecting when skin is more or less red compared to some baseline measurement, and it cannot account for changes in non-hemoglobin chromophores.

Other clinical systems rely on a spatially-fixed spectrally-constrained diffuse reflectance approach.[62] Such systems are capable of accounting for changes in the non-hemoglobin chromophores but may be more sensitive to positioning errors compared to an integrating sphere-based system.

A combination of the two approaches will result in a user-friendly system capable of accounting for all chromophore concentration changes. Thus, a spectrally-constrained model to interpret the total diffuse reflectance spectra obtained with an integrating sphere is proposed. Similar systems have been built by Yudovsky and Pilon,[63, 64] but their derived model was tested on data measured in 1952, and since they did not account for integrating sphere effects, their model did not fit well to the data, particularly outside of the hemoglobin feature wavelengths. As such, careful consideration should be paid when building and characterizing a similar system. In Chapter 2 of this thesis, a paper is presented that outlines the elements of such a system and how its response was characterized. In Chapter 3, the system, combined with a standard erythema index, was used to determine the time to maximal effect of epinephrine. In Chapter 4,

a paper proposing a spectrally-constrained model for interpreting the spectra obtained with the established system is presented. Special consideration is paid to the necessary corrections required when the total diffuse reflectance spectrum is collected instead of the standard fixed-position diffuse reflectance spectrum. The system and model are then combined in Chapter 5 and used to monitor the skin redness of patients undergoing IMRT for cancers of the head and neck. The results are used to outline the proper implementation of quantitative analysis in a study comparing two treatment interventions or management regimens. Such additional consideration is necessary due to the large daily variation in the hemoglobin concentration in skin. Along with the skin redness measurements, weekly TLD readings were performed to confirm the skin dose in the measurement region. These data were later used to determine TLD placement and positioning reproducibility in Chapter 6.

References

[1] Maurene McQuestion. "Evidence-based skin care management in radiation therapy." In: *Seminars in oncology nursing* 22.3 (2006-08), pp. 163–73. ISSN: 0749-2081. DOI: 10.1016/j.soncn.2006.04.004. URL: http://www.ncbi.nlm.nih.gov/pubmed/16893745 (cit. on pp. 2, 16).

[2] B Maciejewski, HR Withers, Jeremy MG Taylor, and Andrzej Hliniak. "Dose fractionation and regeneration in radiotherapy for cancer of the oral cavity and oropharynx: tumor dose-response and repopulation". In: *International Journal of Radiation Oncology*Biology*Physics* 16.3 (1989), pp. 831–843. URL: http://www.sciencedirect.com/science/article/pii/0360301689905038 (cit. on p. 2).

[3] Eric J Hall. "Doses and Risks in Diagnostic Radiology, Interventional Radiology and Cardiology, and Nuclear Medicine". In: *Radiobiology for the Radiologists*. 5th. Philadelphia, PA: Lippincott Williams & Wilkins, 2000. Chap. 14, pp. 199–233 (cit. on p. 2).

[4] D Porock and M U Sinclair. "Factors influencing the severity of radiation skin and oral mucosal reactions : development of a conceptual framework". In: *European journal of cancer care* 11.1 (2002), pp. 33–43 (cit. on p. 2).

[5] Rebecca K S Wong, René-Jean Bensadoun, Christine B Boers-Doets, Jane Bryce, Alexandre Chan, Joel B Epstein, Beth Eaby-Sandy, and Mario E Lacouture. "Clinical practice guidelines for the prevention and treatment of acute and late radiation reactions from the MASCC Skin Toxicity Study Group." In: *Supportive care in cancer : official journal of the Multinational Association of Supportive Care in Cancer* 21.10 (2013-10), pp. 2933–48. ISSN: 1433-7339. DOI: 10.1007/s00520-013-1896-2. URL: http://www.ncbi.nlm.nih.gov/pubmed/23942595 (cit. on p. 2).

[6] Raymond Javan Chan, Joan Webster, Bryan Chung, Louise Marquart, Muhtashimuddin Ahmed, and Stuart Garantziotis. "Prevention and treatment of acute radiation-induced skin reactions: a systematic review and meta-analysis of randomized controlled trials." In: *BMC cancer* 14 (2014-01), p. 53. ISSN: 1471-2407. DOI: 10.1186/1471-2407-14-53. URL: http://www.pubmedcentral.

nih.gov/articlerender.fcgi?artid=3909507%5C&tool=pmcentrez%5C&rendertype=abstract (cit. on p. 2).

[7] Wayne F Larrabee, Brent J Lanier, and David Miekle. "Effect of epinephrine on local cutaneous blood flow". In: *Head & Neck Surgery* 9.5 (1987-05), pp. 287–289. ISSN: 01486403. DOI: 10.1002/hed.2890090507. URL: http://doi.wiley.com/10.1002/hed.2890090507 (cit. on p. 2).

[8] I D Swain and L J Grant. "Methods of measuring skin blood flow". In: *Physics in medicine and biology* 34.2 (1989), pp. 151–175. URL: http://iopscience.iop.org/0031-9155/34/2/001 (cit. on p. 2).

[9] R Richards-Kortum and E Sevick-Muraca. "Quantitative optical spectroscopy for tissue diagnosis." In: *Annual review of physical chemistry* 47 (1996-01), pp. 555–606. ISSN: 0066-426X. DOI: 10.1146/annurev.physchem.47.1.555. URL: http://www.ncbi.nlm.nih.gov/pubmed/8930102 (cit. on pp. 2, 17).

[10] Scott A Prahl and Steven L Jacques. *Optical Properties Spectra*. 2001. URL: http://omlc.org/spectra/ (cit. on pp. 3, 17).

[11] Gregory M. Palmer and Nirmala Ramanujam. "Monte Carlo-based inverse model for calculating tissue optical properties. Part I: Theory and validation on synthetic phantoms". In: *Applied Optics* 45.5 (2006), p. 1062. ISSN: 0003-6935. DOI: 10.1364/AO.45.001062. URL: http://www.opticsinfobase.org/abstract.cfm?URI=AO-45-5-1062 (cit. on p. 3).

[12] Georgios N Stamatas, Barbara Z Zmudzka, Nikiforos Kollias, and Janusz Z Beer. "Review : Innovative Technology Non-Invasive Measurements of Skin Pigmentation In Situ". In: *Pigment Cell Research* 17 (2004), pp. 618–626 (cit. on p. 3).

[13] J B Dawson, D J Barker, D J Ellis, E Grassam, J A Cotterill, G W Fisher, and J W Feather. "A theoretical and experimental study of light absorption and scattering by in vivo skin". In: *Physics in Medicine and Biology* 25.4 (1980-07), pp. 695–709. ISSN: 0031-9155. DOI: 10.1088/0031-9155/25/4/008. URL: http://www.ncbi.nlm.nih.gov/pubmed/7454759%20http://stacks.iop.org/0031-9155/25/i=4/a=008?key=crossref.3a9c201eba5c1754a3a8963193b6ce29 (cit. on p. 3).

[14] B L Diffey, R J Oliver, and P M Farr. "A portable instrument for quantifying erythema induced by ultraviolet radiation." In: *The British journal of dermatology* 111.6 (1984-12), pp. 663–72. ISSN: 0007-0963. URL: http://www.ncbi.nlm.nih.gov/pubmed/6508999 (cit. on p. 3).

[15] J Lock-Andersen, M Gniadecka, F de Fine Olivarius, K Dahlstrom, and H C Wulf. "Skin temperature of UV-induced erythema correlated to laser Doppler flowmetry and skin reflectance measured redness". In: *Skin Research and Technology* 4 (1998), pp. 41–48. URL: http://onlinelibrary.wiley.com/doi/10.1111/j.1600-0846.1998.tb00085.x/abstract (cit. on p. 3).

[16] Mette Bodekaer, Peter Alshede Philipsen, Tonny Karlsmark, and Hans Christian Wulf. "Good agreement between minimal erythema dose test reactions and objective measurements: an in vivo study of human skin." In: *Photodermatology, Photoimmunology & Photomedicine* 29.4 (2013-08), pp. 190–5. ISSN: 1600-0781. DOI: 10.1111/phpp.12049. URL: http://www.ncbi.nlm.nih.gov/pubmed/23815351 (cit. on p. 3).

[17] Georgios N Stamatas, Barbara Z Zmudzka, Nikiforos Kollias, and Janusz Z Beer. "In vivo measurement of skin erythema and pigmentation: new means of implementation of diffuse reflectance spectroscopy with a commercial instrument." In: *The British Journal of Dermatology* 159.3 (2008-09), pp. 683–90. ISSN: 1365-2133. DOI: 10.1111/j.1365-2133.2008.08642.x. URL: http://www.ncbi.nlm.nih.gov/pubmed/18510669 (cit. on p. 3).

[18] Nikiforos Kollias, InSeok Seo, and Paulo R Bargo. "Interpreting diffuse reflectance for in vivo skin reactions in terms of chromophores." In: *Journal of Biophotonics* 3.1-2 (2010-01), pp. 15–24. ISSN: 1864-0648. DOI: 10.1002/jbio.200900066. URL: http://www.ncbi.nlm.nih.gov/pubmed/19946873 (cit. on p. 3).

[19] Igor V Meglinski and Stephen J Matcher. "Quantitative assessment of skin layers absorption and skin reflectance spectra simulation in the visible and near-infrared spectral regions." In: *Physiological measurement* 23.4 (2002-11), pp. 741–53. ISSN: 0967-3334. URL: http://www.ncbi.nlm.nih.gov/pubmed/12450273 (cit. on p. 3).

[20] Bing Yu, Justin Y Lo, Thomas F Kuech, Gregory M Palmer, Janelle E Bender, and Nirmala Ramanujam. "Cost-effective diffuse reflectance spectroscopy device for quantifying tissue absorption and scattering in vivo." In: *Journal of biomedical optics* 13.6 (2008), p. 060505. ISSN: 1083-3668. DOI: 10.1117/1.3041500. URL: http://www.ncbi.nlm.nih.gov/pubmed/19123646 (cit. on p. 3).

[21] Izumi Nishidate, Aditya Wiswadarma, Yota Hase, Noriyuki Tanaka, Takaaki Maeda, Kyuichi Niizeki, and Yoshihisa Aizu. "Noninvasive spectral imaging of skin chromophores based on multiple regression analysis aided by Monte Carlo simulation." In: *Optics letters* 36.16 (2011-08), pp. 3239–41. ISSN: 1539-4794. URL: http://www.ncbi.nlm.nih.gov/pubmed/21847220 (cit. on p. 4).

[22] George Zonios, Julie Bykowski, and Nikiforos Kollias. "Skin melanin, hemoglobin, and light scattering properties can be quantitatively assessed in vivo using diffuse reflectance spectroscopy." In: *The Journal of investigative dermatology* 117.6 (2001-12), pp. 1452–1457. ISSN: 0022-202X. DOI: 10.1046/j.0022-202x.2001.01577.x. URL: http://www.ncbi.nlm.nih.gov/pubmed/11886508 (cit. on p. 4).

[23] George Zonios and Aikaterini Dimou. "Light scattering spectroscopy of human skin in vivo." In: *Optics express* 17.3 (2009-02), pp. 1256–67. ISSN: 1094-4087. URL: http://www.ncbi.nlm.nih.gov/pubmed/19188953 (cit. on p. 4).

[24] Roberto Reif, Mark S Amorosino, Katherine W Calabro, Ousama A'Amar, Satish K Singh, and Irving J Bigio. "Analysis of changes in reflectance measurements on biological tissues subjected to different probe pressures." In: *Journal of biomedical optics* 13.1 (2011), p. 010502. ISSN: 1083-3668. DOI: 10.1117/1.2870115. URL: http://www.ncbi.nlm.nih.gov/pubmed/18315347 (cit. on p. 4).

[25] Sheng-Hao Tseng, Chao-Kai Hsu, Julia Yu-Yun Lee, Shih-Yu Tzeng, Wan-Rung Chen, and Yu-Kai Liaw. "Noninvasive evaluation of collagen and hemoglobin contents and scattering property of in vivo keloid scars and normal skin using diffuse reflectance spectroscopy: pilot study." In: *Journal of biomedical optics* 17.7 (2012-07), p. 077005. ISSN: 1560-2281. DOI: 10.1117/1.JBO.17.7.077005. URL: http://www.ncbi.nlm.nih.gov/pubmed/22894518 (cit. on p. 4).

[26] Dmitry Yudovsky, Aksone Nouvong, and Laurent Pilon. "Hyperspectral imaging in diabetic foot wound care." In: *Journal of Diabetes Science and Technology* 4.5 (2010-09), pp. 1099–113. ISSN: 1932-2968. URL: http://www.pubmedcentral.

nih.gov/articlerender.fcgi?artid=2956800%5C&tool=pmcentrez%5C&rendertype=abstract (cit. on p. 4).

[27] Michael S Chin, Brian B Freniere, Yuan-Chyuan Lo, Jonathan H Saleeby, Stephen P Baker, Heather M Strom, Ronald a Ignotz, Janice F Lalikos, and Thomas J Fitzgerald. "Hyperspectral imaging for early detection of oxygenation and perfusion changes in irradiated skin." In: *Journal of Biomedical Optics* 17.2 (2012-02), p. 026010. ISSN: 1560-2281. DOI: 10.1117/1.JBO.17.2.026010. URL: http://www.ncbi.nlm.nih.gov/pubmed/22463042 (cit. on p. 4).

[28] Markolf H Niemz. "Light and Matter". In: *Laser-Tissue Interactions*. 3rd. Berlin: Springer-Verlag Berlin Heidelberg, 2007. Chap. 2. ISBN: 3-540-40553-4. URL: http://content.schweitzer-online.de/static/catalog%5C_manager/live/media%5C_files/representation/zd%5C_std%5C_orig%5C_%5C_zd%5C_schw%5C_orig/012/629/115/9783642034374%5C_content%5C_pdf%5C_1.pdf (cit. on p. 4).

[29] Randall D Knight. "Ray Optics". In: *Physics for Scientists and Engineers: A Strategic Approach (with Modern Physics)*. 3rd. Glenview, IL: Pearson Education, Inc., 2013. Chap. 23, pp. 655–693 (cit. on p. 4).

[30] Frank L Pedrotti and Leno S Pedrotti. "No Title". In: *Introduction to Optics*. 2nd. Toronto: Prentice Hall, Inc., 1993. Chap. 20, pp. 407–425 (cit. on p. 4).

[31] R M P Doornbos, R Lang, M C Aalders, F W Cross, and H J C M Sterenborg. "The determination of in vivo human tissue optical properties and absolute chromophore concentrations using spatially resolved steady-state diffuse reflectance". In: *Physics in medicine and biology* 44 (1999), pp. 967–981. URL: http://iopscience.iop.org/0031-9155/44/4/012 (cit. on pp. 4, 11).

[32] Steven L Jacques and Michael S Patterson. "Light-tissue interactions". In: *Handbook of Laser Technology and Applications, Volume 3: Applications*. Ed. by Colin E Webb and Julian D C Jones. 1st. Philadephia, Pennslyvania: Institute of Physics Publishing, 2004. Chap. D3.1, pp. 1955–1993. ISBN: 978-0750309660 (cit. on pp. 5, 6).

[33] Paras N Prasad. "Photobiology". In: *Introduction to Biophotonics*. 1st. Toronto: John Wiley & Sons, Inc., 2003. Chap. 6, pp. 159–202 (cit. on p. 5).

[34] Enrico Gratton and Sergio Fantini. "Reflectance and transmittance spectroscopy". In: *Lasers and Current Optical Techniques in Biology*. Ed. by G Palumbo and R Pratesi. 1st. Hong Kong: The Royal Society of Chemistry, 2004. Chap. 11, pp. 211–258 (cit. on p. 5).

[35] Thomas J Farrell and Michael S Patterson. "Diffusion Modeling of Fluorescence in Tissue". In: *Handbook of Biomedical Fluorescence*. Ed. by Mary-Ann Mycek and Brian W Pogue. 1st. New York: Marcel Dekker, Inc., 2003. Chap. 2, pp. 29–60 (cit. on pp. 5, 6).

[36] James J. Duderstadt and Louis J. Hamilton. "Neutron Transport". In: *Nuclear Reactor Analysis*. Toronto: John Wiley & Sons, Inc., 1976. Chap. 4, pp. 103–148. ISBN: 978-0-471-22363-4 (cit. on p. 6).

[37] Brian C Wilson and Michael S Patterson. "The physics, biophysics and technology of photodynamic therapy." In: *Physics in Medicine and Biology* 53.9 (2008-05), R61–109. ISSN: 0031-9155. DOI: 10.1088/0031-9155/53/9/R01. URL: http://www.ncbi.nlm.nih.gov/pubmed/18401068 (cit. on p. 6).

[38] Scott A Prahl. "The Diffusion Approximation in Three Dimensions". In: *Optical-Thermal Response of Laser-Irradiated Tissue*. Ed. by Ashley J Welch and Martin J C van Gemert. 1st. New York: Plenum Press, 1995. Chap. 7, pp. 207–232 (cit. on p. 7).

[39] SA Prahl, M Keijzer, SL Jacques, and AJ Welch. "A Monte Carlo model of light propagation in tissue". In: *Dosimetry of laser radiation in ...* I.1989 (1989), pp. 102–111. URL: http://www.lth.se/fileadmin/atomfysik/Biophotonics/Education/prahl89.pdf (cit. on p. 7).

[40] L Wang, SL Jacques, and L Zheng. "MCML—Monte Carlo modeling of light transport in multi-layered tissues". In: *Computer Methods and Programs in Biomedicine* 47 (1995), pp. 131–146. URL: http://www.sciencedirect.com/science/article/pii/016926079501640F (cit. on p. 7).

[41] Alwin Kienle and Michael S Patterson. "Determination of the optical properties of turbid media from a single Monte Carlo simulation." In: *Physics in Medicine and Biology* 41.10 (1996-10), pp. 2221–7. ISSN: 0031-9155. URL: http://www.ncbi.nlm.nih.gov/pubmed/8912392 (cit. on pp. 7–9).

[42] Erik Alerstam, Stefan Andersson-Engels, and Tomas Svensson. "White Monte Carlo for time-resolved photon migration." In: *Journal of biomedical optics* 13.4 (2013), p. 041304. ISSN: 1083-3668. DOI: 10.1117/1.2950319. URL: http://www.ncbi.nlm.nih.gov/pubmed/19021312 (cit. on p. 7).

[43] Anthony Kim and Brian C. Wilson. "Measurement of Ex Vivo and In Vivo Tissue Optical Properties: Methods and Theories". In: *Optical-Thermal Response of Laser-Irradiated Tissue*. Ed. by Ashley J Welch and M J C van Gemert. 2nd. New York: Springer, 2011. Chap. 8, pp. 267–319. DOI: 10.1007/978-90-481-8831-4_8. URL: http://www.springerlink.com/content/p688r10601w2u2vn/ (cit. on pp. 8, 9, 11).

[44] Alwin Kienle, Lothar Lilge, Michale S Patterson, R Hibst, R Steiner, and Brian C Wilson. "Spatially resolved absolute diffuse reflectance measurements for noninvasive determination of the optical scattering and absorption coefficients of biological tissue." In: *Applied optics* 35.13 (1996-05), pp. 2304–14. ISSN: 0003-6935. URL: http://www.ncbi.nlm.nih.gov/pubmed/21085367 (cit. on p. 9).

[45] Thomas J Farrell and Michael S Patterson. "A diffusion theory model of spatially resolved, stead-state diffuse reflectance for the noninvasive determination of tissue optical properties in vivo". In: *Medical Physics* 19.4 (1992), pp. 879–888 (cit. on p. 10).

[46] Darren Yohan, Anthony Kim, Elina Korpela, Stanley Liu, Carolyn Niu, Brian C Wilson, and Lee Cl Chin. "Quantitative monitoring of radiation induced skin toxicities in nude mice using optical biomarkers measured from diffuse optical reflectance spectroscopy." In: *Biomedical optics express* 5.5 (2014-05), pp. 1309–20. ISSN: 2156-7085. DOI: 10.1364/BOE.5.001309. URL: http://www.pubmedcentral.nih.gov/articlerender.fcgi?artid=4026905%5C&tool=pmcentrez%5C&rendertype=abstract (cit. on p. 11).

[47] P. Clarys, K. Alewaeters, R. Lambrecht, and A. O. Barel. "Skin color measurements: comparison between three instruments: the Chromameter(R), the DermaSpectrometer(R) and the Mexameter(R)." In: *Skin research and technology : official journal of International Society for Bioengineering and the Skin (ISBS) [and] International Society for Digital Imaging of Skin (ISDIS) [and] International Society for Skin Imaging (ISSI)* 6.4 (2000-11), pp. 230–238. ISSN:

1600-0846. URL: http://www.ncbi.nlm.nih.gov/pubmed/11428962 (cit. on pp. 12, 19).

[48] Leonard M Hanssen and Keith A Snail. "Integrating Spheres for Mid- and Near-infrared Reflection Spectroscopy". In: *Handbook of Vibrational Spectroscopy*. Ed. by John M Chalmers and Peter R Griffiths. Wiley & Sons, 2002. URL: http://www.nist.gov/calibrations/upload/HndBkSphere.pdf (cit. on p. 13).

[49] Labsphere. *Application Note No. 01: Quantitation of Single Beam Substitution Correction in Reflectance Spectroscopy Accessories*. Tech. rep. 01. North Sutton, NH: Labsphere. URL: http://www.labsphere.com/uploads/technical-guides/Quantitation%20of%20Single%20Beam%20Substitution%20Correction.pdf (cit. on p. 14).

[50] Labsphere. *Technical Guide: Integrating Sphere Theory and Applications*. Tech. rep. North Sutton, NH: Labsphere, pp. 1–19. URL: http://www.labsphere.com/uploads/technical-guides/a-guide-to-integrating-sphere-theory-and-applications.pdf (cit. on p. 15).

[51] Art W Springsteen. "Reflectance Spectroscopy: An Overview of Classification and Techniques". In: *Applied Spectroscopy: A Compact Reference for Practitioners*. Ed. by Jerry Workman and Art W Springsteen. 1st. New York: Academic Press, 1998. Chap. 6, pp. 193–224 (cit. on p. 15).

[52] Lucian Fodor, Yehuda Ullman, and Monica Elman. "Skin Anatomy". In: *Aesthetic Applications of Intense Pulsed Light*. New York: Springer London, 2011. Chap. 1, pp. 1–10. ISBN: 978-1-84996-455-5. DOI: 10.1007/978-1-84996-456-2. URL: http://link.springer.com/10.1007/978-1-84996-456-2 (cit. on p. 16).

[53] MF Yang, VV Tuchin, and AN Yaroslavsky. "Principles of light-skin interactions". In: *Light-Based Therapies for Skin of ...* Ed. by Elma D Baron. New York: Springer-Verlag London Limited, 2009. Chap. 1, pp. 1–44. ISBN: 9781848823280. URL: http://link.springer.com/chapter/10.1007/978-1-84882-328-0%5C_1 (cit. on p. 16).

[54] David J Wong and Howard Y Chang. "Skin tissue engineering". In: *StemBook* (2009). ISSN: 19403429. DOI: 10.3824/stembook.1.44.1. URL: http://www.stembook.org/node/582 (cit. on p. 16).

[55] Irene E Kochevar, Charles R Taylor, and Jean Krutmann. "Fundamentals of Cutaneous Photobiology and Photoimmunology". In: *Fitzpatrick's Dermatology in General Medicine*. Ed. by L A Goldsmith, S I Katz, Gilchrest B A, A S Paller, D J Leffell, and Wolff K. 8th. New York: McGraw-Hill, 2012. Chap. 90, http://accessmedicine.mhmedical.com/content.aspx?b. URL: http://accessmedicine.mhmedical.com/content.aspx?bookid=392%5C&Sectionid=41138799 (cit. on p. 17).

[56] Noriaki Nakagawa, Masayuki Matsumoto, and Shingo Sakai. "In vivo measurement of the water content in the dermis by confocal Raman spectroscopy." In: *Skin research and technology : official journal of International Society for Bioengineering and the Skin (ISBS) [and] International Society for Digital Imaging of Skin (ISDIS) [and] International Society for Skin Imaging (ISSI)* 16.2 (2010-05), pp. 137–41. ISSN: 1600-0846. DOI: 10.1111/j.1600-0846.2009.00410.x. URL: http://www.ncbi.nlm.nih.gov/pubmed/20456092 (cit. on p. 17).

[57] Paulo R Bargo, S a Prahl, T T Goodell, R a Sleven, G Koval, G Blair, and S L Jacques. "In vivo determination of optical properties of normal and tumor tissue with white light reflectance and an empirical light transport model during endoscopy." In: *Journal of biomedical optics* 10.3 (2005), p. 034018. ISSN: 1083-3668. DOI: 10.1117/1.1921907. URL: http://www.ncbi.nlm.nih.gov/pubmed/16229662 (cit. on p. 17).

[58] J McNulty, Michael Born, and RS Pozos. "Near-Infrared Spectroscopy (NIRS)". In: *Springer Handbook of Medical Technology*. Ed. by Rüdiger Kramme, Klaus-Peter Hoffmann, and Robert S. Pozos. New York: Springer Berlin Heidelberg, 2011. Chap. 22, pp. 423–438. ISBN: 978-3-540-74657-7. DOI: 10.1007/978-3-540-74658-4. URL: http://link.springer.com/chapter/10.1007/978-3-540-74658-4%5C_22%20http://link.springer.com/10.1007/978-3-540-74658-4 (cit. on p. 18).

[59] D L Jr. Kellogg. "Thermoregulation". In: *Fitzpatrick's Dermatology in General Medicine2*. Ed. by L A Goldsmith, S I Katz, Gilchrest B A, A S Paller, D J Leffell, and Wolff K. 8th. New York: McGraw-Hill, 2012. Chap. 93,

http://accessmedicine.mhmedical.com/content.aspx?b. URL: http://accessmedicine.mhmedical.com/content.aspx?bookid=392%5C&Sectionid=41138803 (cit. on p. 18).

[60] T J Fitzgerald, Maryann Bishop Jodoin, Gayle Tillman, Jesse Aronowitz, Richard Pieters, Susan Balducci, Joshua Meyer, M Giulia Cicchetti, Sidney Kadish, Shelagh McCauley, Joanna Sawicka, Marcia Urie, Y C Lo, Charles Mayo, Kenneth Ulin, Linda Ding, Maureen Britton, Jiayi Huang, and Edward Arous. "Radiation therapy toxicity to the skin." In: *Dermatologic Clinics* 26.1 (2008-01), pp. 161–72. ISSN: 0733-8635. DOI: 10.1016/j.det.2007.08.005. URL: http://www.ncbi.nlm.nih.gov/pubmed/18023776 (cit. on p. 19).

[61] Paivi Simonen, Chris Hamilton, Sandra Ferguson, Patricia Ostwald, Maree O'Brien, Peter O'Brien, Michael Back, and Jim Denham. "Do inflammatory processes contribute to radiation induced erythema observed in the skin of humans?" In: *Radiotherapy and Oncology* 46.1 (1998-01), pp. 73–82. ISSN: 01678140. DOI: 10.1016/S0167-8140(97)00115-1. URL: http://linkinghub.elsevier.com/retrieve/pii/S0167814097001151 (cit. on p. 19).

[62] Anthony Kim, Mathieu Roy, Farhan Dadani, and Brian C Wilson. "A fiberoptic reflectance probe with multiple source-collector separations to increase the dynamic range of derived tissue optical absorption and scattering coefficients." In: *Optics express* 18.6 (2010-03), pp. 5580–94. ISSN: 1094-4087. URL: http://www.ncbi.nlm.nih.gov/pubmed/20389574 (cit. on p. 19).

[63] Dmitry Yudovsky and Laurent Pilon. "Rapid and accurate estimation of blood saturation, melanin content, and epidermis thickness from spectral diffuse reflectance." In: *Applied optics* 49.10 (2010-04), pp. 1707–19. ISSN: 1539-4522. URL: http://www.ncbi.nlm.nih.gov/pubmed/20357850 (cit. on p. 19).

[64] Dmitry Yudovsky and Laurent Pilon. "Retrieving skin properties from in vivo spectral reflectance measurements." In: *Journal of biophotonics* 4.5 (2011-05), pp. 305–14. ISSN: 1864-0648. DOI: 10.1002/jbio.201000069. URL: http://www.ncbi.nlm.nih.gov/pubmed/20680977 (cit. on p. 19).

Chapter 2

Paper I - The total diffuse reflectance spectroscopy system

Preamble

Paper I outlines a total diffuse reflectance spectroscopy system for measuring the tissue optical properties of skin. This system incorporates a single integrating sphere geometry and a spectrometer, and was based on previous work by Dr. D. Moscu in 2010.[1] Both Moscu's system and the one outlined in the following paper were made possible by the development of an in-house production method for creating customized integrating spheres from cubes of Spectralon® material by Dr. J. Hayward.

Although the system is not unique in its construction,[2, 3] the intended analysis procedure of fitting the obtained reflectance spectrum with a spectrally-constrained model required the system to be highly characterized. Similar commercially available systems are not accurately calibrated and, as such, can only provide information on increases in chromophore concentrations in terms of arbitrary indices for erythema or melanin. The goal of this paper was to illustrate how an integrating sphere-based system could be calibrated to return the true reflectance spectrum, thereby allowing its use with a spectrally-constrained approach. This makes the system more versatile for use in future studies.

The integrating sphere was prepared by Mr. G. Sawesky at the Juravinski Cancer Centre (Hamilton, Ontario). The remainder of the system was constructed by the author of this thesis (further known as "the author") under the supervision of Drs. T. Farrell and Hayward. All calibration steps were devised and performed by the author. The work from two separate studies was briefly described and shown to illustrate potential uses of the system. The first study involved subcutaneous injections of lidocaine and epinephrine and was jointly achieved by the author and Dr. D. McKee (see Chapter 3) under the supervision of Dr. Hayward. The second study followed radiation therapy patients over the course of treatment and was performed by the author with help from Mrs. L. Doerwald-Munoz and under the supervision of Drs. Farrell, Hayward, O. Ostapiak, and J. Wright (see Chapter 5). Ethics approval was granted for both prospective studies.

An additional benefit to this system was it reduced cost due to the customized integrating sphere. At the time of writing, a call for papers for a special section on "Photonics for Global Health" was issued by the Journal of Biomedical Optics. As a result, the manuscript was prepared with the global health community in mind and special attention was paid to the cost of building and calibrating such a system.

Unfortunately, there was insufficient interest to warrant the special section and the manuscript was published as a general paper. The manuscript was written by the author and edited by Drs. Farrell and Hayward. The manuscript has been altered from its original form to match the style of this thesis.

Contents

Inexpensive diffuse reflectance spectroscopy system for measuring changes in tissue optical properties

Diana L. Glennie, Joseph E. Hayward, Daniel E. McKee, and Thomas J. Farrell
Department of Medical Physics and Applied Radiation Sciences, McMaster University, 1280 Main Street West, Hamilton, Ontario, L8S 1A8
AND
Department of Medical Physics, Juravinski Cancer Centre, 699 Concession Street, Hamilton, Ontario, L8V 5C2

Journal of Biomedical Optics **19**(10), 105005 (October 2014).
http://dx.doi.org/10.1117/1.JBO.19.10.105005

Abstract

The measurement of changes in blood volume in tissue is important for monitoring the effects of a wide range of therapeutic interventions, from radiation therapy to skin-flap transplants. Many systems available for purchase are either expensive or difficult to use, limiting their utility in the clinical setting. A low-cost system, capable of measuring changes in tissue blood volume via diffuse reflectance spectroscopy is presented. The system consists of an integrating sphere coupled via optical fibers to a broadband light source and a spectrometer. Validation data are presented to illustrate the accuracy and reproducibility of the system. The validity and utility of this *in vivo* system were demonstrated in a skin blanching/reddening experiment using epinephrine and lidocaine, and in a study measuring the severity of radiation-induced erythema during radiation therapy.
©2014 Society of Photo-Optical Instrumentation Engineers (SPIE)

2.1 Introduction

The ability to quantify changes in the concentration of chromophores in the skin (particularly oxy- and deoxy-hemoglobin) *in vivo* and in real time has many applications in healthcare. For example, a complication of radiation therapy is radiation-induced erythema, which, if not monitored closely, can progress to painful moist desquamation.[4–7] In photodynamic therapy, tissue oxygenation can be used to indicate treatment efficacy[8] since oxygen is required for the activation of the cytotoxic photochemicals.[9, 10] Finally, in plastic surgery, proper blood flow is integral for the success of free tissue transplants and is used to indicate whether or not a return to the operating room is necessary.[11]

Several methods have been validated for measuring skin redness. In increasing complexity and accuracy they are visual assessment (with or without a color chart), colorimetry/photography, and spectroscopy.[12] Although the visual assessment technique,[13] is the most common, it is qualitative in nature. Due to its subjective nature and the nonlinearity of human vision, it is highly prone to interobserver as well as intraobserver variations.[14] The subjectivity of this method can be minimized by the introduction of color charts; however, a very large number of color shades would be required to best account for the effect of pigmentation on the perceived redness. Despite these difficulties, visual assessment remains the gold standard for measuring skin redness.[15, 16]

Digital photography is usually approached as a two-dimensional implementation of colorimetry. In colorimetry, the color is quantified using a set of three specifically tuned color sensors (usually RGB) that represent the color using a standard color map, such as the L*a*b* system from the International Commission on Illumination (CIE).[17] Colorimetry (and digital photography) is made extremely difficult by the necessity to calibrate and standardize the results to allow for intermeasurement comparison (between days or between individuals).[18] Following correct calibration, both methods are capable of detecting changes in blood and oxygen saturation but, since the relationship between the measured data and skin redness is not fully characterized, they are only capable of indicating whether the skin is more or less red in comparison to previous or baseline measurements.[19–22]

Spectroscopy-based methods, such as reflectance spectroscopy and hyperspectral imaging, are the most complex of the methods used for measuring skin color.[23–27]

Spectroscopy provides quantitative data across a range of wavelengths, allowing for different parameters to be extracted from its measurements, depending on the scope of the investigation and the apparatus used. User-friendly commercial models capable of monitoring relative erythema and tissue oxygen saturation are expensive and use single-use detection probes. For example, the T-Stat®(Spectros, Portola Valley, California) costs approximately $25,000 US.[28] Cheaper models are less user-friendly and mostly only provide a single value for oxygen saturation. As a result, these systems are primarily used by highly trained investigators at research institutions and are rarely utilized in a typical clinical setting where they could be used routinely and would prove most beneficial.

In order to facilitate the translation of spectroscopy systems from the research laboratory to the routine clinical setting for the use on human skin in vivo, an economic integrating sphere-based diffuse reflectance spectroscopy (DRS) unit was developed and characterized. The system designs and specifications will be outlined. To illustrate the validity and utility of the assembled system, the results of two ongoing clinical studies measuring erythema under different conditions will be presented.

2.2 Design of the Total DRS System

Simply, the total DRS system consists of a white light source coupled to an integrating sphere via an optical fiber. A second detection optical fiber directs the reflected light to a spectrometer. The spectrometer is controlled by a computer on which the required processing software was installed. A schematic of the system design is shown in Figure 2.1. A detailed description of the selection of each component is presented below.

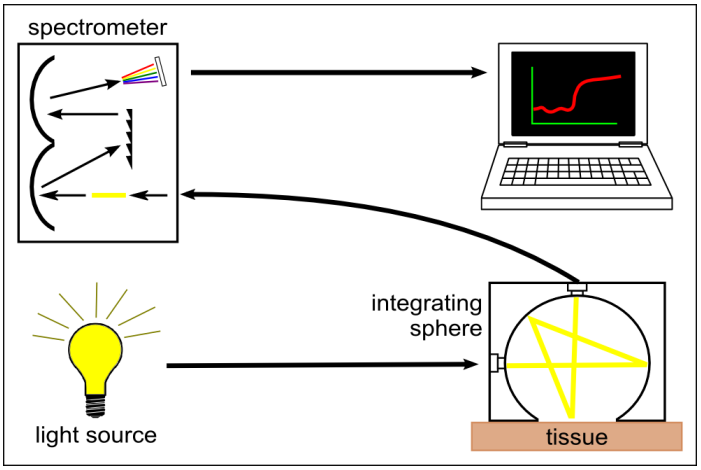

Figure 2.1: A schematic of the measurement system (not to scale). The light source is connected to the side port of the integrating sphere. Light collected through the overhead port is detected by the spectrometer and processed by the laptop.

2.2.1 Light Source

Oxy- and deoxy-hemoglobin have spectral absorption features within the visible light range.[29, 30] Therefore, a light source encompassing this range, without any narrow bandwidth spectral excitation features, is required. In addition, a stable output over the measurement period (minutes to hours) is required for proper reflectance calculation. An Oriel 77501 Radiometric Fiber Optic Source (Newport, Irvine, California) was chosen with a 100 W quartz tungsten halogen lamp to produce a highly stable output within the visible-NIR wavelength range that can be easily coupled to an optical fiber. It also has an adjustable iris to allow for output optimization.

2.2.2 Spectrometer and Optical Fibers

The spectrometer must be capable of detecting light with high sensitivity across the visible spectrum. It must also have sufficient spectral resolution to allow for the differentiation between the spectral features of oxy- and deoxy-hemoglobin (<13 nm for oxy-hemoglobin). An ideal spectrometer would also be small for ease of portability.

The S2000 Miniature Fiber Optic Spectrometer from Ocean Optics (Dunedin, Florida) was chosen for this system. It has a wavelength range of 340 to 1000 nm and a dynamic range of 2000 for a single scan. The 2048-element linear CCD-array results in a pixel width of approximately 0.35 nm and the integration time can range from

3 ms to 60 s. Its small size (<150 mm cube) allows for easy transportation between clinical sites.

The fiber optic connector specifications for the Ocean Optics spectrometer are for an SMA 905 to single-strand 0.22 NA optical fiber. The optical fiber acts in place of a slit in the spectrometer's hardware. A relatively large fiber core of 400 µm was chosen to maximize light collection. This resulted in spectral resolution of 10 nm as determined from the measurement of a mercury–argon calibration source (HG-1 Mercury Argon Calibration Source, Ocean Optics, Dunedin, Florida). The effect of this spectral resolution on the reflectance spectrum analysis is described in Section 2.4.2. The final criterion for the fibers was high transmission in the visible spectrum. Two such fibers, with a wavelength range between 400 and 2200 nm, were purchased from Thorlabs (Newton, New Jersey).

2.2.3 Integrating Sphere

The size of the integrating sphere is dictated by its use to measure light reflectance from human skin. As such, the integrating sphere should be relatively small (on the order of 5 to 10 cm in diameter) so that it can fit onto the various curves of the human body. A small sphere would also be easier to maneuver and keep stationary, resulting in more stable measurements.

The size of the measurement port of the sphere should be sufficiently large that local inhomogeneities in the measurement area (such as small freckles or hairs) do not overwhelm the result, but should result in the sphere's port fraction (the ratio of the total port area to the total internal surface area of the sphere) falling between 2% and 5%.[31] For the range of sphere sizes suggested above, the port diameter would fall somewhere within 1.5 to 5 cm.

The sphere should also have a high internal reflectance (greater than 94%) and produce a uniform light field at the measurement port.[32–34] If the input light is directly incident on the detection port, the sphere should include a baffle, blocking this path. For spheres of the size used in this experiment, baffles should be avoided when possible as they disrupt the internal surface of the sphere, reducing the uniformity of the illumination within the sphere.

The integrating sphere was made from a cube of Spectralon®(Labsphere®, North Sutton, New Hampshire) with side lengths of 2 in. (50.8 mm). The cube was bisected and a hemispherical cavity was machined into both halves using a 1¼ in. (31.75 mm)

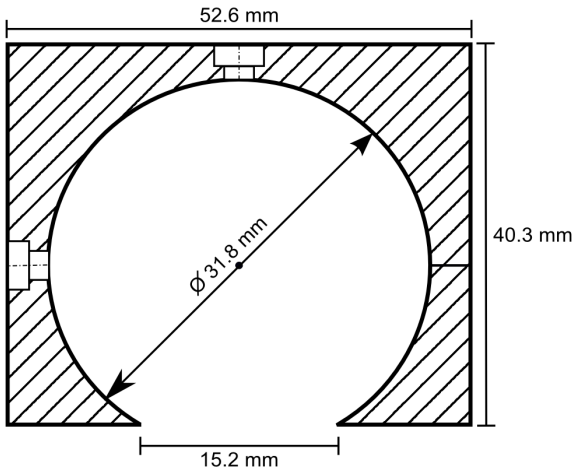

Figure 2.2: A cross-sectional diagram of the integrating sphere. The block of Spectralon® used to make the sphere is bisected before processing and then reattached to form the sphere.

ball-end mill. The bottom of one of these halves was milled down, creating a port measuring 15.2 mm in diameter. The parts were assembled to form the sphere and holes were drilled through the center of the unmilled half as well as through one side at the junction to accommodate SMA 905 connectors which would become the detection and illumination ports, respectively (see Figure 2.2).

2.2.4 Implementation Costs

The specifications for each individual component have some flexibility; therefore, a DRS system can be built within a wide range of costs while still achieving the same measurement results.

In choosing the light source, it is only important that it covers the desired wavelength range and be stable to within 1%. Although a uniform spectral output is ideal to keep the signal uncertainty relatively constant, it is not necessary. A quartz tungsten halogen lamp provides smooth spectral features and high output powers; however, a less expensive alternative would be a white LED. These provide excellent illumination and are relatively stable, although they do have an emission peak in the blue region (~465 nm).

Integrating spheres can be purchased from an optical device supplier; however, spheres can be built for costs as low as $100 US by obtaining a suitable block of Spectralon. Since the sphere is not being used for radiometric purposes, it can deviate

from an ideal integrating sphere and still provide an accurate reflectance measurement. Spheres can also be constructed by vacuum-forming plastic styrene about a spherical mold and coating the inside with barium sulfate paint.[35]

The most expensive component is the spectrometer, and its price will depend on the detection sensitivity and grating size. The average cost for a common fiber-based spectrometer is around $2000 US. Although not recommended, spectrometers can also be built cheaply if necessary.[36]

The computer must be able to interface with the spectrometer and run the necessary software. Therefore, an inexpensive netbook or laptop will be sufficient. Optical fibers are uniformly priced in the market and will contribute very little to the total cost of the system.

A list of itemized expenses is shown in Table 2.1, assuming new materials were required. For comparison, a hand-held colorimeter is available for $6000 US from Derma Spectrometer (MIC Global, London, United Kingdom).

Table 2.1: Cost estimates for the DRS system. Listed prices are based on the purchase of new material.

Component	Pricing (USD)	
	Low	High
Light source	$100	$500
Integrating sphere	$100	$1500
Spectrometer	$500	$3000
Computer	$250	$500
Connection cables	$100	$200
Total	**$1050**	**$5700**

2.3 Procedure and Performance

2.3.1 Integrating Sphere Configuration

The optical fibers are connected to the integrating sphere following a d/0°(diffuse illumination/direct detection) geometry such that the input light is first incident on the sphere wall before encountering the tissue surface and the output fiber is directly across from the measurement port (as shown in Figure 2.1. In this geometry, the

sample is more uniformly illuminated compared with a 0°/d geometry due to the multiple reflections of the light prior to exiting the sphere at the tissue. In addition, since the illumination is diffuse rather than normally incident, the penetration of light is more superficial due to the oblique entrance angle (average 55°). Thus, a greater percentage of spectroscopic information originates from the upper layers of skin where the chromophores of interest are located. Due to the small size of this integrating sphere, a baffle was not used. The geometry and the detector fiber acceptance angle (0.22 NA) allowed only light that was specularly or diffusely reflected from the tissue surface to be collected.

2.3.2 Calculating Spectral Reflectance

The spectral reflectance of a tissue sample was normalized by dividing the spectral count rate with the detection port on the tissue, $S_t(\lambda)$, by the spectral count rate from a highly reflecting standard, $S_{norm}(\lambda)$. Both of these were adjusted by subtracting the background signal rate, $S_{bg}(\lambda)$, so that the modified total diffuse reflectance, $R_m^*(\lambda)$, is given by

$$R_m^*(\lambda) = \frac{S_t(\lambda) - S_{bg}(\lambda)}{S_{norm}(\lambda) - S_{bg}(\lambda)}. \tag{2.1}$$

Normalizing to a reflectance standard eliminates the need to correct the measured signal rate for the system spectral response.

A 99% reflectance standard (SRS-99-010, Labsphere, North Sutton, New Hampshire) was used as the normalization standard while a 2% reflectance standard (SRS-02-010, Labsphere, North Sutton, New Hampshire) was used for the background. The 2% standard was used instead of directing the detection port into a dark room in order to avoid changes in ambient lighting conditions, should the system be used in different locations which would affect the calculated reflectance. This substitution did not affect the accuracy or precision of the measurement. If reflectance standards are not available, a piece of thick, matte black cloth may be substituted for the 2% standard, and a piece of high diffusely reflective material such as a piece of Spectralon or a flat surface coated with barium sulfate may be substituted.

For each spectral count rate measurement, the integration time was set such that the maximum intensity was approximately 90% of the dynamic range. This allowed for optimal precision while ensuring that the signal would not saturate. Five measurements

were averaged to further reduce the noise. The averaged measurements were converted into a count rate by dividing by the integration times.

2.3.3 Sphere Preparation

The measurement port of the integrating sphere was covered with a sheet of occlusive dressing (Tegaderm™film, 3M Health Care, St. Paul, Minnesota) in order to prevent dirt and other material from contaminating the inside of the sphere. A new sheet was applied for each patient before any measurements to ensure sterility. The dressing was left on for the normalization and background measurements and, therefore, did not modify the resulting reflectance. Reflectance measurements were performed on calibrated diffuse reflectance standards ranging from 2% to 99% (RSS-08-010, Labsphere, North Sutton, New Hampshire) with the dressing in place and removed. Both sets of measurements showed no measurable difference.

2.3.4 Correcting for Single Beam Substitution Error

Single beam integrating spheres used for reflectance spectroscopy suffer from single beam substitution error[37, 38] due to the decrease of the total flux within the sphere when the normalization plate is replaced with the sample. This can be corrected using Equation 2.2. The parameters (a, b, c), as a function of wavelength, were determined empirically by measuring the calibrated reflectance standards described in the previous section and developing a relationship between the measured and calibrated reflectances (represented by R_m^* and R_m, respectively), based on the fraction of reflected light. If reflectance standards are not available, Intralipid™(Baxter, Deerfield, Illinois) and India ink liquid phantoms can be used as they have well-characterized extinction coefficients.[39, 40]

$$R_m = \frac{aR_m^* + b}{R_m^* + c} \tag{2.2}$$

These data were fit using a nonlinear least-squares algorithm at each of the wavelengths. A typical fit for a single wavelength is shown in Figure 2.3. This correction was applied to the modified total diffuse reflectance, resulting in a corrected total diffuse reflectance (R_m). A set of colored diffuse reflectance standards (CSS-04-010, Labsphere, North Sutton, New Hampshire) were measured and, following correction,

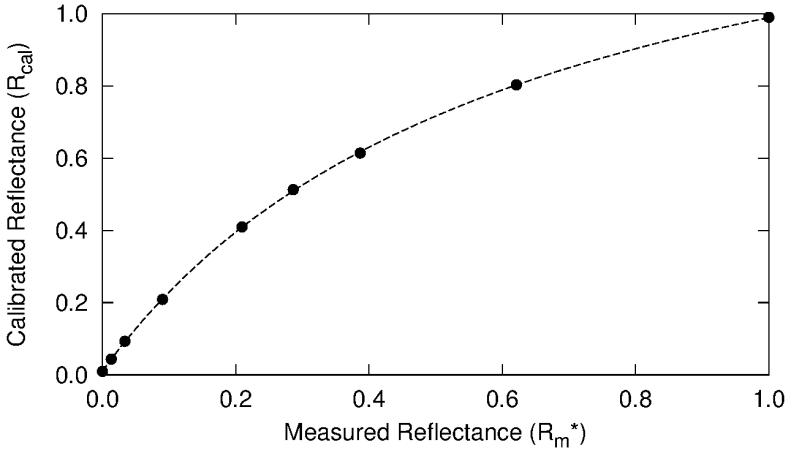

Figure 2.3: The integrating sphere calibration curve at 600 nm. The fitted function corrects the measured reflectance for single-beam substitution error. The dots are the calibrated and measured reflectance pairs and the dashed line is the fit to these data.

the measured reflectance was within 0.01 of the calibrated reflectance specified by the supplier (Figure 2.4).

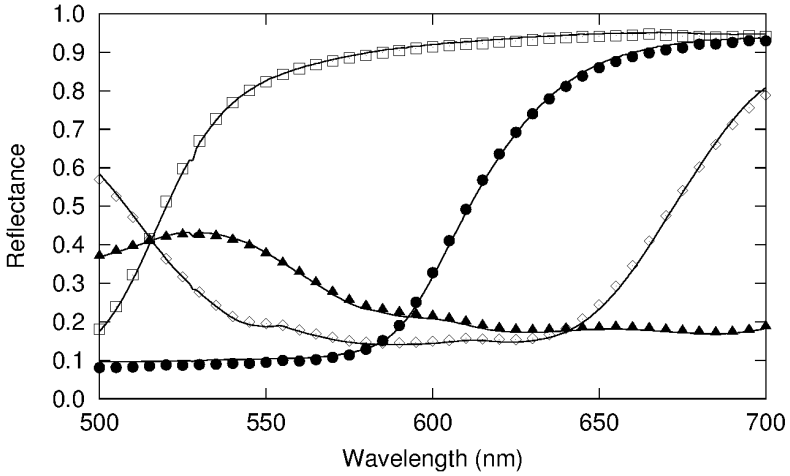

Figure 2.4: The measured (symbols) and calibrated (lines) reflectance spectra for a set of four colored diffuse reflectance standards: red (●), yellow (□), green (▲), and blue (◇). Correction for the single-beam substitution error brought the measured reflectance values to within 0.01 of the calibrated reflectance specified by the supplier.

2.3.5 Reflectance Measurement Reproducibility

The reproducibility of the system was tested using the green reflectance standard (SCS-GN-010) because it had reflectance similar to human skin and spectral features in the same region as hemoglobin. Reflectance was measured every day for 30 days and the standard deviation across the 500 to 700 nm spectral region never exceeded 1%. As expected, it varied with the spectral reflectance of the reflectance standard (i.e., the uncertainty was lower when the reflectance/signal was higher). Reproducibility measurements were also performed on human skin and they had a similar result.

2.4 Experimental Validation

2.4.1 Study Overviews

In order to demonstrate the use and validity of the DRS system, sample data from two ongoing erythema studies are presented. In the first study, erythema and skin blanching were induced via subcutaneous injection of lidocaine (a vasodilator and anesthetic) with or without epinephrine (a vasoconstrictor) over the deltoid muscles of volunteers' upper arms. The aim of this study was to determine the time to maximal

effect of injected epinephrine. In the second study, serial skin reflectance measurements were taken on head and neck cancer patients undergoing intensity-modulated radiation therapy (IMRT). The goal of this study was earlier detection of radiation-induced erythema compared with visual assessment methods. Both studies received Hamilton Health Sciences Research Ethics approval.

2.4.2 Erythema Index Analysis

The measured reflectance spectra were processed using the Dawson erythema index (EI).[41] This model was chosen because of its wide acceptance and use (over 280 citations to date),[42] as well as its straight-forward calculation method. Briefly, the EI is the area under the curve of the log of the inverse reflectance spectrum between 510 and 610 nm (encompassing the absorption features of oxy- and deoxy-hemoglobin). The influence of melanin in the EI can be approximately corrected using reflectance data between 650 and 700 nm (EI). For serial measurements on an individual, a relative erythema index (EI_r) can also be calculated. Simply, a baseline EI_c is obtained either at time zero or at a nearby reference location. This is subtracted from EI_c values measured at later time points such that, in the absence of changes in hemoglobin, EI_r would be zero.

The 10 nm FWHM spectral resolution of the system has the effect of broadening spectral features in the measured reflectance. Although this would be problematic for narrow features, the absorption features in the hemoglobin spectra are very broad and were not strongly affected. To verify the effect on the EI, spectra derived from the literature[43] were convolved with a 10 nm FWHM Gaussian function and the EI calculated before and after. Small differences in the calculated EI were noted (data not shown), however changes in EI with respect to an increase or decrease in hemoglobin were insensitive to the spectrometer's spectral resolution.

2.4.3 Study Results

In the first study, the reflectance was measured serially for 2 h following the injection of lidocaine (with or without epinephrine) and the measurements were processed to calculate the EI_r as a function of time. A time course for one volunteer is shown in Figure 2.5 along with the reflectance spectra at specific time points. For both injections, there was a rapid increase in the EI_r indicating an increase in the hemoglobin content.

The combined lidocaine and epinephrine injection then decreased to a minimum EI_r of approximately -16 at the 22 min mark indicating a reduction in hemoglobin content. An analysis of the EI_r for all subjects indicated that the maximum epinephrine-induced blanching occurred approximately 25 min following injection, after which surgical incision may commence.[44]

In the second study, the reflectance was measured daily over the course of the patients' head and neck IMRT treatments. During this study, it was necessary to have multiple investigators operate the DRS system. This requirement illustrated the ease of training associated with the system, as all investigators were capable of properly using the system following a short 15 min tutorial. Greater variation was observed in the daily measurements compared with the short-term measurements of the first study (see Figure 2.6). The EI_r was not calculated because the baseline consisted of a single measurement. The variation is the result of daily changes such as time of day and patient temperature.[45] An increase in EI_c was observed over the course of the 35 days. Erythema was first visually diagnosed on day 18 of treatment. This study is ongoing.

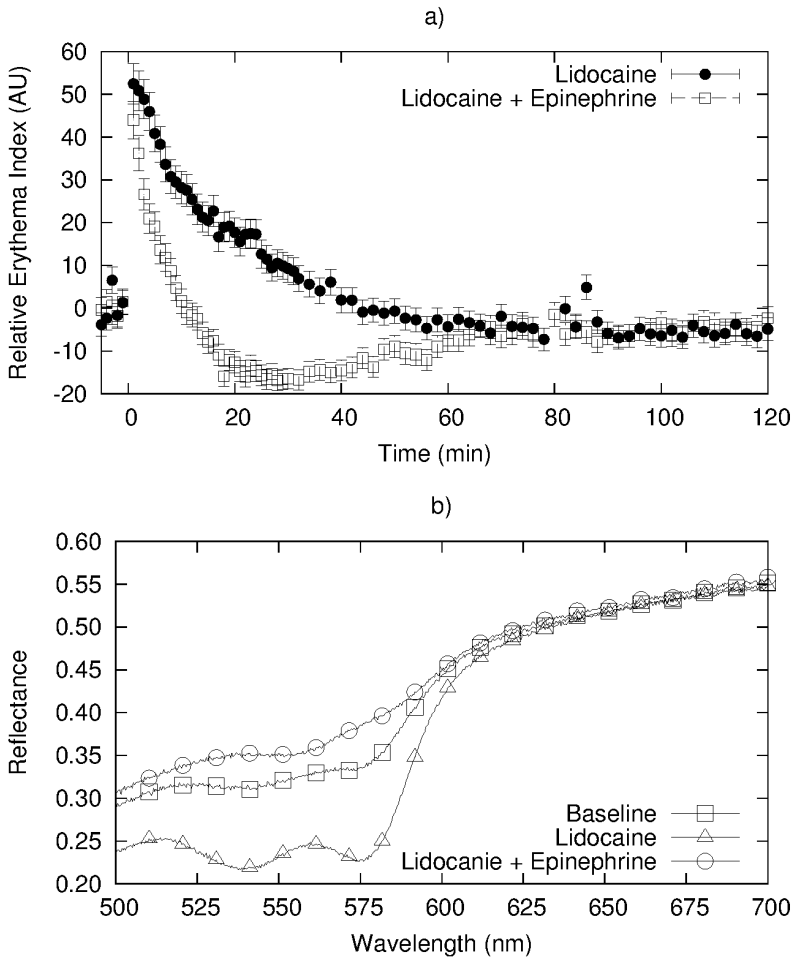

Figure 2.5: (a) A sample time course for one volunteer in the study involving lidocaine and epinephrine. (b) Full reflectance spectra from before injection (□), 1 min following the injection of lidocaine alone (△), and 26 min following the injection of lidocaine and epinephrine (◯).

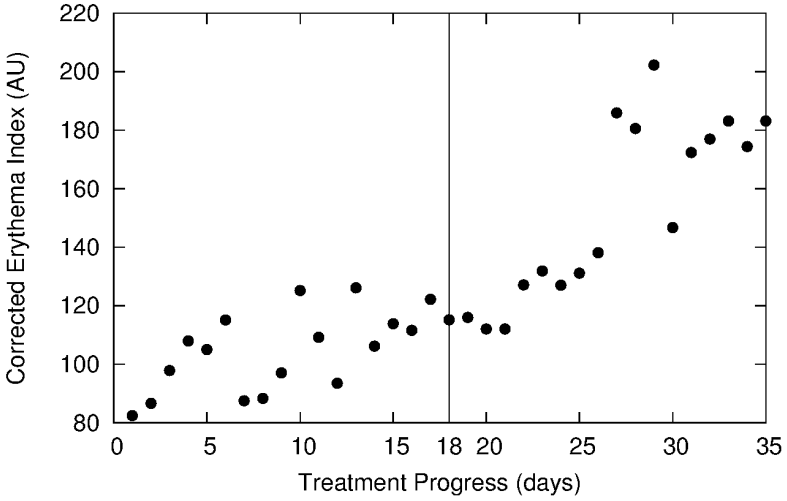

Figure 2.6: Corrected erythema index for a head and neck IMRT cancer patient. Daily measurements were taken over the course of treatment. Erythema was not visually noted until day 18.

2.5 Discussion

This paper illustrates two clinical applications of a DRS system. These results demonstrate that a low-cost spectroscopy system is capable of measuring spectral changes in reflectance due to changes in the concentration of hemoglobin. These changes were quantified using the Dawson EI. The system is easy to operate and yields valuable clinical data with little training required. The system described here may be found to have a wide range of clinical assessment roles, which would make it an even more useful tool for health care practitioners. However, since the system collects a full spectrum, it is capable of generating much more valuable information than just a single EI value. For example, correcting for background chromophores is only approximate and any changes over the measurement period could register as incorrect increases or decreases in skin redness. An alternative modeling approach using a spectrally constrained diffuse reflectance model to fit the measured reflectance spectrum with concentrations of the major tissue chromophores may be advantageous. This will allow for the detection of skin color changes in reference to their responsible chromophore, but would require the measured spectrum to be extremely accurate and precise.

One of the limitations of this spectroscopy system is that the signal is normalized using a highly scattering Spectralon® standard. In comparison, human skin is much

less scattering and therefore the true reflectance is under-represented due to scattering losses. These scattering losses are not large but, since they vary with the tissue optical properties, they would need to be accounted for in a spectrally dependent model.

This paper presents a low-cost, user-friendly DRS system for measurement of changes in skin hemoglobin concentration. The performance of the system was characterized in terms of wavelength accuracy and measurement stability, uncertainty, and reproducibility. The validity and utility of the system were demonstrated through a skin reddening/blanching experiment and a radiation-induced erythema study, followed by analysis with a simple erythema model. Further uses of the system have yet to be investigated.

Acknowledgments

The authors would like to thank Kevin R. Diamond and Gabriel A. Devenyi for their assistance in the preparation of this paper. This work was financially supported by the Natural Sciences and Engineering Research Council of Canada.

References

[1] Diana F Moscu. "Quantifying chromophore concentration in tissue simulating phantoms using an optical detection system based on an integrating sphere". Ph.D. McMaster University, 2010, p. 153. URL: http://library.mcmaster.ca/catalogue/Record/1932096 (cit. on p. 32).

[2] Dmitry Yudovsky and Laurent Pilon. "Rapid and accurate estimation of blood saturation, melanin content, and epidermis thickness from spectral diffuse reflectance." In: *Applied optics* 49.10 (2010-04), pp. 1707–19. ISSN: 1539-4522. URL: http://www.ncbi.nlm.nih.gov/pubmed/20357850 (cit. on p. 32).

[3] Dmitry Yudovsky and Laurent Pilon. "Retrieving skin properties from in vivo spectral reflectance measurements." In: *Journal of biophotonics* 4.5 (2011-05), pp. 305–14. ISSN: 1864-0648. DOI: 10.1002/jbio.201000069. URL: http://www.ncbi.nlm.nih.gov/pubmed/20680977 (cit. on p. 32).

[4] J W Hopewell. "The skin: its structure and response to ionizing radiation*". In: *International Journal of Radiation Biology* 57.4 (1990), pp. 751–773 (cit. on p. 34).

[5] N S Russell, H Knaken, I A Bruinvis, A A Hart, A C Begg, and J V Lebesque. "Quantification of patient to patient variation of skin erythema developing as a response to radiotherapy." In: *Radiotherapy and Oncology* 30.3 (1994-03), pp. 213–21. ISSN: 0167-8140. URL: http://www.ncbi.nlm.nih.gov/pubmed/8209004 (cit. on p. 34).

[6] Josefina Nyström, Paul Geladi, Britta Lindholm-Sethson, Jenny Rattfelt, Ann Christin Svensk, and Lars Franzen. "Objective measurements of radiotherapy-induced erythema." In: *Skin Research and Technology* 10.4 (2004-11), pp. 242–50. ISSN: 0909-752X. URL: http://www.ncbi.nlm.nih.gov/pubmed/15536655 (cit. on p. 34).

[7] T J Fitzgerald, Maryann Bishop Jodoin, Gayle Tillman, Jesse Aronowitz, Richard Pieters, Susan Balducci, Joshua Meyer, M Giulia Cicchetti, Sidney Kadish, Shelagh McCauley, Joanna Sawicka, Marcia Urie, Y C Lo, Charles Mayo, Kenneth Ulin, Linda Ding, Maureen Britton, Jiayi Huang, and Edward Arous. "Radiation therapy toxicity to the skin." In: *Dermatologic Clinics* 26.1 (2008-01),

pp. 161–72. ISSN: 0733-8635. DOI: 10.1016/j.det.2007.08.005. URL: http://www.ncbi.nlm.nih.gov/pubmed/18023776 (cit. on p. 34).

[8] Josephine H Woodhams, Alexander J MacRobert, and Stephen G Bown. "The role of oxygen monitoring during photodynamic therapy and its potential for treatment dosimetry". In: *Photochemical & Photobiological Sciences* 6.12 (2007-12), pp. 1246–1256. ISSN: 1474-905X. DOI: 10.1039/b705461k. URL: http://www.ncbi.nlm.nih.gov/pubmed/18046478 (cit. on p. 34).

[9] Michael S Patterson, Ephraim Schwartz, and Brian C Wilson. "Quantitative reflectance spectrophotometry for the noninvasive measurement of photosensitizer concentraion in tissue during photodynamic therapy". In: *SPIE Vol. 1065 Photodynamic Therapy: Mechanisms*. Vol. 1065. 1989, pp. 115–122 (cit. on p. 34).

[10] Brian C Wilson and Michael S Patterson. "The physics, biophysics and technology of photodynamic therapy." In: *Physics in Medicine and Biology* 53.9 (2008-05), R61–109. ISSN: 0031-9155. DOI: 10.1088/0031-9155/53/9/R01. URL: http://www.ncbi.nlm.nih.gov/pubmed/18401068 (cit. on p. 34).

[11] Matthew H Steele. "Three-year experience using near infrared spectroscopy tissue oximetry monitoring of free tissue transfers." In: *Annals of Plastic Surgery* 66.5 (2011-05), pp. 540–5. ISSN: 1536-3708. DOI: 10.1097/SAP.0b013e31820909f9. URL: http://www.ncbi.nlm.nih.gov/pubmed/21301288 (cit. on p. 34).

[12] Pierre Agache. "Assessment of Erythema and Pallor". In: *Measuring the skin*. Ed. by Pierre Agache and Philippe Humbert. 1st. New York: Springer-Verlag, 2004. Chap. 58, pp. 591–601. ISBN: 978-3-540-01771-4 (cit. on p. 34).

[13] Andy Trotti, A.Dimitrios Colevas, Ann Setser, Valerie Rusch, David Jaques, Volker Budach, Corey Langer, Barbara Murphy, Richard Cumberlin, C.Norman Coleman, and Philip Rubin. "CTCAE v3.0: development of a comprehensive grading system for the adverse effects of cancer treatment". In: *Seminars in Radiation Oncology* 13.3 (2003), pp. 176–181. URL: http://www.sciencedirect.com/science/article/pii/S1053429603000316 (cit. on p. 34).

[14] Mette Bodekaer, Peter Alshede Philipsen, Tonny Karlsmark, and Hans Christian Wulf. "Good agreement between minimal erythema dose test reactions and objective measurements: an in vivo study of human skin." In: *Photodermatology,*

Photoimmunology & Photomedicine 29.4 (2013-08), pp. 190–5. ISSN: 1600-0781. DOI: 10.1111/phpp.12049. URL: http://www.ncbi.nlm.nih.gov/pubmed/23815351 (cit. on p. 34).

[15] David Basketter, Fiona Reynolds, Matt Rowson, Claire Talbot, and Ed Whittle. "Visual assessment of human skin irritation: a sensitive and reproducible tool". In: *Contact Dermititis* 37.5 (1997), pp. 218–220. URL: http://onlinelibrary.wiley.com/doi/10.1111/j.1600-0536.1997.tb02438.x/abstract (cit. on p. 34).

[16] Yvonne Wengström, Christina Forsberg, Ingemar Näslund, and Jonas Bergh. "Quantitative assessment of skin erythema due to radiotherapy—evaluation of different measurements". In: *Radiotherapy and Oncology* 72.2 (2004-08), pp. 191–197. ISSN: 01678140. DOI: 10.1016/j.radonc.2004.04.011. URL: http://linkinghub.elsevier.com/retrieve/pii/S0167814004003032 (cit. on p. 34).

[17] CIE. *Colorimetry - Part 3: CIE Tristimulus Values. CIE S 014-3/E:2011 (ISO 11664-3:2012)*. Tech. rep. International Commission on Illumination, 2012, p. 14. URL: http://www.techstreet.com/cie/products/1844374 (cit. on p. 34).

[18] Byungjo Jung, Soobyeong Kim, Yunjin Bae, Heesung Kang, Yongheum Lee, and J Stuart Nelson. "Real-time measurement of skin erythema variation by negative compression: pilot study." In: *Journal of Biomedical Optics* 17.8 (2012-08), pp. 081422–1. ISSN: 1560-2281. DOI: 10.1117/1.JBO.17.8.081422. URL: http://www.ncbi.nlm.nih.gov/pubmed/23224183 (cit. on p. 34).

[19] Nikiforos Kollias and Georgios N Stamatas. "Optical non-invasive approaches to diagnosis of skin diseases." In: *The Journal of Investigative Dermatology* 7.1 (2002-12), pp. 64–75. ISSN: 1087-0024. DOI: 10.1046/j.1523-1747.2002.19635.x. URL: http://www.ncbi.nlm.nih.gov/pubmed/12518795 (cit. on p. 34).

[20] Jennifer Canning, Brian Barford, David Sullivan, Randy Wickett, and Marty Visscher. "Use of digital photography and image analysis techniques to quantify erythema in health care workers." In: *Skin Research and Technology* 15.1 (2009-02), pp. 24–34. ISSN: 1600-0846. DOI: 10.1111/j.1600-0846.2008.00333.x. URL: http://www.ncbi.nlm.nih.gov/pubmed/19152575 (cit. on p. 34).

[21] Izumi Nishidate, Noriyuki Tanaka, Tatsuya Kawase, Takaaki Maeda, Tomonori Yuasa, Yoshihisa Aizu, Tetsuya Yuasa, and Kyuichi Niizeki. "Noninvasive imaging of human skin hemodynamics using a digital red-green-blue camera". In: *Journal of Biomedical Optics* 16.8 (2011-08), p. 086012. ISSN: 1560-2281. DOI: 10.1117/1.3613929. URL: http://www.ncbi.nlm.nih.gov/pubmed/21895324 (cit. on p. 34).

[22] Michele Setaro and Adele Sparavigna. "Quantification of erythema using digital camera and computer-based colour image analysis: a multicentre study". In: *Skin Research and Technology* 8.2 (2002-05), pp. 84–8. ISSN: 0909-752X. URL: http://www.ncbi.nlm.nih.gov/pubmed/12060471%20http://onlinelibrary.wiley.com/doi/10.1034/j.1600-0846.2002.00328.x/full (cit. on p. 34).

[23] Rong Zhang, Wim Verkruysse, Bernard Choi, John a Viator, Byungjo Jung, Lars O Svaasand, Guillermo Aguilar, and J Stuart Nelson. "Determination of human skin optical properties from spectrophotometric measurements based on optimization by genetic algorithms." In: *Journal of Biomedical Optics* 10.2 (2005), p. 024030. ISSN: 1083-3668. DOI: 10.1117/1.1891147. URL: http://www.ncbi.nlm.nih.gov/pubmed/15910103 (cit. on p. 34).

[24] Georgios N Stamatas, Barbara Z Zmudzka, Nikiforos Kollias, and Janusz Z Beer. "In vivo measurement of skin erythema and pigmentation: new means of implementation of diffuse reflectance spectroscopy with a commercial instrument." In: *The British Journal of Dermatology* 159.3 (2008-09), pp. 683–90. ISSN: 1365-2133. DOI: 10.1111/j.1365-2133.2008.08642.x. URL: http://www.ncbi.nlm.nih.gov/pubmed/18510669 (cit. on p. 34).

[25] Nikiforos Kollias, InSeok Seo, and Paulo R Bargo. "Interpreting diffuse reflectance for in vivo skin reactions in terms of chromophores." In: *Journal of Biophotonics* 3.1-2 (2010-01), pp. 15–24. ISSN: 1864-0648. DOI: 10.1002/jbio.200900066. URL: http://www.ncbi.nlm.nih.gov/pubmed/19946873 (cit. on p. 34).

[26] Dmitry Yudovsky, Aksone Nouvong, and Laurent Pilon. "Hyperspectral imaging in diabetic foot wound care." In: *Journal of Diabetes Science and Technology* 4.5 (2010-09), pp. 1099–113. ISSN: 1932-2968. URL: http://www.pubmedcentral.nih.gov/articlerender.fcgi?artid=2956800%5C&tool=pmcentrez%5C&rendertype=abstract (cit. on p. 34).

[27] Michael S Chin, Brian B Freniere, Yuan-Chyuan Lo, Jonathan H Saleeby, Stephen P Baker, Heather M Strom, Ronald a Ignotz, Janice F Lalikos, and Thomas J Fitzgerald. "Hyperspectral imaging for early detection of oxygenation and perfusion changes in irradiated skin." In: *Journal of Biomedical Optics* 17.2 (2012-02), p. 026010. ISSN: 1560-2281. DOI: 10.1117/1.JBO.17.2.026010. URL: http://www.ncbi.nlm.nih.gov/pubmed/22463042 (cit. on p. 34).

[28] PM Fox, Kamakshi Zeidler, Joseph Carey, and GK Lee. "White light spectroscopy for free flap monitoring". In: *Microsurgery* 33.3 (2012), pp. 198–202. DOI: 10.1002/micr. URL: http://onlinelibrary.wiley.com/doi/10.1002/micr.22069/full (cit. on p. 35).

[29] Anthony R Young. "Chromophores in human skin." In: *Physics in Medicine and Biology* 42.5 (1997-05), pp. 789–802. ISSN: 0031-9155. URL: http://www.ncbi.nlm.nih.gov/pubmed/9172259 (cit. on p. 36).

[30] Tom Lister, Philip A Wright, and Paul H Chappell. "Optical properties of human skin". In: *Journal of Biomedical Optics* 17.9 (2012), p. 090901. DOI: 10.1117/1.JBO.17.9.090901 (cit. on p. 36).

[31] Leonard M Hanssen and Keith A Snail. "Integrating Spheres for Mid- and Near-infrared Reflection Spectroscopy". In: *Handbook of Vibrational Spectroscopy*. Ed. by John M Chalmers and Peter R Griffiths. Wiley & Sons, 2002. URL: http://www.nist.gov/calibrations/upload/HndBkSphere.pdf (cit. on p. 37).

[32] Labsphere. *Technical Guide: Integrating Sphere Theory and Applications*. Tech. rep. North Sutton, NH: Labsphere, pp. 1–19. URL: http://www.labsphere.com/uploads/technical-guides/a-guide-to-integrating-sphere-theory-and-applications.pdf (cit. on p. 37).

[33] Labsphere. *Technical Guide: Integrating Sphere Radiometry and Photometry*. North Sutton, NH. URL: http://www.labsphere.com/uploads/technical-guides/a-guide-to-integrating-sphere-radiometry-and-photometry.pdf (cit. on p. 37).

[34] Labsphere. *Technical Guide: Reflectance Spectroscopy*. Tech. rep. North Sutton, NH: Labsphere, pp. 1–40. URL: http://www.labsphere.com/uploads/

technical-guides/A%20Guide%20to%20Reflectance%20Spectroscopy.pdf (cit. on p. 37).

[35] Diana L Glennie. "Use of integrating spheres for improved skin PDT treatment". Masters of Science. McMaster University, 2009, pp. 1–96 (cit. on p. 39).

[36] Sarun Sumriddetchkajorn and Yuttana Intaravanne. "Home-made N-channel fiber-optic spectrometer from a web camera." In: *Applied spectroscopy* 66.10 (2012-10), pp. 1156–62. ISSN: 1943-3530. DOI: 10.1366/11-06522. URL: http://www.ncbi.nlm.nih.gov/pubmed/23031698 (cit. on p. 39).

[37] Art W Springsteen. "Reflectance Spectroscopy: An Overview of Classification and Techniques". In: *Applied Spectroscopy: A Compact Reference for Practitioners*. Ed. by Jerry Workman and Art W Springsteen. 1st. New York: Academic Press, 1998. Chap. 6, pp. 193–224 (cit. on p. 41).

[38] Labsphere. *Application Note No. 01: Quantitation of Single Beam Substitution Correction in Reflectance Spectroscopy Accessories*. Tech. rep. 01. North Sutton, NH: Labsphere. URL: http://www.labsphere.com/uploads/technical-guides/Quantitation%20of%20Single%20Beam%20Substitution%20Correction.pdf (cit. on p. 41).

[39] S T Flock, S L Jacques, B C Wilson, W M Star, and M J van Gemert. "Optical properties of Intralipid: a phantom medium for light propagation studies." In: *Lasers in surgery and medicine* 12.5 (1992-01), pp. 510–9. ISSN: 0196-8092. URL: http://www.ncbi.nlm.nih.gov/pubmed/1406004 (cit. on p. 41).

[40] S J Madsen, M S Patterson, and B C Wilson. "The use of India ink as an optical absorber in tissue-simulating phantoms." In: *Physics in medicine and biology* 37.4 (1992-05), pp. 985–93. ISSN: 0031-9155. URL: http://www.ncbi.nlm.nih.gov/pubmed/1589459 (cit. on p. 41).

[41] J B Dawson, D J Barker, D J Ellis, E Grassam, J A Cotterill, G W Fisher, and J W Feather. "A theoretical and experimental study of light absorption and scattering by in vivo skin". In: *Physics in Medicine and Biology* 25.4 (1980-07), pp. 695–709. ISSN: 0031-9155. DOI: 10.1088/0031-9155/25/4/008. URL: http://www.ncbi.nlm.nih.gov/pubmed/7454759%20http://stacks.iop.org/0031-9155/25/i=4/a=008?key=crossref.3a9c201eba5c1754a3a8963193b6ce29 (cit. on p. 44).

[42] B Riordan, S Sprigle, and M Linden. "Testing the validity of erythema detection algorithms." In: *Journal of Rehabilitation Research and Development* 38.1 (2001), pp. 13–22. ISSN: 0748-7711. URL: http://www.ncbi.nlm.nih.gov/pubmed/11322466 (cit. on p. 44).

[43] Steven L Jacques. *Skin Optics Summary*. 1998. URL: http://omlc.ogi.edu/news/jan98/skinoptics.html (cit. on p. 44).

[44] Daniel E McKee, Donald H Lalonde, Achilleas Thoma, Diana L Glennie, and Joseph E Hayward. "Optimal time delay between epinephrine injection and incision to minimize bleeding." In: *Plastic and Reconstructive Surgery* 131.4 (2013-04), pp. 811–4. ISSN: 1529-4242. DOI: 10.1097/PRS.0b013e3182818ced. URL: http://www.ncbi.nlm.nih.gov/pubmed/23249984 (cit. on p. 45).

[45] A Fullerton, T Fischer, A Lahti, and KP Wilhelm. "Guidelines for measurement skin colour and erythema: A report from the Standardization Group of the European Society of Contact Dermatitis*". In: *Dermatitis* 35 (1996), pp. 1–10. URL: http://onlinelibrary.wiley.com/doi/10.1111/j.1600-0536.1996.tb02258.x/abstract (cit. on p. 45).

Chapter 3

Paper II - Application of system in plastic surgery

Preamble

Paper II employs the system developed in Chapter 2 to determine the time to maximum vasoconstriction of subcutaneously injected epinephrine. Previous work was performed with porcine models using laser Doppler flowmetry and estimated the time interval to be 7 to 10 minutes in length.[1] This work was performed in 1987 and there had been no further investigation to confirm this result prior to this work. In this paper, lidocaine was injected into volunteers upper arms with and without epinephrine to induce reddening or blanching respectively, and DRS measurements were performed every 1 to 2 minutes over the course of 2 hours. Since work was still being performed on a spectrally-constrained model (see Chapter 4), the measurements were analyzed with the commonly cited Dawson erythema index.[2]

The protocol used during this investigation was developed primarily by the author of this thesis (further known as "the author") with contributions by Dr. D. McKee (the first author of the paper). In addition, the majority of the material required for the Research Ethics Board application was prepared by the author. Injection of the lidocaine (and epinephrine) was performed by Dr. McKee while all subsequent measurements were performed by the author with assistance from Dr. McKee. The program for converting the measurements into corrected Dawson erythema indices was written and executed by the author while the error analysis and the interpretation of the time course results were undertaken by Dr. McKee. The manuscript was prepared primarily by Dr. McKee under the supervision of Drs. D. Lalonde and A. Thoma. The author and Dr. J. Hayward did not contribute major changes to the manuscript. The manuscript has been altered from its original form to match the style of this thesis.

Contents

Optimal Time Delay between Epinephrine Injection and Incision to Minimize Bleeding

Daniel E. McKee, Donald H. Lalonde, Achilleas Thoma, Diana L. Glennie, and Joseph E. Hayward

Division of Plastic and Reconstructive Surgery, Department of Surgery, and the Department of Medical Physics and Applied Radiation Sciences, McMaster University,

1280 Main Street West, Hamilton, Ontario, L8S 1A8
AND
Saint John Regional Hospital, Dalhousie University

Journal of Plastic and Reconstructive Surgery **131**(4), 811-814 (April 2013).
http://dx.doi.org/10.1097/PRS.0b013e3182818ced

Abstract

Background: The time until maximal cutaneous vasoconstriction after injection of lidocaine with epinephrine is often given in textbooks and multiple choice examinations as 7 to 10 minutes. However, in our experience, there is significantly less cutaneous bleeding if one waits considerably longer than 7 to 10 minutes after injection of local anesthesia with epinephrine for most procedures on human skin.
Methods: This was a prospective, randomized, triple-blind study where 12 volunteers were injected simultaneously in each arm with either 1% lidocaine with epinephrine (study group) or 1% plain lidocaine (control group), after which the relative hemoglobin concentration of the underlying skin and soft tissues was measured over time using spectroscopy.
Results: In the epinephrine group, the mean time at which the lowest cutaneous hemoglobin level was obtained was 25.9 minutes (95 percent CI, 25.9 $\pm$ 5.1 minutes). This was significantly longer than the historical literature values of 7 to 10 minutes for maximum vasoconstriction after injection. Mean hemoglobin index values at every time measurement after postinjection minute 1 were significantly different between the study group and the control group, with use of a two-tailed paired t test ($p < 0.01$).
Conclusions: If optimal visualization is desired, the ideal time for the surgeon to begin the incision should be 25 minutes after injection of local anesthetic with epinephrine. It takes considerably longer than 7 to 10 minutes for a new local equilibrium to be obtained in relation to hemoglobin quantity.
CLINICAL QUESTION/LEVEL OF EVIDENCE: Therapeutic, I.
©2013 American Society of Plastic Surgeons

3.1 Introduction

Epinephrine is routinely used with local anesthetic in surgical procedures to provide hemostasis, where visualization of underlying intricate anatomy is important. The time until maximal cutaneous vasoconstriction after injection of lidocaine with epinephrine is often listed in textbooks[3, 4] and multiple-choice examinations as 7 to 10 minutes. This value originated from a 1987 study using a laser Doppler flowmeter on pig skin after injection of 1% lidocaine with epinephrine at several concentrations, including 1:100,000.[1] In our clinical experience, there is significantly less cutaneous bleeding if one waits considerably longer than 7 to 10 minutes after injection of local anesthesia with epinephrine for most procedures on human skin.

The purpose of this study was to see how long it really takes to obtain the lowest cutaneous hemoglobin concentration after lidocaine with epinephrine injection in the human arm. In this prospective, randomized, triple-blind study, volunteers were injected simultaneously in each arm with either 1% lidocaine (plain) or 1% lidocaine with epinephrine. The underlying skin and soft-tissue perfusion changes were monitored with diffuse reflectance spectroscopy to estimate relative hemoglobin concentration changes over time. The time until the lowest concentration of hemoglobin was obtained for each volunteer injected with lidocaine with epinephrine.

3.2 Patients and Methods

This study was given final full approval on December 8, 2011, from the Research Ethics Board affiliated with Hamilton Health Sciences and McMaster University (project no. 11-543) and all volunteers gave informed written consent. Between March and May of 2012, 12 volunteer university students with ages ranging from 21 to 31 years, and a male-to-female ratio of 50:50, received two injections within 1 minute of each other just under the dermis on the lateral arm over the deltoid insertion. One person was responsible for injecting all volunteers: 5 cc of 1% lidocaine with 1:100,000 epinephrine (0.01 mg/ml) in one arm and 5 cc of 1% lidocaine (plain) in the other arm (AstraZeneca Canada, Inc., Mississauga, Ontario, Canada). By opaque envelope, volunteers were assigned randomly with details of arm allocation so that they had a 50:50 chance of receiving the epinephrine injection in either their left or right arm. The study was triple-blinded: neither the volunteer, the person injecting the local anesthetic, nor

the spectroscopy technician knew which arm was injected with which solution. With regard to volunteer skin type, 11 volunteers were white and one was of eastern Asian heritage.

Spectroscopy measurements were taken every minute from each arm for 5 minutes before injections and for 30 minutes after injections. Subsequently, measurements were taken every 2 minutes until 100 minutes after injection. Reflectance measurements for this study were achieved by attaching an integrating sphere to a white light source and a spectrometer by means of fiberoptic cables. The incident light was provided by a 7-W tungsten-halogen white light source (360- to 2000-nm optical bandwidth) (HL-2000-FHSA; OceanOptics, Dunedin, Fla.). The diffuse reflectance from the skin was captured by a circular port opening that was 1.6 cm in diameter and was detected by a spectrometer (SD 2000; OceanOptics) with a usable wavelength range of 300 to 1000 nm. From each spectral measurement, a hemoglobin index (E) was calculated as follows[2]:

$$E = 100[r + 1.5(q + s) - 2(p + t)], \tag{3.1}$$

where p, q, r, s, and t are the logarithm of the inverse of reflectance at wavelengths 510, 542, 560, 576, and 610 nm, respectively. This index correlates with total hemoglobin concentration in vivo and corrects for the concentration of melanin in the skin. For each arm injected with epinephrine, the time until lowest hemoglobin concentration (most negative hemoglobin index) was obtained by averaging every three consecutive time points to reduce noise error.

3.2.1 Statistical Analysis

Two sample size calculations were performed using the parameters alpha error = 0.05 and beta error = 0.05 and using values obtained from a pilot study with eight experiments on volunteers. The first calculation used a difference of means of 29.3 (SD 8.0 and 20.2, respectively) for hemoglobin index measured by spectroscopy at 30 minutes after injection, between the lidocaine with epinephrine group and the plain lidocaine group. The second calculation compared the time until lowest hemoglobin concentration obtained in the pilot study (37.3 ± 27.4 minutes) to a literature value of 10 minutes. A sample size of 12 was determined for the study as the largest sample size resulting from the two calculations.

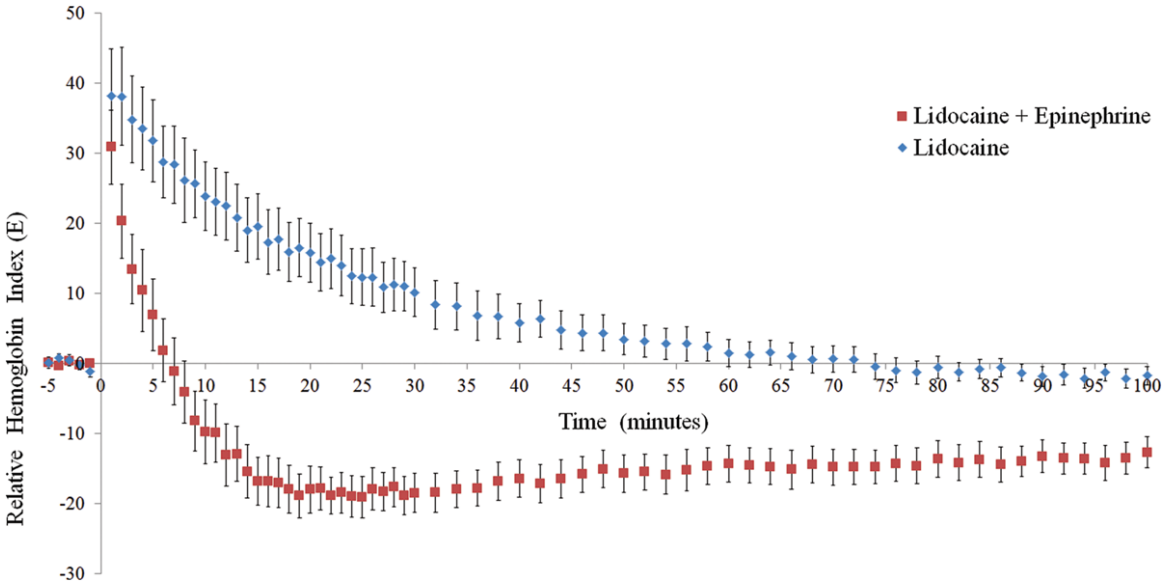

Figure 3.1: Mean relative hemoglobin index (unitless) (y axis) versus time (in minutes) (x axis). Time = 0 is the injection of plain lidocaine (blue) and lidocaine plus epinephrine (red). Time < 0 represents baseline measurements. Error bars = SEM. The lowest point on the lidocaine plus epinephrine curve was -19.1, occurring at 25 minutes.

3.3 Results

Mean relative hemoglobin index versus time was plotted for both groups (Figure 3.1). Mean relative hemoglobin index values at every time measurement after 1 minute after injection were significantly different between the lidocaine plus epinephrine group and the plain lidocaine group, using a two-tailed paired t test ($p < 0.01$). On the lidocaine plus epinephrine curve, the lowest mean relative hemoglobin index was obtained at 25 minutes. For every volunteer, the time until lowest hemoglobin concentration was obtained, and the average was 25.9 minutes (95 percent CI, 25.9 $\pm$ 5.1 minutes). This was found to be significantly different and longer than the commonly quoted historical literature value of 7 to 10 minutes, using a two-tailed one-sample t test ($p < 0.001$).

3.4 Discussion

This study revealed that the time when the lowest cutaneous hemoglobin concentration was obtained after injection of 1% lidocaine with 1:100,000 epinephrine in the human

arm was 25.9 minutes. This is considerably longer than the frequently quoted 7 to 10 minutes for maximal cutaneous vasoconstriction.[1]

Several studies have used laser Doppler flowmetry in humans to correlate epinephrine concentration with arterial blood flow.[5, 6] No studies to date have used tissue reflectance spectroscopy to characterize the actual quantity of blood in soft tissue injected with lidocaine with epinephrine over time. This technique provides a more direct estimate of potential intraoperative bleeding, as opposed to measuring arterial blood flow alone.

Hemoglobin has a distinct spectral response and well-described absorption properties. Tissue reflectance spectroscopy is a validated reproducible technique for measuring oxygenated and deoxygenated hemoglobin concentrations in soft tissue at a depth of up to 1 cm.[2, 7] A widely used application of tissue spectroscopy in medicine is pulse oximetry. A pulse oximeter is specifically calibrated to distinguish the concentration of oxygenated hemoglobin in an arterial pulse from the soft tissue's total background hemoglobin concentration. In the present study, we were solely interested in background total hemoglobin. Tissue reflectance spectroscopy has been recently tested in plastic surgery for several novel purposes, including continuous noninvasive monitoring of tissue perfusion in free flaps, where changes in oxygenated hemoglobin concentration have been used to guide early reoperation in failing flaps.[8, 9] Spectroscopy is more reproducible, sensitive, and objective than color judgments made by the human eye when measuring degrees of paleness or erythema. In this study, spectral responses were found to be a reliable method used to distinguish the epinephrine and control groups. Mean relative hemoglobin index values at every time point after post injection minute 1 were significantly different between groups. The authors observed a correlation between spectroscopy measurements (relative hemoglobin index) and subjective visual observations (relative skin redness and whiteness) over time; however, this correlation was not quantified.

For each group, there was an immediate transient increase in hemoglobin index shown by spectroscopy that was statistically significant at 1 minute compared with baseline, using an unpaired two-tailed t test ($p < 0.01$). This immediate increase in hemoglobin is likely caused by local histamine release by mast cells because of tissue trauma from the injection and by the chemical sympathectomy effect of lidocaine, resulting in immediate vasodilation. In the plain lidocaine group, the hyperemia effect lasted up to 80 minutes on average. In the epinephrine group, hemoglobin concentration

returned to baseline at roughly 7 minutes after injection, and continued to decrease until a new equilibrium was reached at roughly 25 minutes, with a hemoglobin concentration less than the baseline concentration. When using lidocaine, epinephrine should be added whenever possible to decrease bleeding during surgery.[10, 11]

Epinephrine's vasoconstriction effect is complex, and vasoconstriction intensity differs depending on vessel type: arteries, arterioles, precapillary sphincters, capillaries, venules, and veins.[12] Although epinephrine's maximal effect on arterial vasoconstriction may occur at 7 to 10 minutes, it takes considerably longer for a new local equilibrium to be obtained with regard to hemoglobin quantity.

If optimal visualization is desired, the ideal time for the surgeon to begin the incision should be the time when local hemoglobin concentration is lowest. Waiting 25 minutes after injection of local anesthetic with epinephrine before making an incision will result in less intraoperative bleeding. Plastic surgeons already using this concept may inject local anesthetic; leave the injected patient temporarily, to perform other tasks such as injecting other patients; and later return after roughly 25 minutes, to begin the procedure on the first patient.[13]

One limitation of this study was that there was no surgery performed on volunteers. Ideally, two standard bilateral incisions during a surgical procedure could be made at both 7 and 25 minutes after lidocaine plus epinephrine injection to see whether there was any difference in volume of blood loss between sites. Future studies could use spectroscopy to measure hemoglobin concentration in the head and neck or in the hand, as epinephrine likely has slightly different effects, depending on location.

References

[1] Wayne F Larrabee, Brent J Lanier, and David Miekle. "Effect of epinephrine on local cutaneous blood flow". In: *Head & Neck Surgery* 9.5 (1987-05), pp. 287–289. ISSN: 01486403. DOI: 10.1002/hed.2890090507. URL: http://doi.wiley.com/10.1002/hed.2890090507 (cit. on pp. 58, 60, 63).

[2] J B Dawson, D J Barker, D J Ellis, E Grassam, J A Cotterill, G W Fisher, and J W Feather. "A theoretical and experimental study of light absorption and scattering by in vivo skin". In: *Physics in Medicine and Biology* 25.4 (1980-07), pp. 695–709. ISSN: 0031-9155. DOI: 10.1088/0031-9155/25/4/008. URL: http://www.ncbi.nlm.nih.gov/pubmed/7454759%20http://stacks.iop.org/0031-9155/25/i=4/a=008?key=crossref.3a9c201eba5c1754a3a8963193b6ce29 (cit. on pp. 58, 61, 63).

[3] D M Knize. "Forehead lift". In: *Grabb & Smith's Plastic Surgery*. Ed. by C H Thorne, R W Beasley, S J Aston, S P Bartlett, G C Gurtner, and S L Spear. 6th. Philadelphia: Wolters Kluwer Health/Lippincott Williams & Wilkins, 2007, pp. 509–517 (cit. on p. 60).

[4] Z Kryger and Z Sisco. "Practical plastic surgery". In: *Local Anesthetics*. Ed. by Z B Kryger and T Yagmour. 1st. Austin, Texas: Landes Bioscience, 2007, pp. 29–32 (cit. on p. 60).

[5] T Dunlevy, T P O'Malley, and G N Postma. "Optimal concentration of epinephrine for vasoconstriction in neck surgery". In: *Laryngoscope* 106 (1996), pp. 1412–1414 (cit. on p. 63).

[6] T P O'Malley, G N Postma, M Holtel, and D A Girod. "Effect of local epinephrine on cutaneous bloodflow in the human neck". In: *Laryngoscope* 105 (1995), pp. 140–143 (cit. on p. 63).

[7] Brian C Wilson and Michael S Patterson. "The physics, biophysics and technology of photodynamic therapy." In: *Physics in Medicine and Biology* 53.9 (2008-05), R61–109. ISSN: 0031-9155. DOI: 10.1088/0031-9155/53/9/R01. URL: http://www.ncbi.nlm.nih.gov/pubmed/18401068 (cit. on p. 63).

[8] A Najefi, D R Leff, M Nocolaou, C Nduka, G Z Yang, and A W Darzi. "Monitoring of free flaps using near-infrared spectroscopy: A systematic review of the initial trials". In: *Plastic and reconstructive surgery* 125 (2010), 182e–184e (cit. on p. 63).

[9] M H Stelle. "Three-year experience using near infrared spectroscopy tissue oximetry monitoring of free tissue transfer". In: *Annals of Plastic Surgery* 66 (2011), pp. 540–545 (cit. on p. 63).

[10] A Higgins, Donald H Lalonde, M Bell, Daniel E McKee, and J F Lalonde. "Avoiding flexor tendon repair rupture with intraoperative total active movement examination". In: *Plastic and reconstructive surgery* 126 (2010), pp. 941–945 (cit. on p. 64).

[11] Donald H Lalonde. "Reconstruction of the hand with wide awake surgery". In: *Clinical Plastic Surgery* 38 (2011), pp. 761–769 (cit. on p. 64).

[12] R E Lee and E A Holze. "The peripheral vascular system in the bulbar conjunctiva of young normotensive adults at rest". In: *Journal of Clinical Investigation* 29 (1050), pp. 146–150 (cit. on p. 64).

[13] M Gibson. "Outpatient carpal tunnel decompression without tourniquet: A simple local anaesthetic technique". In: *Annals of The Royal College of Surgeons of England* 72 (1990), pp. 408–409 (cit. on p. 64).

Chapter 4

Paper III - A model for analyzing system-measured spectra

Preamble

Paper III proposes a spectrally-constrained model for interpreting the total diffuse reflectance spectra obtained with the integrating sphere-based system outlined in Chapter 2. The model was developed from the one dimensional diffusion theory approximation of the radiation transport equation[1] where each scatter point acts as a point source. The coefficients for the solution to the resulting ordinary differential equation were determined by applying the extrapolated boundary condition.

The necessary corrections to modify a measured reflectance spectrum into the true reflectance spectrum were thoroughly considered. The Single Beam Substitution Error (SBSE) was previously addressed in Chapter 2, while the scattering losses that result from calibration with a highly scattering Spectralon® standard were investigated in this paper. To determine the functional form of this correction factor (SLCF), mono Monte Carlo simulations were performed and then confirmed with tissue-simulating liquid phantoms.

The order in which these corrections are applied in the fitting algorithm was determined based on the required parameters for each step. The robustness of the model was then tested for effects of noise, and changes in the scattering and background absorption coefficients. Finally, the model was used to interpret the previously collected lidocaine & epinephrine data from Chapter 3 and compared to the previous Dawson erythema index analysis.[2]

All of the work undertaken for this paper was performed by the author of this thesis (further known as "the author") under the supervision of Drs. T. Farrell and J. Hayward with the following exceptions; As previously mentioned, the epinephrine study was jointly undertaken by the author and Dr. D. McKee, the liquid phantoms were prepared by Mr. D. Gallino, the spatially-resolved diffuse reflectance measurements were collected and analyzed with the help of Mr. D. Cappon, and the Monte Carlo simulation code was written with significant help by Dr. G. Devenyi. The manuscript was written by the author and edited by Drs. Farrell and Hayward. The manuscript has been altered from its original form to match the style of this thesis.

Contents

Modeling changes in the hemoglobin concentration of skin with total diffuse reflectance spectroscopy

Diana L. Glennie, Joseph E. Hayward, and Thomas J. Farrell

Department of Medical Physics and Applied Radiation Sciences, McMaster University, 1280 Main Street West, Hamilton, Ontario, L8S 1A8

AND

Department of Medical Physics, Juravinski Cancer Centre, 699 Concession Street, Hamilton, Ontario, L8V 5C2

Submitted to the *Journal of Biomedical Optics* on September 25, 2014.

Abstract

The ability to monitor changes in the concentration of hemoglobin in the blood of the skin in real time is a key component to personalized patient care. Since hemoglobin has a unique absorption spectrum in the visible light range, diffuse reflectance spectroscopy is the most common approach. Although the collection of the diffuse reflectance spectrum with an integrating sphere has several calibration challenges, this collection method is sufficiently user-friendly that it may be worth overcoming the initial difficulty. Once the spectrum is obtained, it is commonly interpreted with a log-inverse-reflectance (LIR) or "absorbance" analysis that can only accurately monitor changes in the hemoglobin concentration when there are no changes to the non-hemoglobin chromophore concentrations. This paper addresses the difficulties associated with collection of the diffuse reflectance spectrum with an integrating sphere and proposes a model capable of retrieving relative changes in hemoglobin concentration from the visible light spectrum. The model is capable of accounting for concentration changes in the non-hemoglobin chromophores and is first characterized with theoretical spectra and liquid phantoms. The model is then used in comparison with an LIR analysis on temporal measurements from blanched and reddened human skin.

4.1 Introduction

The knowledge of changes in blood volume in tissue is a valuable asset when monitoring the effects of a wide range of therapeutic interventions, from radiation therapy[3–6] to skin-flap transplants.[7] The most common method of monitoring changes in skin perfusion or blanching is by visual inspection.[6, 8] While widely accessible, this approach is subjective and is prone to inter- and intra- observer error.[9] Monitoring changes in skin perfusion to gauge patient progress would be more reliable if an objective, quantitative approach were available.

Steady-state diffuse reflectance spectroscopy (DRS) measures the wavelength-dependent intensity of light that has entered and scattered back out from a sample.[10] Since the amount of reflected light is dependent on the absorption coefficient μ_a, which is itself a function of the individual chromophore concentrations (such as oxy- and deoxy-hemoglobin, and melanin), it is a good candidate for the task. There are several different approaches and technologies available for obtaining a diffuse reflectance spectrum, each with their own set of advantages and disadvantages.

4.1.1 Measurement of Diffuse Reflectance Spectra

Spatially-resolved diffuse reflectance (SRDR) is one of the most common approaches for determining optical properties from reflectance spectra. Typically, fiber optics are placed at increasing radial distances from a source fiber and the measured intensities can be used to determine both the absorption and reduced scattering coefficients.[10] However, SRDR is rarely used in the clinical setting due to the many difficulties associated with its implementation. SRDR returns most accurate results when there is good coupling between the fiber optics and the measurement surface. Also, the results may be sensitive to local inhomogeneities, such as freckles, hair, and localized vasculature that may alter the individual fiber measurements. Since the signal drops off rapidly with distance, a high quality spectrometer is required to span the required dynamic range and establish the rate of decrease in intensity as a function of radial distance, making it expensive and difficult to calibrate.

An alternative is to use a single fiber-optic source-collector pair geometry. This has many of the same complications as the spatially-resolved approach except it is not as expensive and is much easier to calibrate. It is still error prone if tissue contact is

compromised or if there is a local inhomogeneity, but the source/detector geometry can be selected to match a specific range of expected optical properties and minimize the effect of high scattering.

Another measurement technique is an integrating sphere (IS) based system.[11, 12] In these systems, the total light diffusely reflected by a single integrating sphere from a sample is compared with that collected from a highly reflective calibration plate. Such systems do not have any of the difficulties associated with fiber-based geometries. They are inexpensive, easy to ensure sample coupling, and are insensitive to pathlength considerations and local inhomogeneities since they measure the average reflectance over an area. However, this approach has its own set of challenges that must be addressed before an accurate reflectance spectrum can be obtained. Once they have been overcome, this method is easily implemented and has a low assembly cost.

4.1.2 Analysis of a Diffuse Reflectance Spectrum

The absorption spectrum for a purely absorbing (no scattering) solution can be determined with the Beer-Lambert law by measuring the light transmitted through a sample in a cuvette with a spectrophotometer.[13] Since the pathlength is fixed, the transmission measurement is often expressed as the common logarithm of the ratio of the incident intensity to the transmitted intensity, known as the "absorbance". This approach has been adopted in tissue optics to analyze a diffuse reflectance spectrum by calculating the common logarithm of the reciprocal (inverse) of the reflectance spectrum (known as "LIR").[2, 14] However, *in vivo*, only the reflected light intensity as opposed to the transmitted light intensity can be measured due to the different geometry. Also, since the tissue is highly scattering, the pathlength is no longer fixed and known. This is accounted for by introducing a pathlength correction factor $l(\lambda)$ into the LIR term. Since this factor is wavelength-dependent and unknown, only changes in chromophore concentrations are possible with this approach. The change in LIR (including the unknown pathlength correction factor) is equated directly to the absorption from the individual chromophores, which is expressed as the products of the concentrations c_i, and extinction coefficients $\varepsilon_i(\lambda)$,[15]

$$\begin{aligned}\Delta LIR(\lambda)/l(\lambda) = \Delta c_{HbO}(\lambda)\varepsilon_{HbO}(\lambda) + \Delta c_{Hb}(\lambda)\varepsilon_{Hb}(\lambda) + \Delta c_{mel}(\lambda)\varepsilon_{mel}(\lambda) \\ + \Delta c_{H_2O}(\lambda)\varepsilon_{H_2O}(\lambda) + \Delta c_{scat}(\lambda)\varepsilon_{scat}(\lambda)\end{aligned} \tag{4.1}$$

It is common to use the LIR values at wavelengths above 650 nm to approximate the contribution from the non-hemoglobin chromophores, and to use the LIR value at 550 nm to approximate the contribution from scatter.[16] This approach is intended to remove all but the hemoglobin terms and has been shown to successfully approximate changes in skin perfusion, but only in the instance where there are no changes in the non-hemoglobin chromophore concentrations or scattering conditions. Otherwise, the correction method fails and the recovered hemoglobin concentrations are no longer linear with respect to actual changes to the LIR spectrum.

Depending on the duration over which the measurements are performed, it may be reasonable to assume that there are no changes to the melanin and background absorption components or to the reduced scattering coefficient. However, if these values have changed, a robust model should have the ability to account for them. A spectrally-constrained theoretical approach relies on known absorption and scattering coefficient spectra to model the diffuse reflectance spectrum. Since there exists a large body of data on the extinction coefficients for the major constituents of human skin in the visible-to-near-infrared region, this approach may be an ideal solution. In this manuscript, such a model will be applied to total diffuse reflectance spectra obtained with an inexpensive IS-based DRS measurement system. Next, deviations to the model introduced by the use of an IS will be identified and addressed. Finally, the fully-characterized system and model will be used in an in vivo study in which the results will be compared to a common LIR analysis.

4.2 Theory

An appropriate model is required to interpret the total diffuse reflectance spectra obtained from an IS. For a sufficiently large illumination port geometry, the incident light on the skin can be accurately approximated by a broad beam light source perpendicularly incident on a semi-infinite, homogeneous medium. However, for realistic IS sizes, there are a number of factors that introduce deviations from the simple model that will require corrections. While it may be standard procedure to

apply all of the corrections to the calculated spectrum, the available information mandates that some of the corrections be applied to the collected spectrum. Therefore, special consideration is required during the development of a fitting algorithm.

4.2.1 Forward Model Derivation

There are several different ways of modeling light transport in tissue. One such approach is the Boltzmann Radiative Transport Equation (RTE), which describes the stochastic behavior of neutral particles such as photons.[17] When sufficiently far from a boundary within a turbid material, the RTE can be accurately approximated by the steady-state diffusion equation,[1]

$$\nabla^2\Psi(r) - \frac{\mu_a}{D}\Psi(r) = S(r). \tag{4.2}$$

The light fluence rate $\Psi(r)$, is dependent only on the absorption coefficient μ_a, the reduced scattering coefficient μ_s', and the source term $S(r)$. The sum of absorption and reduced scattering coefficients is the reduced total interaction coefficient μ_t'. The source term, that represents photons scattered out of the primary beam, is typically approximated by an isotropic spherical harmonic term $-S_0(r)/D$, where $S_0(r)$ decays with depth and D is the diffusion constant,

$$D = \frac{1}{3\mu_t'}. \tag{4.3}$$

For a normally incident, semi-infinite broad beam light source, Equation 4.2 collapses into one dimension,

$$\frac{d^2\Psi(z)}{dz^2} - \mu_{eff}^2\Psi(z) = -\frac{\mu_s'}{D}I_0 e^{-\mu_t' z}, \tag{4.4}$$

where

$$\mu_{eff}^2 \equiv \frac{\mu_a}{D}. \tag{4.5}$$

This equation has a closed form solution that can be determined by considering the boundary conditions.[1]

By applying the definition that total diffuse reflectance is the fraction of the incident photon current exiting the tissue surface to the solution to Equation 4.4, an equation for the wavelength-dependent diffuse reflectance is produced,

$$R_d = \frac{\mu_s'}{[\mu_t' + \mu_{eff}]\,[1 + 2AD\mu_{eff}]}. \tag{4.6}$$

4.2.2 Integrating Sphere Effects on Reflectance Measurements

When the total diffuse reflectance spectrum is collected with an IS, the finite geometry violates some of the assumptions made in Section 4.2.1 regarding the broad beam geometry. Corrections can be applied to account for these deviations from the theoretical model, thereby restoring some of its accuracy. There are three major violations which must be addressed: (1) the specular reflectance, (2) the single-beam substitution error, and (3) the scattering losses.

Specularly reflected light has not penetrated the tissue of interest and, therefore, carries no information about the tissue optical properties. The amount of light that penetrates the tissue or is specularly reflected depends on the index of refraction of the material and is on the order of four percent for human tissue.[18] If the specularly reflected light were to be collected in addition to the diffusely reflected light, it could account for a significant portion of the total detected signal (depending on the skin type) which would yield inaccurate results. To reduce the contribution from specularly reflected light, an illumination geometry should be chosen such that none of the specularly reflected light can enter the detection fiber. In this way, only light that has penetrated, and been remitted from, the tissue will be detected. This can also be achieved through the implementation of a baffle; however it is not generally preferred as it disrupts the internal surface of the sphere, leading to substantial non-uniformities in smaller spheres.[19]

Single-beam substitution error (SBSE) is due to the normalization procedure that converts a single intensity measurement s_m, into reflectance by subtracting the background signal s_{bg}, and comparing it to the signal from a highly reflective calibration standard s_{cal},[20]

$$R_m = \frac{s_m - s_{bg}}{s_{cal} - s_{bg}}. \tag{4.7}$$

When the calibration standard is replaced with the sample to be measured, there is a decrease in the total flux within the sphere due to the considerably higher absorption in

the sample as well as multiple scattering, which leads to a lower reflectance. Therefore, a correction factor for SBSE would be both sphere and reflection dependent, and can be determined empirically with a set of diffuse reflectance standards.[21, 22]

The final IS effect to be accounted for is the decrease in detected signal due to the finite port size. Near the edge of the detection port, there is an annular region where the light that enters the sample will migrate away from the detection port, resulting in a small decrease in the reflected signal. For the calibration standard, which has a significantly higher scattering coefficient compared with human tissue,[23] this region (and the deviation from the model) is small. However, as the reduced scattering coefficient decreases, the pathlength increases and the region and its influence increases. This phenomenon, similar to that investigated by Zhu *et al.*,[24] can be accounted for with a scattering losses correction factor (SLCF) that is a function of both the absorption and reduced scattering coefficients, and can be determined empirically or with Monte Carlo (MC) methods.

4.2.3 The Fitting Algorithm

In the absence of any IS effects, the calculated broad beam diffuse reflectance model would simply be fit to the measured reflectance spectrum using the concentrations of absorbers as parameters in a spectrally-constrained least-squares approach. The concentrations of the major chromophores c_i, would be the fitting parameters multiplied with their corresponding extinction coefficient spectra $\varepsilon_i(\lambda)$, to produce the absorption coefficient spectrum,

$$\mu_a(\lambda) = \sum_i c_i \times \varepsilon_i(\lambda). \tag{4.8}$$

In the visible light spectrum, the three major chromophores that contribute to the absorption coefficient are oxy-hemoglobin, deoxy-hemoglobin, and melanin. Each has a well-established extinction coefficient spectrum as shown in Figure 1.[25] While both eumelanin (black/brown) and pheomelanin (yellow/red) are found in human skin, eumelanin is the dominant form, therefore its spectrum was selected for use in the fitting algorithm. Additional chromophores such as bilirubin and water do not contribute significantly in this region, however a fourth term can be included to account for the base absorption by all other minor chromophores in the skin layers. The shape of this component is exponential with respect to wavelength, according to

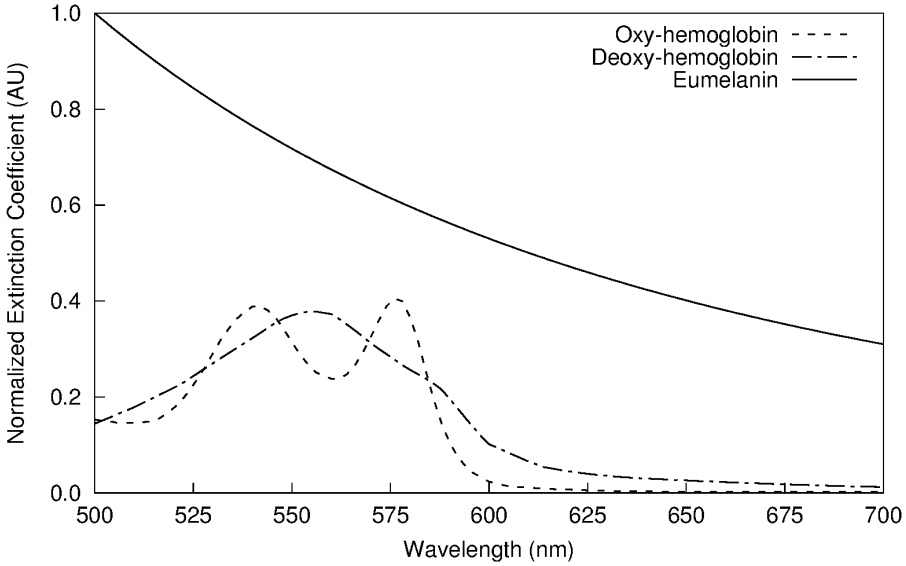

Figure 4.1: Normalized extinction coefficient spectra for the three major chromophores found in human skin.

the Huang and Jacques data from bloodless rat skin,[26]

$$\mu_{a\ base} = a \times \exp\left[\frac{-(\lambda - 154)}{66.2}\right] + b \quad \left[mm^{-1}\right] \tag{4.9}$$

where a and b are scaling (fitting) parameters.

This baseline absorption spectrum has a similar broad-spectral shape to the melanin extinction coefficient spectrum. Therefore, it will be impossible to separate the contributions from these two concentrations. Since the goal of this study is to monitor changes in hemoglobin concentration, these two absorption components were combined following fitting and considered together as a single background absorption term. The final absorption term consisted of five components with five fitting parameters.

With only a single measurement (that of the total diffuse reflectance), the contributions from absorption and scattering are not separable. Therefore, an assumption of the reduced scatter spectrum is necessary to extract information on the absorption coefficient spectrum. This approach was deemed valid since there is only a small amount of variation in scatter between individuals for a particular tissue type.[10] The chosen spectrum should closely approximate scatter in both the epidermis and dermis since the skin is being modeled as a homogeneous slab of tissue. Due to the protein structure of these two layers (e.g keratin, collagen fibers), the reduced scattering

spectrum for visible light has both Rayleigh and Mie scattering contributions and can be determined as the sum of these two components,[26]

$$\mu'_{s\ Mie}(\lambda) = 2 \times 10^4 \lambda^{-1.5} \quad [mm^{-1}] \tag{4.10}$$

$$\mu'_{s\ Rayleigh}(\lambda) = 2 \times 10^{11} \lambda^{-4} \quad [mm^{-1}] \tag{4.11}$$

The resultant absorption and reduced scattering coefficient spectra would then be used to calculate the spectral broad beam reflectance, according to Equation 4.6. The correct concentrations would be those parameters that minimize the sum-of-squares.

However, as previously stated, the effects of the IS must be accounted for and the model should be adjusted accordingly. Ideally, all corrections would be made to the measured reflectance spectrum to reproduce the broad beam reflectance spectrum being modeled in the calculated spectrum. Since the SLCF is a function of the absorption and scattering coefficients, it was easier to apply the SLCF to the calculated reflectance spectrum where the input optical properties are known.

In addition to the IS effects, the fitting algorithm must account for the spectral resolution of the spectrometer. Depending on the full-width-at-half-max (FWHM) of the spectral response function, it may be necessary to de-convolve the measured reflectance spectrum with the chosen response function. However, since deconvolutions are prone to noise amplification and signal stability issues, they are not preferred.[27, 28] Instead, the calculated reflectance spectrum was convolved with the instrument response function and compared with the measured spectrum. A flow chart for the fitting algorithm is shown in Figure 4.2.

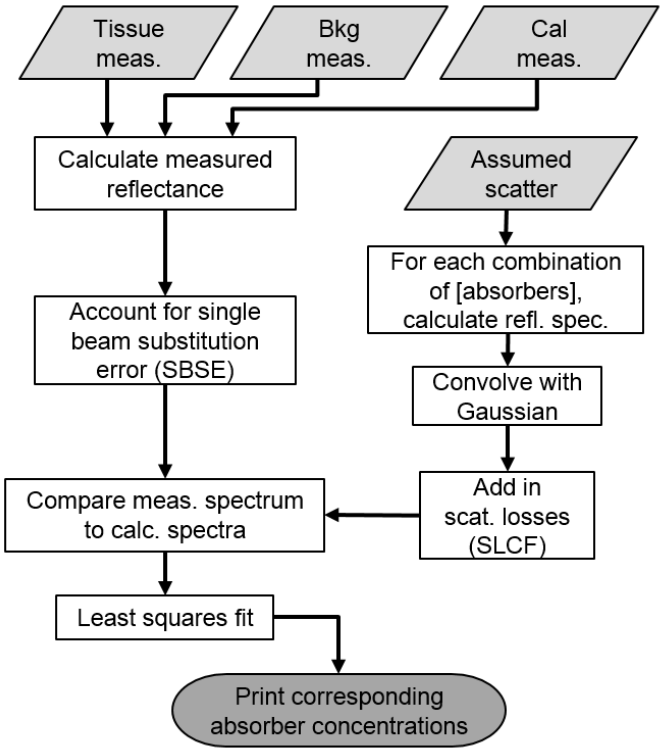

Figure 4.2: A flow chart describing the fitting algorithm to be applied to total diffuse reflectance measurements. The single beam substitution error is applied to the measured spectrum while all other corrections are applied to the calculated spectrum.

4.3 Methods & Materials

The robustness of the model was tested using reflectance spectra representing a variety of tissue optics situations. Following the characterization of the model, the SBSE correction factor and the SLCF were determined. The SBSE correction factors were established following an accepted empirical approach.[21] Since there was no established method for accurately assessing and correcting for the scattering losses, one was developed using Monte Carlo simulations and tissue-simulating phantoms. Following a complete characterization of the model, it was used in an in vivo study to extract blood concentrations in human skin from diffuse reflectance spectra obtained with an IS.

The IS-based system used to collect total diffuse reflectance spectra throughout this paper has been described previously.[22] Briefly, the system consists of a tungsten halogen light source coupled via optical fibers to an IS (manufactured in-house) and a computer-based spectrometer. The collection fiber directly illuminates the grating of the spectrometer, acting in place of a slit. The spectral resolution of the system, measured using a mercury-argon calibration source, is 10 nm FWHM. The spectrometer range was 340-997 nm, encompassing 2048 discrete wavelengths. Since the chromophores of interest do not have significant spectral features below 500 nm or above 700 nm, the measurement spectra were analyzed only within this wavelength range. The typical measurement uncertainty did not exceed two percent across this interval for true reflectance values above 20 percent.

4.3.1 Characterization of the Model

In order to investigate the robustness of the model, sample spectra were generated using the forward model described in Section 4.2.1 which were then convolved with the IS system spectral response (represented by a Gaussian function). Two melanin concentrations were selected to yield Type III and Type V representative skin types on the Fitzpatrick scale.[29] For each melanin concentration, three hemoglobin concentrations were chosen, corresponding to blanched, normal, and reddened skin respectively, for a total of six representative baseline diffuse reflectance spectra. When these unmodified spectra were fitted with the model, the hemoglobin concentrations were recovered to within 0.2 percent of the input values. These spectra were then used to determine the

effect of noise on the model's performance as well as the impact of an incorrect reduced scattering coefficient spectra or of a change in the background absorption spectrum.

4.3.1.1 Testing the Effect of Noise

To test the effect of noise in the signal on the model performance, Gaussian random noise ranging from one to ten percent was added to each of the six sample spectra. This process was repeated five times for each baseline spectrum in order to perform a statistical analysis on the results. The noisy spectra were then fitted with the model and the hemoglobin concentrations were recovered. The mean and standard deviation of the difference between the recovered concentration and the input concentrations for oxy- and deoxy-hemoglobin were determined for each noise level.

4.3.1.2 Testing the Effect of an Incorrect Scatter Coefficient Spectrum

Since the scattering properties of human epidermis and dermis do not vary widely between individuals, the model incorporates a constant average reduced scattering coefficient spectrum. While it is probable that it does not accurately represent the scattering for a given individual, the deviation from this chosen spectrum is expected to be small. To investigate the possible effect of these differences, eight Fitzpatrick Type III reflectance spectra were produced with decreasing and increasing amounts of total hemoglobin concentrations from 25 to 200 percent of a baseline amount (oxygen saturation of 84 percent)[30] and with two percent noise. Each spectrum was fit using a different assumed, reduced scattering coefficient spectrum, from 25 to 200 percent of the original, input reduced scattering spectrum. The differences between the recovered total hemoglobin concentration and the input concentration were calculated.

4.3.1.3 Testing the Effect of Changes in Background Absorption

As mentioned in Section 4.2.3, absorption by melanin and the structural components in skin were combined into a single background absorption term. Depending on the timeline over which measurements are taken, it is possible that the contributing absorber concentrations may change. The model is expected to correctly account for this change and to accurately recover the hemoglobin concentrations. To verify this expectation, a set of Fitzpatrick Type III spectra were produced with simultaneously increasing hemoglobin (up to 200 percent) and background absorbers (up to 40 percent).

If the increase in background absorption was due solely to the increase in melanin concentration, a 40 percent increase would correspond to a reclassification of a Type III skin type into a Type IV skin type, which is highly improbable but would be visibly noticeable and so represents the upper limit of absorption increase. These spectra were fitted and the hemoglobin concentrations were recovered and compared to the input values.

4.3.2 Determination of the Scattering Losses Correction Factor

The magnitude of the scattering losses is sphere dependent and inversely proportional to the absorption and reduced scattering coefficients, i.e., for a given IS geometry, it will increase as either the absorption or scattering coefficients decrease. Monte Carlo (MC) simulations were used to determine the functional form of the SLCF and empirical measurements were used to verify and obtain the exact parameters of the functional form. A variation of the standard MC simulation called a Mono MC[31] (or "White MC")[32] was used to economize the computationally expensive simulation. Under this approach, photons were tracked through the material with only scattering properties defined, and the effect of absorption was applied afterward. The MC geometry matched the actual IS measurements, with a sphere wall reflectance coefficient of 0.95. The semi-infinite homogeneous tissue was assigned a refractive index of 1.33 and an anisotropy factor of 0.9.[33] Simulations were performed for a range of reduced scattering coefficients from 0.50 to 4.00 mm^{-1}. For each simulation, a range of absorption coefficients from 0.01 to 10.00 mm^{-1} was applied to obtain simulated reflectance values R_{sim}, which represented the reflectance measured with the IS. These values were then combined with reflectance values calculated with the model R_{calc}, to achieve SLCFs as follows,

$$SLCF\left(\mu_a, \mu_s'\right) = \frac{R_{sim}\left(\mu_a, \mu_s'\right)}{R_{calc}\left(\mu_a, \mu_s'\right)}. \tag{4.12}$$

Once the functional form was determined, twenty liquid phantoms were measured with the IS to confirm the fit. These phantoms included different concentrations of commercially available green food coloring and Intralipid®(Baxter, Toronto, Ontario) such that the absorption ranged from 0.01 to 0.38 mm^{-1} and the reduced scattering coefficient ranged from 0.45 to 3.5 mm^{-1}. Both extinction coefficient spectra were deter-

mined with a spatially-resolved diffuse reflectance spectrometer while that of the green food coloring was additionally characterized with a UV/Visible Spectrophotometer (Varian Cary 50 Bio, Cary, NC).

The phantoms were measured with the IS system as well as with the spatially-resolved system. The SBSE was applied to the measured reflectance, and the concentrations extracted from the spatially-resolved system were used to calculate the diffuse reflectance with the model which was then convolved with the spectral response function. The ratios of these two sets (representing the SLCF), combined with the absorption and reduced scattering coefficients created a set of triplets which was fitted using the previously obtained function form for the SLCF.

4.3.3 *In Vivo* Study

An *in vivo* experiment was performed to determine the time to maximal vasoconstriction following the injection of epinephrine. Volunteers were made to lay quietly on a bed for ten minutes, during which time five baseline measurements were performed. They were then injected subcutaneously in both upper arms with either 5 cc of 1 percent lidocaine (plain) or 5 cc of 1 percent lidocaine with 1:100,000 epinephrine (0.01 mg/mL) (AstraZeneca Canada, Inc., Mississauga, Ontario) in order to induce perfusion or blanching, respectively. Reflectance spectra were obtained with the IS system every minute for 30 minutes and then every two minutes for another 90 minutes. The spectra were processed using the model and the hemoglobin concentration over this period of time were recovered.

4.4 Results & Discussion

4.4.1 Model Characterization

4.4.1.1 Effect of Noise

Test spectra with varying levels of noise were processed via the fitting algorithm to obtain the best fit parameters. For each set of five spectra, the mean and standard error of the percent difference between the recovered and input oxy- and deoxy- hemoglobin concentrations were calculated. The results for the Fitzpatrick Type III, normal hemoglobin concentration spectra are shown in Figure 4.3. The average oxy-, deoxy-,

and total hemoglobin concentrations for each noise level agreed with the corresponding input concentrations, with the total hemoglobin having the smallest standard deviation. This observation, that the two hemoglobin concentrations are coupled parameters, can be explained by the spectral similarities between the oxy- and deoxy- hemoglobin extinction coefficient spectra. The two spectra vary only within a small wavelength range (500-600 nm), and since these two chromophores only contribute a small fraction to the total absorption in skin, a portion of one of the chromophore concentrations may be erroneously attributed to the other without substantially impacting the fit. Therefore, future analysis should focus on the recovered total hemoglobin rather than the two individual hemoglobin chromophores as it has been shown to return a more consistently accurate result.

The results are the same for the Type V reflectance spectra, which suggests that melanin, a broad spectrum absorber, does not mask the absorption effects of hemoglobin within the wavelength range of interest.

Further inspection of Figure 4.3c indicates that the noise generally increases the uncertainty for single measurements. This is expected, since the hemoglobin spectral features become harder to differentiate as the noise increases, particularly for higher melanin and/or lower hemoglobin concentrations. For the noise levels associated with the IS system (two percent), the difference between the input and recovered total hemoglobin concentrations did not exceed five percent for any of the 240 individual test spectra processed. Since this level of variation is of the same order as the observed daily variation in hemoglobin concentration,[34] it is considered acceptable.

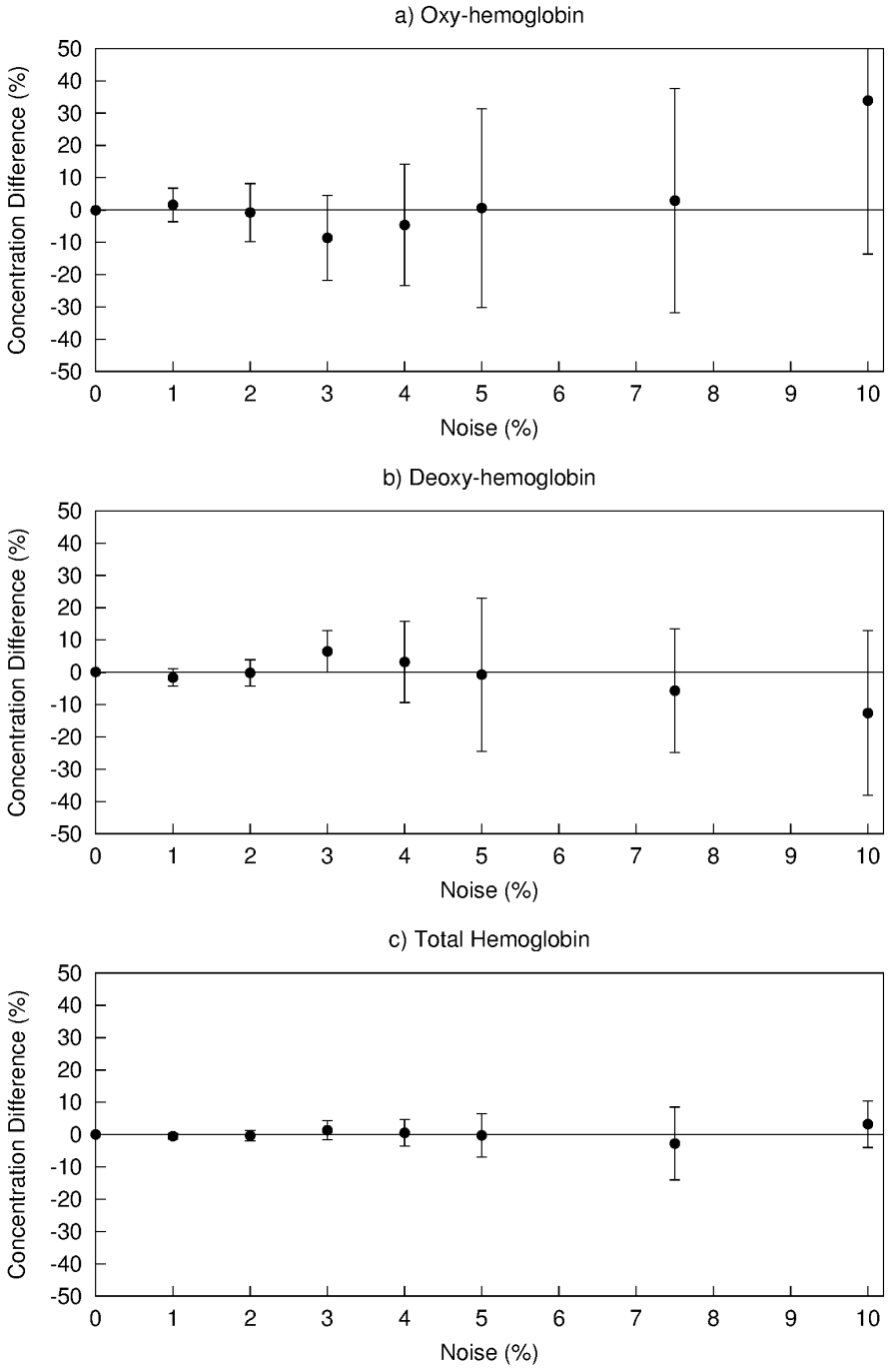

Figure 4.3: Percent differences between the recovered and input concentrations for a) oxy-hemoglobin and b) deoxy-hemoglobin. When combined into a total hemoglobin concentration (c), the standard deviation (represented by error bars) is consistently reduced.

4.4.1.2 Effect of an Incorrect Scatter Coefficient Spectrum

The eight Fitzpatrick Type III reflectance spectra with increasing total hemoglobin concentrations and characteristic noise were processed using the model and different assumed reduced scattering coefficient spectra. The maximum percent difference between the recovered and input total hemoglobin concentrations increased linearly with the reduced scattering coefficient spectrum (not shown). For example, if the model employed an assumed reduced scattering coefficient spectrum that was ten percent higher than the actual input scatter coefficient spectrum, the recovered total hemoglobin concentration also had a maximum difference on the order of ten percent. This agrees with what is known about the coupled nature of the scattering and absorption coefficients: that if both of the coefficients are increased by the same factor, they produce the same total diffuse reflectance.

There is a large body of research regarding the reduced scattering coefficient spectrum of skin and therefore, it is unlikely that the assumed reduced scatter spectrum will ever exceed an absolute difference of ten percent unless the individual suffers from a condition that causes abnormal keratin or collagen fiber growth. As such, it is expected that the total hemoglobin concentration for most individuals can be recovered to within ten percent.

The diffuse reflectance model assumed a homogeneous single layer, while skin is actually a layered structure with melanin in the epidermal layer and hemoglobin in the dermal layer. Consequently, only the recovery of a perceived or apparent chromophore concentration is possible with the model. The recovered total hemoglobin concentrations expressed as a percent increase relative to an initial, baseline measurement can act as a proxy measure of the actual hemoglobin concentration found in the dermal layer. It also has the added benefit of removing any effects caused by an incorrectly assumed reduced scattering coefficient, as shown in Figure 4.4. When expressed in this manner, the percent difference only exceeds five percent for atypical skin conditions such as when the hemoglobin concentration is alarmingly low (25 percent) or when the assumed reduced scattering coefficient deviates from average values by greater than 50 percent.

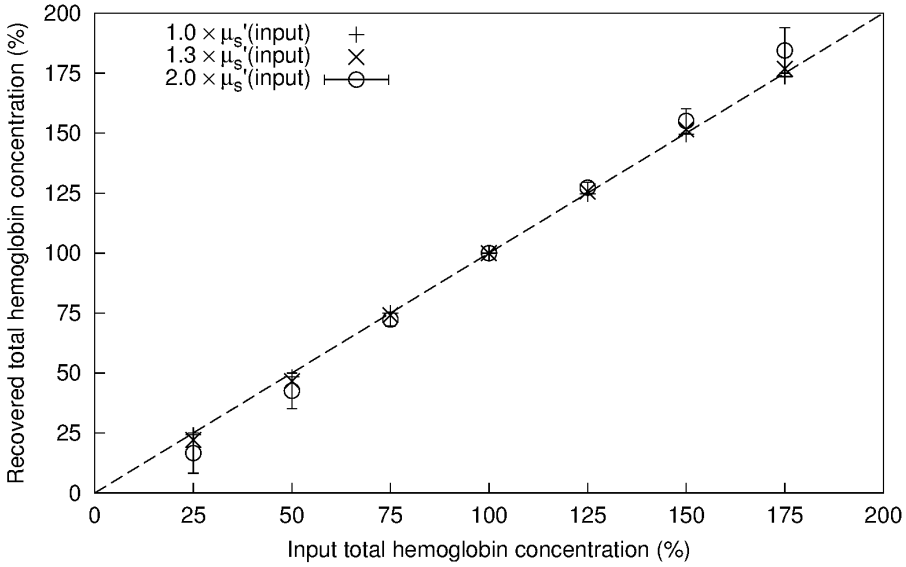

Figure 4.4: Total hemoglobin concentration recovered with the erroneous reduced scattering coefficients (μ_s') as a function of input total hemoglobin concentration. When the hemoglobin concentration is expressed as a fraction of a baseline measurement, the effects of an incorrectly assumed reduced scatter coefficient spectrum are removed. The line of unity has been added for visualization purposes. Error bars are only shown for the $2.0 \times \mu_s'$ data series.

4.4.1.3 Effect of Changes to Background Absorption

The relative total hemoglobin concentrations were recovered from the Fitzpatrick Type III reflectance spectra containing simultaneously increasing hemoglobin and background absorber concentrations (including melanin) using the model. In order to compare the performance of the model with common LIR techniques, the Dawson corrected Erythema Index[2] (EI_c) was also calculated. The Dawson model was chosen because it was one of the first models created and is commonly cited in the literature. The total hemoglobin concentrations, expressed as a percent increase from the baseline measurement, are shown in Figure 4.5 for both approaches.

Increases in the background absorption were found to have no impact on the relative total hemoglobin concentrations recovered with the model, as it was able to adjust the background absorption parameters to account for these changes. However, since the EI_c equates relative hemoglobin changes to a change in the area under the LIR curve, the decrease in area due to the increased background absorption is erroneously interpreted, resulting in an under-estimation of the relative total hemoglobin.

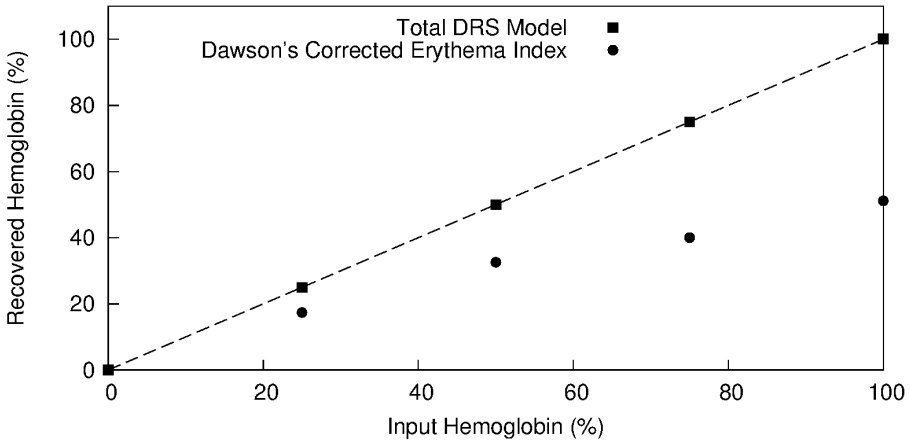

Figure 4.5: Percent increases in the total hemoglobin for reflectance spectra with simultaneously increasing hemoglobin and background absorbers. The model was able to account for changes in the background absorption and follows the line of unity, while the Dawson approach underestimates the increase in hemoglobin concentration.

4.4.2 Empirical Determination of the Scattering Losses Correction Factor

Consideration of the SLCFs from the MC simulations (Section 4.3.2) as a function of the absorption and reduced scattering coefficients indicated that there were two distinct regions within the data that roughly corresponded to values for which the diffusion approximation was valid, and for which the diffusion approximation did not hold. Inspection of the boundaries of the diffusion theory region suggested that it was approximately limited to values where the absorption coefficient was less than or equal to 5 percent of the reduced scattering coefficient. This agrees with the generally accepted limit on the diffusion theory which states that the absorption coefficient should be less than 10 percent of the reduced scattering coefficient. Since the model and the prediction of the SLCF both depend on diffusion theory, only those points in the calculated reflectance spectra (and their corresponding points in the measured spectra) that meet the optical property criterion of diffusion theory may be used in the fitting algorithm. SLCFs within the diffusion theory region ranged from 0.5 to 1.0 while values outside of the diffusion theory region exceeded 1.0, which could only be possible if additional light was being scattered into the IS. Only points where the relationship between the absorption and reduced scattering coefficient satisfied the diffusion theory were used to determine the functional form of the SLCF.

Scatter plots of the SLCF as a function of the absorption coefficient for single values of the reduced scattering coefficient (iso-lines) indicated a linear relationship with respect to the natural logarithm of the absorption coefficient. The scaling coefficient has a power-law relationship with the reduced scattering coefficient, resulting in a function form of,

$$SLCF(\mu_a, \mu_s') = a \times \mu_s'^{b} \ln(\mu_a) + c \tag{4.13}$$

The Intralipid® phantom measurements were used to confirm Equation 4.13, with triplets outside of the diffusion theory region omitted. This empirical fit was used to correct for scattering losses in the *in vivo* study analysis.

4.4.3 *In Vivo* Study Analysis

Each IS measurement from the *in vivo* study was processed with the model and fitting algorithm as well as with the Dawson model for comparison purposes. A complete report of the analysis of the Dawson model was performed by McKee et al. (2013).[35] A sample fit of the total DRS model to an individual IS measurement is shown in Figure 4.6. Measured spectra with greater hemoglobin concentrations were observed to yield better fits with the model within the 520-580 nm region. This may be attributed to the difficulty of, and ambiguity in, combining the available extinction coefficient spectra in the absence of distinct hemoglobin spectral features.

Based on the observations from Section 4.4.1 that: (1) it is difficult to separate the oxy- and deoxy-hemoglobin contributions, and (2) that a relative increase in hemoglobin concentration removes any effects due to an incorrectly assumed reduced scattering coefficient spectrum, both the total hemoglobin concentration and corrected erythema index were expressed as a percent increase from the average of the baseline measurements. A sample time series of one of the volunteers is shown in Figure 4.7.

The two methods agree everywhere except immediately following the injection. This difference may be due to initial bleeding and/or swelling following the insertion of the needle, which would have led to changes in the scattering and/or the relative concentrations of the chromophores from the baseline measurements. Since the LIR approach was shown in Section 4.4.1.3 to be unable to correctly interpret changes to non-hemoglobin chromophore concentrations, it is most likely that the erythema index is underestimating the skin redness in this situation.

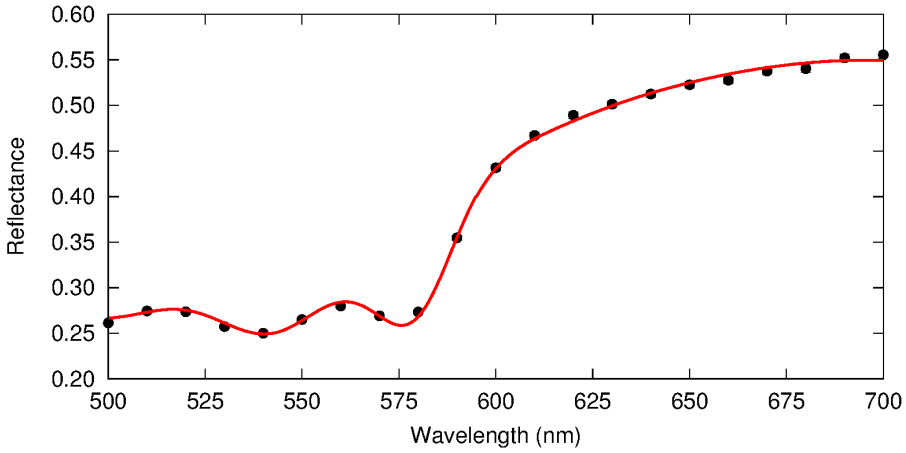

Figure 4.6: Sample spectrum (•) and fit (red line). The measured spectrum has been down-sampled for illustration purposes. Measurement error bars are too small to be visible.

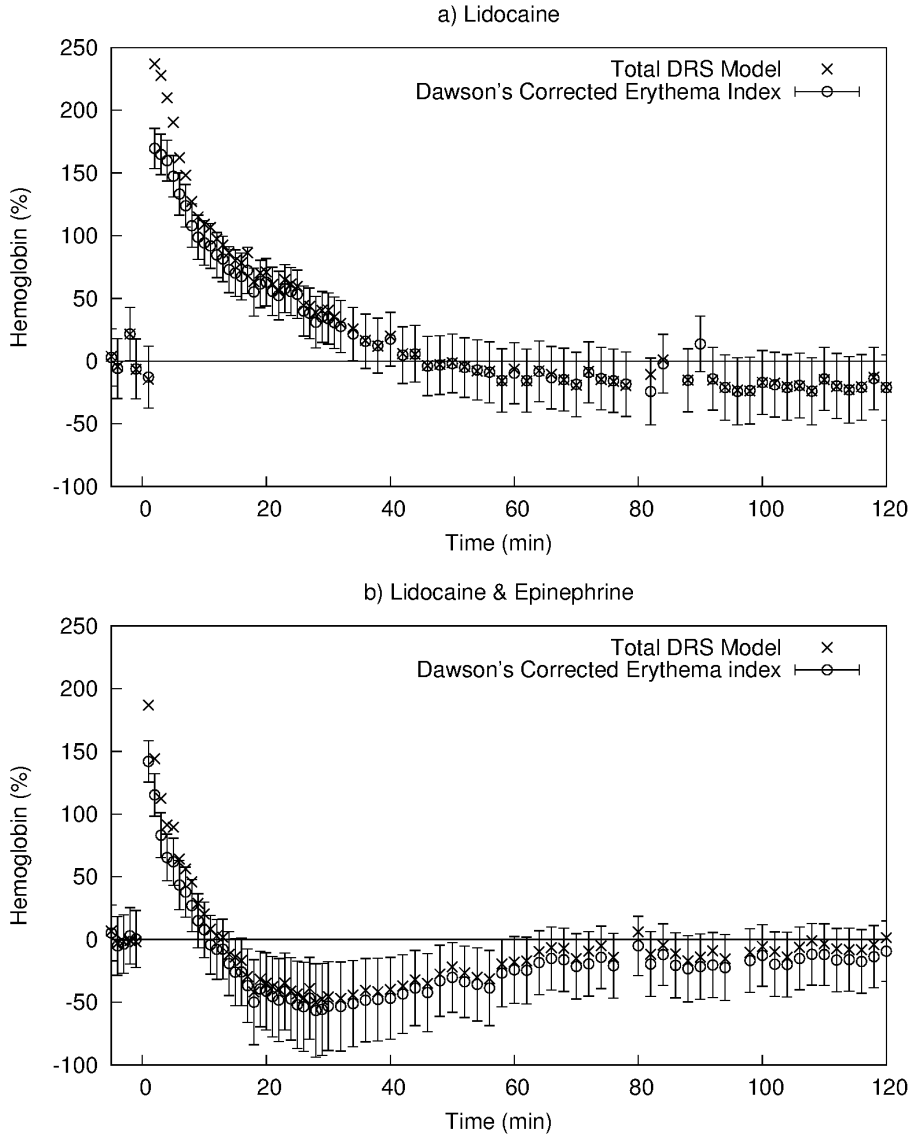

Figure 4.7: Sample time series for a single volunteer using both the total DRS model and the Dawson EI model. Error bars are shown only for the Dawson model as the returned standard deviation for the total DRS model is consistently less than 2 percent and not visible on this scale. Measurement error was determined for the Dawson model by propagating the system measurement error at each wavelength through the calculations.

4.5 Conclusion

In this paper, a model was derived for the total diffuse reflectance spectrum based on a semi-infinite, broad beam homogeneous geometry. The model was then used to interpret total diffuse reflectance spectra obtained with an integrating sphere placed on the skin, following corrections for the perturbations associated with this measurement technique. Characterization of the model and system showed that this approach was insensitive to characteristic noise, and able to account for any deviations from the assumed reduced scattering coefficient spectrum. When compared to a common log inverse reflectance approach, the model proved superior in its ability to successfully interpreted changes to background absorber concentrations. Finally, the model was applied to reflectance spectra obtained during an in vivo study and compared to analysis using the Dawson erythema index. The two methods agreed over the majority of the measurement period, but differed immediately following injection, most likely due to the Dawson model incorrectly interpreting the acute response to the needle insertion.

Acknowledgments

The authors would like to thank Dr. Daniel E. McKee for his help with the in vivo study and Dr. Gabriel A. Devenyi for his help with the Monte Carlo simulations. Monte Carlo simulations were performed using the facilities at SHARCNET (Shared Hierarchical Research Computing Network: `www.sharcnet.ca`) and Compute/Calcul Canada. This work was financially supported by the Natural Sciences and Engineering Research Council of Canada (NSERC).

References

[1] Thomas J Farrell and Michael S Patterson. "A diffusion theory model of spatially resolved, stead-state diffuse reflectance for the noninvasive determination of tissue optical properties in vivo". In: *Medical Physics* 19.4 (1992), pp. 879–888 (cit. on pp. 68, 73).

[2] J B Dawson, D J Barker, D J Ellis, E Grassam, J A Cotterill, G W Fisher, and J W Feather. "A theoretical and experimental study of light absorption and scattering by in vivo skin". In: *Physics in Medicine and Biology* 25.4 (1980-07), pp. 695–709. ISSN: 0031-9155. DOI: 10.1088/0031-9155/25/4/008. URL: http://www.ncbi.nlm.nih.gov/pubmed/7454759%20http://stacks.iop.org/0031-9155/25/i=4/a=008?key=crossref.3a9c201eba5c1754a3a8963193b6ce29 (cit. on pp. 68, 71, 87).

[3] Jocelyn Farrell. *Management of skin toxicity in the patient receiving radiation therapy.* 2004. URL: http://www.nlhba.nl.ca/Web%5C_Site%5C_Files/AOTY/AOTY.htm (cit. on p. 70).

[4] T J Fitzgerald, Maryann Bishop Jodoin, Gayle Tillman, Jesse Aronowitz, Richard Pieters, Susan Balducci, Joshua Meyer, M Giulia Cicchetti, Sidney Kadish, Shelagh McCauley, Joanna Sawicka, Marcia Urie, Y C Lo, Charles Mayo, Kenneth Ulin, Linda Ding, Maureen Britton, Jiayi Huang, and Edward Arous. "Radiation therapy toxicity to the skin." In: *Dermatologic Clinics* 26.1 (2008-01), pp. 161–72. ISSN: 0733-8635. DOI: 10.1016/j.det.2007.08.005. URL: http://www.ncbi.nlm.nih.gov/pubmed/18023776 (cit. on p. 70).

[5] N S Russell, H Knaken, I A Bruinvis, A A Hart, A C Begg, and J V Lebesque. "Quantification of patient to patient variation of skin erythema developing as a response to radiotherapy." In: *Radiotherapy and Oncology* 30.3 (1994-03), pp. 213–21. ISSN: 0167-8140. URL: http://www.ncbi.nlm.nih.gov/pubmed/8209004 (cit. on p. 70).

[6] Yvonne Wengström, Christina Forsberg, Ingemar Näslund, and Jonas Bergh. "Quantitative assessment of skin erythema due to radiotherapy—evaluation of different measurements". In: *Radiotherapy and Oncology* 72.2 (2004-08), pp. 191–197. ISSN: 01678140. DOI: 10.1016/j.radonc.2004.04.011. URL:

http://linkinghub.elsevier.com/retrieve/pii/S0167814004003032 (cit. on p. 70).

[7] Matthew H Steele. "Three-year experience using near infrared spectroscopy tissue oximetry monitoring of free tissue transfers." In: *Annals of Plastic Surgery* 66.5 (2011-05), pp. 540–5. ISSN: 1536-3708. DOI: 10.1097/SAP.0b013e31820909f9. URL: http://www.ncbi.nlm.nih.gov/pubmed/21301288 (cit. on p. 70).

[8] NIH. *Common Terminology Criteria for Adverse Events (CTCAE) v4.03*. Tech. rep. U.S. Department of Health and Human Services, National Institutes of Health, National Cancer Institute, 2010, p. 80. URL: http://evs.nci.nih.gov/ftp1/CTCAE/About.html (cit. on p. 70).

[9] B L Diffey and P M Farr. "Quantitative aspects of ultraviolet erythema." In: *Clinical physics and physiological measurement : an official journal of the Hospital Physicists' Association, Deutsche Gesellschaft für Medizinische Physik and the European Federation of Organisations for Medical Physics* 12.4 (1991-11), pp. 311–25. ISSN: 0143-0815. URL: http://www.ncbi.nlm.nih.gov/pubmed/1778030 (cit. on p. 70).

[10] Anthony Kim and Brian C. Wilson. "Measurement of Ex Vivo and In Vivo Tissue Optical Properties: Methods and Theories". In: *Optical-Thermal Response of Laser-Irradiated Tissue*. Ed. by Ashley J Welch and M J C van Gemert. 2nd. New York: Springer, 2011. Chap. 8, pp. 267–319. DOI: 10.1007/978-90-481-8831-4_8. URL: http://www.springerlink.com/content/p688r10601w2u2vn/ (cit. on pp. 70, 76).

[11] R Marchesini, M Brambilla, C Clemente, M Maniezzo, a E Sichirollo, a Testori, D R Venturoli, and N Cascinelli. "In vivo spectrophotometric evaluation of neoplastic and non-neoplastic skin pigmented lesions–I. Reflectance measurements." In: *Photochemistry and photobiology* 53.1 (1991-01), pp. 77–84. ISSN: 0031-8655. URL: http://www.ncbi.nlm.nih.gov/pubmed/2027910 (cit. on p. 71).

[12] Lianshun Zhang, Aijuan Shi, and Hongguang Lu. "Determination of optical coefficients of biological tissue from a single integrating-sphere". In: *Journal of Modern Optics* 59.2 (2012-01), pp. 121–125. ISSN: 0950-0340. DOI: 10.1080/09500340.2011.631052. URL: http://www.tandfonline.com/doi/abs/10.1080/09500340.2011.631052 (cit. on p. 71).

[13] Markolf H Niemz. "Light and Matter". In: *Laser-Tissue Interactions*. 3rd. Berlin: Springer-Verlag Berlin Heidelberg, 2007. Chap. 2. ISBN: 3-540-40553-4. URL: http://content.schweitzer-online.de/static/catalog%5C_manager/live/media%5C_files/representation/zd%5C_std%5C_orig%5C_%5C_zd%5C_schw%5C_orig/012/629/115/9783642034374%5C_content%5C_pdf%5C_1.pdf (cit. on p. 71).

[14] J W Feather, M Hajizadeh-Saffar, G Leslie, and J B Dawson. "A portable scanning reflectance spectrophotometer using visible wavelengths for the rapid measurement of skin pigments." In: *Physics in medicine and biology* 34.7 (1989-07), pp. 807–20. ISSN: 0031-9155. URL: http://www.ncbi.nlm.nih.gov/pubmed/2780799 (cit. on p. 71).

[15] Nikiforos Kollias, InSeok Seo, and Paulo R Bargo. "Interpreting diffuse reflectance for in vivo skin reactions in terms of chromophores." In: *Journal of Biophotonics* 3.1-2 (2010-01), pp. 15–24. ISSN: 1864-0648. DOI: 10.1002/jbio.200900066. URL: http://www.ncbi.nlm.nih.gov/pubmed/19946873 (cit. on p. 71).

[16] M Hajizadeh-Saffar, J W Feather, and J B Dawson. "An investigation of factors affecting the accuracy of in vivo measurements of skin pigments by reflectance spectrophotometry." In: *Physics in medicine and biology* 35.9 (1990-09), pp. 1301–15. ISSN: 0031-9155. URL: http://www.ncbi.nlm.nih.gov/pubmed/2236210 (cit. on p. 72).

[17] James J. Duderstadt and Louis J. Hamilton. "Neutron Transport". In: *Nuclear Reactor Analysis*. Toronto: John Wiley & Sons, Inc., 1976. Chap. 4, pp. 103–148. ISBN: 978-0-471-22363-4 (cit. on p. 73).

[18] Ashley J Welch, Martin J C van Gemert, and Willem M Star. "Definitions and Overview of Tissue Optics". In: *Optical-Thermal Response of Laser-Irradiated Tissue*. Ed. by Ashley J. Welch and Martin J.C. Gemert. 2nd. Dordrecht: Springer Netherlands, 2011. Chap. 3, pp. 27–64. ISBN: 978-90-481-8830-7. DOI: 10.1007/978-90-481-8831-4. URL: http://link.springer.com/10.1007/978-90-481-8831-4 (cit. on p. 74).

[19] Labsphere. *Technical Guide: Integrating Sphere Radiometry and Photometry*. North Sutton, NH. URL: http://www.labsphere.com/uploads/technical-

guides/a-guide-to-integrating-sphere-radiometry-and-photometry.pdf (cit. on p. 74).

[20] Art W Springsteen. "Reflectance Spectroscopy: An Overview of Classification and Techniques". In: *Applied Spectroscopy: A Compact Reference for Practitioners*. Ed. by Jerry Workman and Art W Springsteen. 1st. New York: Academic Press, 1998. Chap. 6, pp. 193–224 (cit. on p. 74).

[21] Labsphere. *Application Note No. 01: Quantitation of Single Beam Substitution Correction in Reflectance Spectroscopy Accessories*. Tech. rep. 01. North Sutton, NH: Labsphere. URL: http://www.labsphere.com/uploads/technical-guides/Quantitation%20of%20Single%20Beam%20Substitution%20Correction.pdf (cit. on pp. 75, 79).

[22] Diana L Glennie, Joseph E Hayward, and Thomas J Farrell. "Modelling changes in the hemoglobin concentration of skin with total diffuse reflectance spectroscopy". In: *Manuscript submitted for publication* (2014) (cit. on pp. 75, 79).

[23] Sheng-Hao Tseng, Alexander Grant, and Anthony J Durkin. "In vivo determination of skin near-infrared optical properties using diffuse optical spectroscopy." In: *Journal of biomedical optics* 13.1 (2008), 014016(1–7). ISSN: 1083-3668. DOI: 10.1117/1.2829772. URL: http://www.pubmedcentral.nih.gov/articlerender.fcgi?artid=2626348%5C&tool=pmcentrez%5C&rendertype=abstract (cit. on p. 75).

[24] Dan Zhu, Wei Lu, Shaoqun Zeng, and Qingming Luo. "Effect of light losses of sample between two integrating spheres on optical properties estimation." In: *Journal of biomedical optics* 12.6 (2014), p. 064004. ISSN: 1083-3668. DOI: 10.1117/1.2815691. URL: http://www.ncbi.nlm.nih.gov/pubmed/18163820 (cit. on p. 75).

[25] Scott A Prahl and Steven L Jacques. *Optical Properties Spectra*. 2001. URL: http://omlc.org/spectra/ (cit. on p. 75).

[26] Steven L Jacques. *Skin Optics Summary*. 1998. URL: http://omlc.ogi.edu/news/jan98/skinoptics.html (cit. on pp. 76, 77).

[27] Deepa Kundur and Dimitrios Hatzinakos. "Blind image deconvolution". In: *Signal Processing Magazine, IEEE* May (1996-05), pp. 43–64. URL: http://ieeexplore.ieee.org/xpls/abs%5C_all.jsp?arnumber=489268 (cit. on p. 77).

[28] Rafael C Gonzalez, Richard E Woods, and Steven L Eddins. *Digital Image Processing Using MATLAB*. 1st. Upper Saddle River, New Jersey: Pearson Prentice Hall, 2003. ISBN: 0130085197 (cit. on p. 77).

[29] Thomas B. Fitzpatrick. "The Validity and Practicality of Sun-Reactive Skin Types I Through VI". In: *Archives of Dermatology* 124.6 (1988-06), pp. 869–871. ISSN: 0003-987X. DOI: 10.1001/archderm.1988.01670060015008. URL: http://archderm.jamanetwork.com/article.aspx?articleid=549509 (cit. on p. 79).

[30] Hidenobu Arimoto. "Multispectral polarization imaging for observing blood oxygen saturation in skin tissue." In: *Applied spectroscopy* 60.4 (2006-04), pp. 459–64. ISSN: 0003-7028. DOI: 10.1366/000370206776593672. URL: http://www.ncbi.nlm.nih.gov/pubmed/16613644 (cit. on p. 80).

[31] Alwin Kienle and Michael S Patterson. "Determination of the optical properties of turbid media from a single Monte Carlo simulation." In: *Physics in Medicine and Biology* 41.10 (1996-10), pp. 2221–7. ISSN: 0031-9155. URL: http://www.ncbi.nlm.nih.gov/pubmed/8912392 (cit. on p. 81).

[32] Erik Alerstam, Stefan Andersson-Engels, and Tomas Svensson. "White Monte Carlo for time-resolved photon migration." In: *Journal of biomedical optics* 13.4 (2013), p. 041304. ISSN: 1083-3668. DOI: 10.1117/1.2950319. URL: http://www.ncbi.nlm.nih.gov/pubmed/19021312 (cit. on p. 81).

[33] L Wang, SL Jacques, and L Zheng. "MCML—Monte Carlo modeling of light transport in multi-layered tissues". In: *Computer Methods and Programs in Biomedicine* 47 (1995), pp. 131–146. URL: http://www.sciencedirect.com/science/article/pii/016926079501640F (cit. on p. 81).

[34] A Fullerton, T Fischer, A Lahti, and KP Wilhelm. "Guidelines for measurement skin colour and erythema: A report from the Standardization Group of the European Society of Contact Dermatitis*". In: *Dermatitis* 35 (1996), pp. 1–10.

URL: http://onlinelibrary.wiley.com/doi/10.1111/j.1600-0536.1996.tb02258.x/abstract (cit. on p. 83).

[35] Daniel E McKee, Donald H Lalonde, Achilleas Thoma, Diana L Glennie, and Joseph E Hayward. "Optimal time delay between epinephrine injection and incision to minimize bleeding." In: *Plastic and Reconstructive Surgery* 131.4 (2013-04), pp. 811–4. ISSN: 1529-4242. DOI: 10.1097/PRS.0b013e3182818ced. URL: http://www.ncbi.nlm.nih.gov/pubmed/23249984 (cit. on p. 89).

Chapter 5

Paper IV - Application of system and model in radiation therapy

Preamble

Following the full characterization of the measurement system (Chapter 2) and the spectrally-constrained model (Chapter 4), a study was devised to employ both in the clinical setting. In radiation therapy, it is common to compare two treatment or skin care management regimens using only visual assessment (VA) and patient questionnaires. Both of these evaluation techniques are subjective in nature, meaning that there is a large amount of inter- and intra- observational variation. The spectrally-constrained integrating sphere-based diffuse reflectance spectroscopy approach outline in the previous papers provides a quantitative, objective way to quantify patient skin reactions. However, it is not as easily implemented as VA.

This paper explains where the difficulty in implementation comes from, and how it can be best addressed. This is a very important step in making the system and accompanying model accessible to the clinical community. More clinicians may adopt this assessment method if they have a set of recommendations on how it should be used to optimize clarity in the results.

This study required research ethics board (REB) approval. The application was prepared by the author of this thesis (further known as "the author") with significant assistance from Mrs. L. Doerwald-Munoz and under the guidance of Drs. T. Farrell, J. Hayward, O. Ostapiak, and J. Wright. The daily measurements were very time-consuming and required much assistance from Mrs. Doerwald-Munoz with occasional help from Miss. C. Cook and Dr. P. Muruganandam. All analysis was performed by the author. The manuscript was written by the author under the guidance of Drs. Farrell and Hayward and was additionally editted by the other authors, Drs. Ostapiak and Wright, and Mrs. Doerwald-Munoz. The manuscript has been altered from its original form to match the style of this thesis.

Contents

Diffuse reflectance spectroscopy for monitoring erythema in head & neck intensity modulated radiation therapy

Diana L. Glennie, Joseph E. Hayward, Orest Z. Ostapiak, James Wright, Lilian Doerwald-Munoz, and Thomas J. Farrell

Department of Medical Physics and Applied Radiation Sciences, McMaster University, 1280 Main Street West, Hamilton, Ontario, L8S 1A8

AND

Department of Medical Physics, Juravinski Cancer Centre, 699 Concession Street, Hamilton, Ontario, L8V 5C2

Submitted to the *Journal of Radiation Oncology* on November 5, 2014.

Abstract

Objectives To outline the best practices for obtaining and interpreting quantitative measurements of erythema in radiation therapy patients with a diffuse reflectance spectroscopy (DRS) system.

Methods Ten patients receiving intensity modulated radiation therapy (IMRT) for head & neck cancer were enrolled in a prospective observational study. Prior to the delivery of each fraction of radiation, DRS measurements were recorded. In addition, weekly dose measurements and visual assessments were performed. The daily variation in the total hemoglobin in skin was determined and used to identify the first day of significant increase in total hemoglobin. The impact of measurement frequency and data smoothing was investigated.

Results The daily variation in the total hemoglobin in a control region of skin was found to be 15.6% (st. dev.). To reduce the impact of this on serial erythema measurements, a 3-point centered moving average was applied. The range of maximum increase in the relative total hemoglobin concentration for the patients in this study was 36-254%. The daily variation in the total hemoglobin was used to calculate a minimum detectable increase threshold. It was possible to detect skin redness from 1 to 19 days before visual assessment.

Conclusion DRS offers a quantitative alternative to the subjective visual assessment method of evaluating radiation-induced erythema. It can be easily implemented into interventional studies to compare patient skin response.

5.1 Introduction

Intensity Modulated Radiation Therapy (IMRT) is the standard of care for head and neck (H&N) cancers as it is capable of delivering the prescribed dose to the tumor

target while sparing nearby radiosensitive organs.[1] However, H&N IMRT is often accompanied by higher rates of acute toxicity in the treatment field, commonly in the form of erythema, that can often be severe and painful for the patient.[2] The prevailing hypothesis is that the thermoplastic masks, required for patient immobilization, have a bolus-like effect on the skin.[3] In addition, since skin is hard to contour in the treatment planning software, the true skin dose is usually underestimated.[4] Moreover, since skin is not considered to be a radio-sensitive organ, its dose is not always purposefully minimized.[5]

Radiation-induced erythema, or radiation dermatitis, begins as an inflammatory response to the destruction of basal cells in the epidermal layer of skin that results in the cells migrating to the surface at an increased rate.[6] Since erythema is a deterministic effect there is a threshold dose and, following incidence, the severity increases with dose. Acute erythema typically appears two to three weeks following the start of IMRT and peaks around five weeks into treatment. In addition to the patient-specific response, erythema also depends on the volume of tissue involved. Due to these many factors, it is impossible to reliably predict the extent and latency period of a specific patient's reaction.[7]

Erythema can be extremely painful and there is a risk of infection. Severe cases of erythema may lead to an interruption in the treatment delivery, possibly compromising the treatment efficacy.[8] There is also a risk of permanent damage such as skin discoloration due to the migration of the melanocytes to the more superficial layers of the epidermis,[6] or tissue necrosis which may occur up to 2-4 years following the radiation treatment.[3] Therefore, it is important to properly monitor and manage a patient's skin response.

Radiation-induced erythema is commonly managed with proper hygiene and skin care.[6] Patients are often prescribed a topical treatment to soothe the skin and potentially minimize the reaction. In reviews on skin-care management for radiation therapy patients, nearly all of the reviewed studies relied on visual assessment (VA) (along with patient questionnaires) to compare the efficacies of the two management regimens.[6, 9, 10] With VA, the skin area of interest is observed by a researcher and classified using one of any number of skin reaction scales. These scales can be divided up into two main types; those with four or fewer classifications,[11–14] and those with more.[15–17] Scales with four or fewer classifications are not precise enough to differentiate between the various levels of erythema. For example, the prevalent

Common Terminology for Adverse Events (CTCAE v4.03)[19] has four categories ranging from faint/dull erythema to complete necrosis. Patients experiencing skin reactions will continue to be classified as a "1" until moist desquamation is observed. Although this scale is easier and more consistent to use, it does not provide enough information for comparison purposes. Scales with greater than four classifications are able to capture the different stages of an erythematic response (e.g. "mild" vs "moderate" levels), but there will be large inter- and intra- observer differences when comparing between different days, observers, and studies. These scales are also more difficult to use for more heavily pigmented individuals in which an increase in skin redness may not be easily observed.

In an effort to establish a quantitative evaluation technique, recent work has focused on using diffuse reflectance spectroscopy (DRS) to monitor skin redness. DRS relies on the properties of both oxy- and deoxy-hemoglobin that allow them to preferentially absorb green light. When skin appears redder to the human eye, it is not because more red light is being reflected, but because less green light is being scattered back out of the tissue (see Figure 5.1). Therefore, as the concentration of hemoglobin increases, more green light is absorbed. Previous systems commonly used only two small ranges of wavelengths (one red, and one green) to measure skin redness,[15, 18–20] but they were unable to account for the effect of melanin on the reflected light intensities. More recent systems use the entire visible light spectrum.[21–23] Hemoglobin is located in the dermis, below the melanin-containing epidermis. Since the thickness and melanin-content of the epidermal layer is unknown, the recovered hemoglobin concentrations from any reflectance method are apparent concentrations for a homogeneous single layered tissue and not the true concentrations found in the dermal layer. These results can, however, be accurately expressed as a percent difference from a baseline measurement.

While qualitative evaluations, such as VA, have a straight-forward implementation due to their simplicity, quantitative approaches, such as DRS, require more thorough consideration prior to use. This is primarily due to the daily variation in the blood concentration of skin. Although there is no consensus on the diurnal variation, a review by Brown et al. found it to be on the order of 10% with a maximum ranging from 15 to 30%.[24] While these changes in concentration levels may not be visibly detected, they will likely appear in the quantitative measurements, making it difficult to interpret trends in the recovered hemoglobin concentrations.

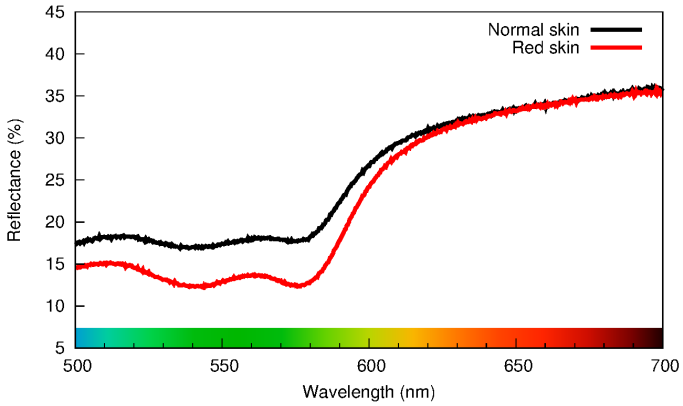

Figure 5.1: Total diffuse reflectance spectra for the same area of skin before and after the inducement of skin reddening. The amount (percent) of red light is the same for both measurements but there is a decrease in the amount of green light reflected from the reddened skin.

The purpose of this article is to outline the best methods for collecting data with a DRS system, as well as describe how to process the results to improve interpretation. This objective was achieved through a prospective, observational study in which patients treated with IMRT underwent daily DRS measurements over the course of their treatment. From the collected data, the daily variation in the reflectance of non-irradiated skin was established. This result was then used to establish the optimum measurement frequency and what (if any) data smoothing should be applied. Finally, the first day of measurable skin redness was identified for each volunteer following the newly established approach and was compared to the date of the first erythema note from the patient charts.

5.2 Materials & Methods

5.2.1 Subject Selection

Patients at the Juravinski Cancer Centre (Hamilton, Ontario, Canada) were eligible for inclusion in the study if they were receiving IMRT for a head and neck cancer between October 2010 and March 2011. Prescribed radiation doses were either 60 or 70 Gy, given daily at a rate of 2 Gy per fraction. None of the enrolled participants were receiving concurrent chemotherapy. A total of 14 volunteers were enrolled, with 10 successfully completing the study. Four of the participants did not complete the

study due to personal reasons or health concerns. Of those that successfully completed the study, one volunteer was retroactively removed due to bolus modification during the course of treatment. In total, nine complete data sets were collected. Completed volunteers were all Caucasian males between the ages of 41 and 79, although neither gender, nor age, nor race were screening criteria. Hamilton Health Sciences Research Ethics Board approval was obtained for this prospective study.

5.2.2 Measurement System

The diffuse reflectance spectroscopy system used in this study has been discussed elsewhere.[25] Briefly, the measurement area is illuminated with white light delivered through a highly reflective integrating sphere. Light reflected back into the sphere is collected by an optical fiber and delivered to a spectrometer. The collected spectrum is then processed to extract a total hemoglobin concentration[26] which is expressed as a percent difference from an established baseline measurement.

5.2.3 Study Protocol

Prior to the first fraction of radiation and the first DRS measurement, participants' radiation treatment plans were assessed to determine the location of the projected maximum skin dose. A measurement location was chosen on the skin that was close to this area while being sufficiently flat to ensure good contact between the collection port of the measurement device and the skin. The location was marked on the skin with an indelible marker to ensure daily placement accuracy. A back-up template was also created on an 8.5 inch x 11 inch transparency film, using topographical landmarks such as freckles, moles, and scars for alignment. A patch of skin was selected outside of the radiation field on the upper lateral portion of the left arm that was relatively free of hair and other irregularities to collect control data.

Before each fraction of radiation, participants were escorted to a private room and asked to sit quietly for 5 minutes in an attempt to reduce the effects of vasodilation due to exertion and external temperature exposure. Three measurements were then taken on the arm, followed by three measurements on the head/neck. The entire collection procedure lasted less than 15 minutes. No fractions were delivered on weekends or statutory holidays.

Weekly questionnaires were used to monitor changes in participant behavior that might affect the study results, such as voluntary sun exposure and any skin care regimens. VAs of the volunteer skin conditions were performed by the attending oncologists during their weekly patient assessment. Each week, thermoluminescent detectors (TLDs) arrays were placed inside patient masks over the DRS measurement areas to determine the skin dose received per fraction.

5.2.4 Data Analysis

For each day and measurement location (head/neck and arm), the three measured spectra were averaged to increase the signal to noise ratio.[27] Each averaged spectrum was background subtracted and normalized to a calibration measurement in order to obtain reflectance spectra. These were then analyzed to recover the total hemoglobin concentration. The first measurement (taken prior to the first fraction of radiation) was assigned as the baseline and all subsequent measurements were expressed as a percent difference from this value.

5.3 Results & Discussion

5.3.1 Variation in DRS Measurement & Minimum Detectable Difference in Blood Concentration of Hemoglobin

Previously, the DRS system was characterized and was able to recover chromophore concentrations to within 5% in tissue-simulating phantoms.[26] However, the daily variation of the hemoglobin concentration in skin has been reported as low as 2% and as high as 30%.[24] Therefore, the measurements performed on volunteer arms were analyzed to determine the daily variation for this particular study sample.

The measurement location on the arm was well outside of the treatment field and as such, was not expected to vary appreciably over the course of treatment. However, there may have been slight variations in the hemoglobin concentrations over time from external factors such as environmental temperatures. To account for this possibility, the measured hemoglobin for each individual patient (expressed as a percent difference from the first measurement) was plotted against time and a straight line was fit to

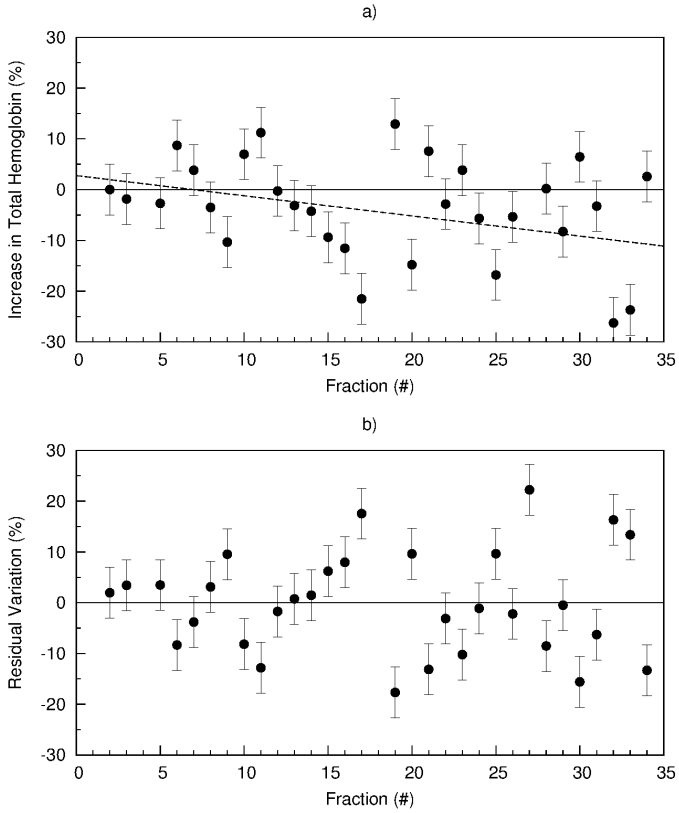

Figure 5.2: a) The total hemoglobin at the control site, expressed as a percent difference from the first measurement for a typical patient along with a linear fit. b) The residuals when the measurements were subtracted from the line of best fit.

these data and subtracted to obtain the residuals (See Figure 5.2 for data from a representative patient).

The standard deviation in the percent difference in hemoglobin concentration for each volunteer was calculated. The typical, or population, standard deviation for the patients in the study was 15.6%.[28] A minimum detectable difference in hemoglobin concentration could be defined as the 95% confidence interval for this population. Since only an increase in total hemoglobin concentration in the form of erythema is under investigation, the 95% confidence interval for a one-tailed test can be determined from the 90% confidence interval (1.64*st. dev.) for a two-tailed test. Thus, the minimal detectable increase (MDI) is 25.6%.

5.3.2 Skin Erythema Measurements

Skin erythema measurements were collected daily at the treatment site and were processed as a percentage difference from the first result. Figure 5.3a shows the daily measurements from one study volunteer with the MDI, plotted as a dotted line. While the daily variation makes it difficult to interpret, there is a noticeable increase in the total hemoglobin over time. However, there are also many excursions of the data across the MDI threshold.

To improve the interpretation of the results, some form of data smoothing was considered. Since the percent increase in total hemoglobin is a scalar observation recorded over time with a constant measurement interval, data smoothing techniques for univariate time series were considered to improve the diagnostic value of the data.[29] A moving average is the most common smoothing filter for time series analysis. It reduces the daily variation in the total hemoglobin concentration and can highlight any long term trends in the data. The period of the moving average should be relatively short, based on the total number of observations made. If using a centered instead of a leading moving average, odd numbered periods work best. On the scale of 30-35 measurements, a moving average of three should provide sufficient smoothing without obscuring possible smaller trends (e.g. weekly trends). Given the amount of daily variation in the measurements and the chosen period, there is no significant improvement in the data smoothing when employing a weighted moving average over a simple moving average (data not shown). Therefore, a 3-point centered moving average (3PCMA) was applied to the data collected in this study.

Since a moving average decreases the magnitude of the daily variation, the MDI was recalculated. The control measurements were reprocessed with a 3PCMA and the percent standard deviation was determined to be 11.8%. This value was confirmed by applying quadrature error propagation to the previously determined percent standard deviation. Using the same confidence interval as before, the MDI for the 3PCMA smoothed data was found to be 19.4%. The data from Figure 5.3a is shown with a 3PCMA smoothing filter and the new MCI in Figure 5.3b.

For the patient data shown in Figure 5.3b, the percent increase in total hemoglobin remains relatively constant at the baseline concentration from the first fraction's measurement. It begins to increase around fraction 15, corresponding to the third week of treatment. This is consistent with the clinically observed trends discussed in

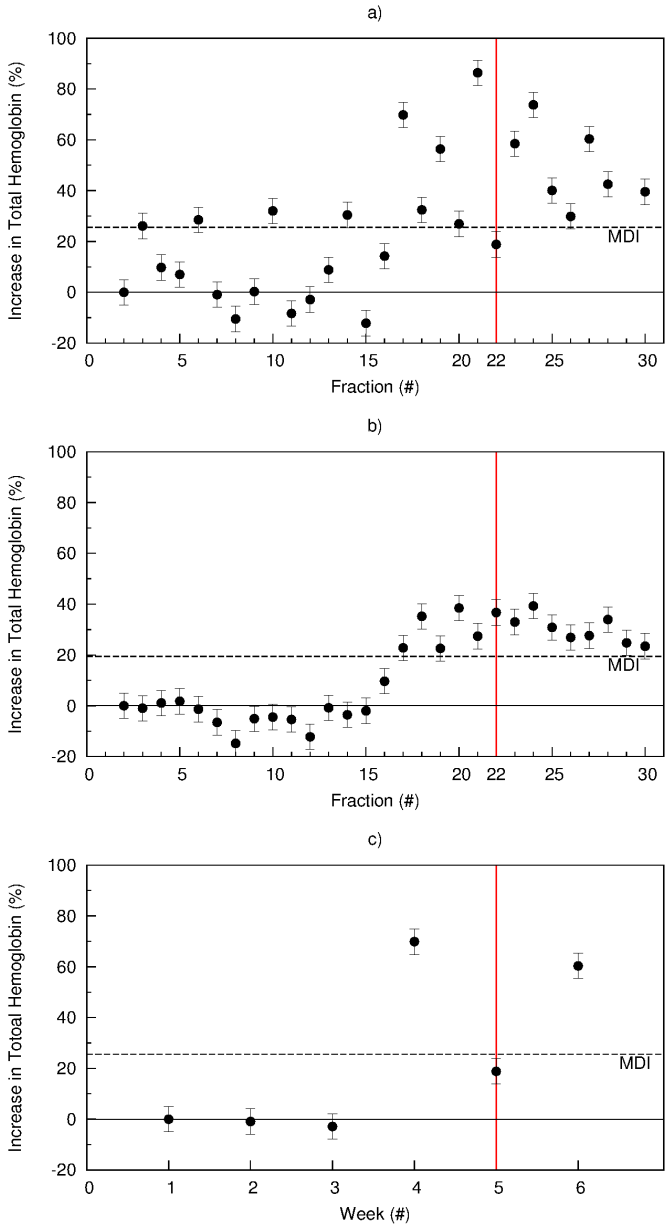

Figure 5.3: a) Daily total hemoglobin measurements expressed as a percent difference from the first measurement for a typical volunteer. b) The same data with a 3-point centered moving average applied and a recalculated MDI threshold. c) One of every five data points from the same volunteer representing weekly measurements. For this volunteer, erythema was first noted visually on Fraction 22/Week 5 as indicated by the red line.

the introduction. Following this change, the percent increase in total hemoglobin levels off above the MDI threshold at approximately 40%. Similar trends were seen in all the study volunteers. For patients where the percent increase in total hemoglobin exceeded the MDI, the range of maximum erythema levels was 36-254%. The majority of papers that monitored UV-induced erythema did not analyze the results in a similar way and cannot be used for comparison,[30–32] except for Stamatas et al.[21] who reported a range of (dose dependent) relative increase in oxy-hemoglobin of 4-237%. In the lone study on radiation-induced erythema, Yohan et al.[22] exposed nude mice to a single fraction of 40 Gy and recovered relative increases in total hemoglobin concentration of 14-256%.

If the MDI is used to indicate the point at which skin redness is distinguishable from daily fluctuations, the first signs of erythema should be visually identified on Day 17 for this specific volunteer – five days prior to the actual visual identification. Table 5.1 shows a summary of the number of fractions leading up to the identification of erythema with both the visual and MDI methods. For seven of the nine volunteers, the MDI assessment method identified erythema earlier than the visual method. In one volunteer, no notes were made in the patient chart regarding skin redness, although the MDI method did detect skin redness during treatment. In another volunteer, the MDI threshold was never reached in the DRS measurements although a note identifying erythema was made in the patient chart. For this particular volunteer, the visual identification was made during the fourth week of treatment. Given that the skin dose was relatively low (55 cGy/frac), the visually noted erythema may be due to empirical bias. While it should be reiterated that oncologists only saw patients once a week for VA, the MDI detection method preceeded the visual detection method by more than five fractions (i.e. one week) for the majority of volunteers.

Table 5.1: Days until the first assessment of erythema using visual identification and the MDI threshold.

Volunteer	1	2	3	4	5	6	7	8	9
Skin Dose (cGy)	123	150	134	58	138	136	142	139	55
Visual ID (fraction)	22	24	25	11	-*	26	14	25	20
MDI Threshold (fraction)	17	12	8	7	12	7	13	19	-**
Difference (MDI - Visual)	-5	-12	-17	-4	N/A	-19	-1	-6	N/A

* No note was made in the patient's chart regarding skin redness.
** Increase in total hemoglobin did not exceed MDI.

5.3.3 Optimal Frequency of DRS Measurements

While daily measurements may be time consuming, it is likely that weekly measurements (one per week for 6-7 weeks) are insufficient to establish any possible underlying trends in the data that would otherwise be hidden by the daily fluctuations. To illustrate this concern, the representative volunteer data from Figure 5.3a was reduced to only one of every five measurements in order to simulate a graph of single weekly measurements (see Figure 5.3c). In this graph, Week 4 and 6 are exceptionally high and Week 5 is exceptionally low (as compared to the surrounding points in Figure 5.3a). Without any additional information, one might interpret these results in one of two ways. First, that Week 5 is an anomaly and that skin redness should have been observed earlier, or second, that Week 4 is an anomaly and no substantial increase in skin redness should have been observed in Week 5. Since data smoothing on so few points is not advisable, it is recommended that daily measurements be performed.

In this study, while daily DRS measurements were shown to be ideal, the VAs made by the attending oncologists were only performed weekly. In order to better compare the two assessment methods, a study should be performed in which daily VAs are also performed alongside the daily DRS measurements. In addition to creating a better comparison between the two techniques, such a study would also provide an idea as to how much of an increase in hemoglobin concentration is necessary before visible detection, as well as what concentration changes are typical of the different stages of visually assessed erythema.

5.4 Conclusion

DRS provides a quantitative method for monitoring erythema in patients receiving radiation therapy. When using a DRS system, daily measurements should be performed. On each day, three spectra should be collected for each location and averaged prior to processing. The single measurement daily variation of the hemoglobin concentration in skin was determined to be 15.6% (st. dev.). This value may be reduced to 11.8% (st. dev.) if a simple 3-point centered moving average is applied as a smoothing filter to the recovered total hemoglobin results. The range of maximum increase in the relative total hemoglobin concentration for the patients in this study was 36-254%. By setting a detection threshold at the MDI, the quantitative DRS system was capable of detecting skin reddening between 1 and 19 days earlier than the standard VA approach.

Acknowledgments

The authors report that they have no conflicts of interest to disclose. This work was financially supported by the Natural Sciences and Engineering Research Council of Canada.

References

[1] Nancy Lee, DR Puri, and AI Blanco. "Intensity-modulated radiation therapy in head and neck cancers: An update". In: *Journal of the sciences and specialties of the head and neck* 29.4 (2007), pp. 387–400. DOI: 10.1002/hed. URL: http://onlinelibrary.wiley.com/doi/10.1002/hed.20332/full (cit. on p. 102).

[2] Franco De Conno and Vittorio Ventaftidda. "Skin Problems in Advanced and Terminal Cancer Patients". In: *Journal of Pain and Symptom Management* 6.4 (1991), pp. 247–256 (cit. on p. 102).

[3] Nancy Lee, Cynthia Chuang, Jeanne M Quivey, Theodore L Phillips, Pam Akazawa, Lynn J Verhey, and Ping Xia. "Skin toxicity due to intensity-modulated radiotherapy for head-and-neck carcinoma." In: *International journal of radiation oncology, biology, physics* 53.3 (2002-07), pp. 630–7. ISSN: 0360-3016. URL: http://www.ncbi.nlm.nih.gov/pubmed/12062606 (cit. on p. 102).

[4] Laurence E Court, Roy Tishler, Hong Xiang, Aaron M Allen, Mike Makrigiorgos, and Lee Chin. "Experimental evaluation of the accuracy of skin dose calculation for a commercial treatment planning system." In: *Journal of applied clinical medical physics / American College of Medical Physics* 9.1 (2008-01), p. 2792. ISSN: 1526-9914. URL: http://www.ncbi.nlm.nih.gov/pubmed/18449168 (cit. on p. 102).

[5] Elantholi P Saibishkumar, Marc a MacKenzie, Diane Severin, Alina Mihai, John Hanson, Helene Daly, Gino Fallone, Matthew B Parliament, and Bassam S Abdulkarim. "Skin-sparing radiation using intensity-modulated radiotherapy after conservative surgery in early-stage breast cancer: a planning study." In: *International journal of radiation oncology, biology, physics* 70.2 (2008-02), pp. 485–91. ISSN: 0360-3016. DOI: 10.1016/j.ijrobp.2007.06.049. URL: http://www.ncbi.nlm.nih.gov/pubmed/17881140 (cit. on p. 102).

[6] Maurene McQuestion. "Evidence-based skin care management in radiation therapy." In: *Seminars in oncology nursing* 22.3 (2006-08), pp. 163–73. ISSN: 0749-2081. DOI: 10.1016/j.soncn.2006.04.004. URL: http://www.ncbi.nlm.nih.gov/pubmed/16893745 (cit. on p. 102).

[7] D Porock and M U Sinclair. "Factors influencing the severity of radiation skin and oral mucosal reactions : development of a conceptual framework". In: *European journal of cancer care* 11.1 (2002), pp. 33–43 (cit. on p. 102).

[8] B Maciejewski, HR Withers, Jeremy MG Taylor, and Andrzej Hliniak. "Dose fractionation and regeneration in radiotherapy for cancer of the oral cavity and oropharynx: tumor dose-response and repopulation". In: *International Journal of Radiation Oncology*Biology*Physics* 16.3 (1989), pp. 831–843. URL: http://www.sciencedirect.com/science/article/pii/0360301689905038 (cit. on p. 102).

[9] Rebecca K S Wong, René-Jean Bensadoun, Christine B Boers-Doets, Jane Bryce, Alexandre Chan, Joel B Epstein, Beth Eaby-Sandy, and Mario E Lacouture. "Clinical practice guidelines for the prevention and treatment of acute and late radiation reactions from the MASCC Skin Toxicity Study Group." In: *Supportive care in cancer : official journal of the Multinational Association of Supportive Care in Cancer* 21.10 (2013-10), pp. 2933–48. ISSN: 1433-7339. DOI: 10.1007/s00520-013-1896-2. URL: http://www.ncbi.nlm.nih.gov/pubmed/23942595 (cit. on p. 102).

[10] Raymond Javan Chan, Joan Webster, Bryan Chung, Louise Marquart, Muhtashimuddin Ahmed, and Stuart Garantziotis. "Prevention and treatment of acute radiation-induced skin reactions: a systematic review and meta-analysis of randomized controlled trials." In: *BMC cancer* 14 (2014-01), p. 53. ISSN: 1471-2407. DOI: 10.1186/1471-2407-14-53. URL: http://www.pubmedcentral.nih.gov/articlerender.fcgi?artid=3909507%5C&tool=pmcentrez%5C&rendertype=abstract (cit. on p. 102).

[11] S Wan, J a Parrish, and K F Jaenicke. "Quantitative evaluation of ultraviolet induced erythema." In: *Photochemistry and photobiology* 37.6 (1983-06), pp. 643–8. ISSN: 0031-8655. URL: http://www.ncbi.nlm.nih.gov/pubmed/6611670 (cit. on p. 102).

[12] J D Cox, J Stetz, and T F Pajak. "Toxicity criteria of the Radiation Therapy Oncology Group (RTOG) and the European Organization for Research and Treatment of Cancer (EORTC)". In: *International journal of radiation oncology, biology, physics* 31.5 (1995-03), pp. 1341–6. ISSN: 0360-3016. DOI: 10.1016/

0360-3016(95)00060-C. URL: http://www.ncbi.nlm.nih.gov/pubmed/7713792 (cit. on p. 102).

[13] J Lock-Andersen, M Gniadecka, F de Fine Olivarius, K Dahlstrom, and H C Wulf. "Skin temperature of UV-induced erythema correlated to laser Doppler flowmetry and skin reflectance measured redness". In: *Skin Research and Technology* 4 (1998), pp. 41–48. URL: http://onlinelibrary.wiley.com/doi/10.1111/j.1600-0846.1998.tb00085.x/abstract (cit. on p. 102).

[14] Youlia M Kirova, Isabelle Fromantin, Yann De Rycke, Alain Fourquet, Esra Morvan, Solene Padiglione, Marie-Christine Falcou, Francois Campana, and Marc a Bollet. "Can we decrease the skin reaction in breast cancer patients using hyaluronic acid during radiation therapy? Results of phase III randomised trial." In: *Radiotherapy and oncology : journal of the European Society for Therapeutic Radiology and Oncology* 100.2 (2011-08), pp. 205–9. ISSN: 1879-0887. DOI: 10.1016/j.radonc.2011.05.014. URL: http://www.ncbi.nlm.nih.gov/pubmed/21624699 (cit. on p. 102).

[15] A D Pearse, C Edwards, S Hill, and R Marks. "Portable erythema meter and its application to use in human skin." In: *International journal of cosmetic science* 12.2 (1990-04), pp. 63–70. ISSN: 0142-5463. DOI: 10.1111/j.1467-2494.1990.tb00521.x. URL: http://www.ncbi.nlm.nih.gov/pubmed/19456960 (cit. on pp. 102, 103).

[16] Yvonne Wengström, Christina Forsberg, Ingemar Näslund, and Jonas Bergh. "Quantitative assessment of skin erythema due to radiotherapy—evaluation of different measurements". In: *Radiotherapy and Oncology* 72.2 (2004-08), pp. 191–197. ISSN: 01678140. DOI: 10.1016/j.radonc.2004.04.011. URL: http://linkinghub.elsevier.com/retrieve/pii/S0167814004003032 (cit. on p. 102).

[17] Mette Bodekaer, Peter Alshede Philipsen, Tonny Karlsmark, and Hans Christian Wulf. "Good agreement between minimal erythema dose test reactions and objective measurements: an in vivo study of human skin." In: *Photodermatology, Photoimmunology & Photomedicine* 29.4 (2013-08), pp. 190–5. ISSN: 1600-0781. DOI: 10.1111/phpp.12049. URL: http://www.ncbi.nlm.nih.gov/pubmed/23815351 (cit. on p. 102).

[18] J B Dawson, D J Barker, D J Ellis, E Grassam, J A Cotterill, G W Fisher, and J W Feather. "A theoretical and experimental study of light absorption and scattering by in vivo skin". In: *Physics in Medicine and Biology* 25.4 (1980-07), pp. 695–709. ISSN: 0031-9155. DOI: 10.1088/0031-9155/25/4/008. URL: http://www.ncbi.nlm.nih.gov/pubmed/7454759%20http://stacks.iop.org/0031-9155/25/i=4/a=008?key=crossref.3a9c201eba5c1754a3a8963193b6ce29 (cit. on p. 103).

[19] B L Diffey, R J Oliver, and P M Farr. "A portable instrument for quantifying erythema induced by ultraviolet radiation." In: *The British journal of dermatology* 111.6 (1984-12), pp. 663–72. ISSN: 0007-0963. URL: http://www.ncbi.nlm.nih.gov/pubmed/6508999 (cit. on p. 103).

[20] J W Feather, D J Ellis, and G Leslie. "A portable reflectometer for the rapid quantification of cutaneous haemoglobin and melanin." In: *Physics in medicine and biology* 33.6 (1988-06), pp. 711–22. ISSN: 0031-9155. URL: http://www.ncbi.nlm.nih.gov/pubmed/3406055 (cit. on p. 103).

[21] Georgios N Stamatas, Barbara Z Zmudzka, Nikiforos Kollias, and Janusz Z Beer. "In vivo measurement of skin erythema and pigmentation: new means of implementation of diffuse reflectance spectroscopy with a commercial instrument." In: *The British Journal of Dermatology* 159.3 (2008-09), pp. 683–90. ISSN: 1365-2133. DOI: 10.1111/j.1365-2133.2008.08642.x. URL: http://www.ncbi.nlm.nih.gov/pubmed/18510669 (cit. on pp. 103, 110).

[22] Darren Yohan, Anthony Kim, Elina Korpela, Stanley Liu, Carolyn Niu, Brian C Wilson, and Lee Cl Chin. "Quantitative monitoring of radiation induced skin toxicities in nude mice using optical biomarkers measured from diffuse optical reflectance spectroscopy." In: *Biomedical optics express* 5.5 (2014-05), pp. 1309–20. ISSN: 2156-7085. DOI: 10.1364/BOE.5.001309. URL: http://www.pubmedcentral.nih.gov/articlerender.fcgi?artid=4026905%5C&tool=pmcentrez%5C&rendertype=abstract (cit. on pp. 103, 110).

[23] Nikiforos Kollias, InSeok Seo, and Paulo R Bargo. "Interpreting diffuse reflectance for in vivo skin reactions in terms of chromophores." In: *Journal of Biophotonics* 3.1-2 (2010-01), pp. 15–24. ISSN: 1864-0648. DOI: 10.1002/jbio.200900066. URL: http://www.ncbi.nlm.nih.gov/pubmed/19946873 (cit. on p. 103).

[24] A. Brown and A. L. Goodall. "Normal variations in blood haemoglobin concentration". In: *The Journal of physiology* 104.4 (1946), pp. 404–407. URL: http://jp.physoc.org/content/104/4/404.full.pdf (cit. on pp. 103, 106).

[25] Diana L Glennie, Joseph E Hayward, Daniel E McKee, and Thomas J Farrell. "Inexpensive diffuse reflectance spectroscopy system for measuring changes in tissue optical properties". In: *Journal of Biomedical Optics* 19.10 (2014-10), p. 105005. ISSN: 1083-3668. DOI: 10.1117/1.JBO.19.10.105005. URL: http://biomedicaloptics.spiedigitallibrary.org/article.aspx?doi=10.1117/1.JBO.19.10.105005 (cit. on p. 105).

[26] Diana L Glennie, Joseph E Hayward, and Thomas J Farrell. "Modelling changes in the hemoglobin concentration of skin with total diffuse reflectance spectroscopy". In: *Manuscript submitted for publication* (2014) (cit. on pp. 105, 106).

[27] A Fullerton, T Fischer, A Lahti, and KP Wilhelm. "Guidelines for measurement skin colour and erythema: A report from the Standardization Group of the European Society of Contact Dermatitis*". In: *Dermatitis* 35 (1996), pp. 1–10. URL: http://onlinelibrary.wiley.com/doi/10.1111/j.1600-0536.1996.tb02258.x/abstract (cit. on p. 106).

[28] Keith Knight. "Random vectors and joint distributions". In: *Mathematical Statistics*. Boca Raton, FL: Chapman & Hall/CRC, 1999. Chap. 2, pp. 55–112. ISBN: 1-58488-178-X (cit. on p. 107).

[29] Jack Prins. *Chapter 6: Process or Product Monitoring and Control*. 2013. URL: http://www.itl.nist.gov/div898/handbook/ (cit. on p. 108).

[30] Graham I Harrison and Antony R Young. "Ultraviolet radiation-induced erythema in human skin." In: *Methods (San Diego, Calif.)* 28.1 (2002-09), pp. 14–19. ISSN: 1046-2023. URL: http://www.ncbi.nlm.nih.gov/pubmed/12231183 (cit. on p. 110).

[31] Jennifer K Wagner, Celina Jovel, Heather L Norton, Esteban J Parra, and Mark D Shriver. "Comparing quantitative measures of erythema, pigmentation and skin response using reflectometry." In: *Pigment cell research / sponsored by the European Society for Pigment Cell Research and the International Pigment*

Cell Society 15.5 (2002-10), pp. 379–84. ISSN: 0893-5785. URL: http://www.ncbi.nlm.nih.gov/pubmed/12213095 (cit. on p. 110).

[32] Terence H. Wong, Ian J. Jackson, and Jonathan L. Rees. "The physiological and phenotypic determinants of human tanning measured as change in skin colour following a single dose of ultraviolet B radiation". In: *Experimental Dermatology* 19.7 (2010-06), pp. 667–673. ISSN: 09066705. DOI: 10.1111/j.1600-0625.2010.01078.x. URL: http://doi.wiley.com/10.1111/j.1600-0625.2010.01078.x (cit. on p. 110).

Chapter 6

Paper V - TLD reproducibility

Preamble

During the erythema study (Chapter 5), weekly dose measurements were performed by placing thermoluminscent detectors (TLDs) inside patient masks in the DRS measurement area. This data was used in that paper to interpret patient responses to radiation therapy. Since the measurements were taken every week on every patient, there was the possibility of further analysis on the collected data. TLDs are used for so many purposes across so many disciplines, that their dose response uncertainties are well understood to be around 2-3%, depending on the calibration procedure. However, this does not address what kind of differences should be expected for repeat measurements in-phantom or *in vivo*. To determine a representative uncertainty, the TLD results were statistically analyzed and a limited investigation into the source of the variation was completed.

Outside of the assistance provided for the previous paper, the majority of the work was performed by the author of this thesis (further known as "the author"). The TLD measurements were all performed by the author, although they could not have been collected without the cooperation of the radiation therapy teams at the Juravinksi Cancer Centre (JCC). The author was trained in the use of the TLD reader and proper TLD calibration techniques by Ms. L Gamble and was supported in the endeavor by all of the members of the Physics Quality Assurance team at the JCC. The manuscript was prepared in collaboration with Dr. O. Ostapiak and was additionally reviewed by Drs. T. Farrell, J. Hayward, J. Wright, and Mrs. Doerwald-Munoz. The manuscript has been altered from its original form to match the style of this thesis.

Contents

Department of Medical Physics, Juravinski Cancer Centre, 699 Concession Street, Hamilton, Ontario, L8V 5C2

Submitted to the *Journal of Applied Clinical Medical Physics* on November 5, 2014.

6.1 Introduction

Thermoluminescent dosimeters (TLDs) are commonly used for phantom and *in vivo* dosimetry to confirm radiation therapy dose calculations[1, 2] and a large amount of research has established the random and systematic uncertainties related to the TLD dose measurement procedure.[3, 4] On average, TLDs are expected to have a standard deviation of 2-3% when properly calibrated.[1, 5] However, this uncertainty is expressed for TLDs irradiated in a uniform treatment field where there is no added uncertainty due to patient or TLD positioning. In the case where TLD measurements must be performed several times during a single patient's radiation therapy treatment to monitor progress or to confirm the calculated dose, it would be useful to have a measure of the TLD reproducibility that includes possible treatment setup errors and TLD positioning errors. Currently, *in vivo* dosimetry research with TLDs focuses on the difference between the TLD measurements and the calculated dose,[6–8] not on measurement reproducibility due to patient and TLD positioning uncertainty. This knowledge would allow for the determination as to whether or not separate session measurement differences in the TLD reading from are significant and should be further investigated.

6.2 Methods

Ten patients undergoing radiation therapy for head and neck cancer at the Juravinski Cancer Centre (Hamilton, Ontario, Canada) were enrolled in a prospective, observational study to monitor radiation-induced erythema.[9] The prescribed doses were either 60 or 70 Gy to a reference point within the tumor target, delivered in 2 Gy fractions. All treatments were planned using intensity modulated radiation therapy (IMRT) and required an immobilizing thermoplastic mask. In order to compare the erythema to the received skin dose, TLD measurements were performed weekly throughout treatment.

6.2.1 TLD Measurements

Each week, during the course of treatment, a TLD array was placed inside the patient masks. The TLD array consisted of five packets of two TLDs placed in a cross configuration on a square piece of paper (approximately 7 cm x 7 cm). The group of TLDs were maintained on site, and were batched such that each had a calibrated uncertainty of 2.9%. The location of the array was selected based on the area of projected maximum skin dose as determined from the radiation therapy plan developed using the Pinnacle3 (Philips, Andover, MA) Radiation Therapy Planning System (TPS).

Following each measured irradiation, the TLDs were read on site with a commercial TLD reader (Harshaw TLD 5500, Saint-Gobain Crystals & Detectors, Hiram, OH). None of the TLD pairs differed by more than the reading uncertainty (2.9%), although there were 7 instances where one of the TLDs returned an error during the reading process. Given this low difference between the TLDs in a pair, their average was used as the dose for each TLD packet location. When one of the TLDs returned an error, the single remaining TLD dose was used instead of the average. For each location on the skin, there was a TLD data set of 5-7 measurements collected over the course of treatment.

6.2.2 Statistical Analysis

A descriptive statistical analysis of the results requires that there be no trends in the sets of TLD data, such as time dependence. Time dependence is a valid concern, as weight loss is often observed over the course of treatment of head and neck cancer, which could affect the mask fitting and consequently, the measured dose. Since the Pearson correlation coefficient (r) for a completely uncorrelated parent population is 0, the correlation coefficient for a sample can be used to test whether that sample is a member of the uncorrelated parent population (this is the null hypothesis). For this test, the p-value for a given coefficient represents the probability that a random subset of N observations of the uncorrelated population would result in an equal or greater correlation coefficient. The p-value can be determined from a two-dimensional Gaussian distribution which is tabulated numerically. A p-value greater than the desired significance level (5%) indicates that the null hypothesis can be accepted and that the sample likely comes from an uncorrelated parent population. Conversely, a

p-values less than the desired significance level indicates that the null hypothesis should be rejected and that the sample likely came from a correlated parent population. To test whether each data set is time independent, the dose-time Pearson correlation coefficient (r) was calculated for each TLD position and the p-values were determined.[10]

The mean and standard deviation for each of the measured TLD dose data sets was calculated. Following a test for a dose dependence of the standard deviations, descriptive statistics were performed on the standard deviations and further dependence tests were performed to determine the source of the variation.

6.2.3 TPS Calculated Dose at TLD Location

Information regarding the calculated dose at the TLD site was determined using the TPS. Following the final radiation fraction, radio-opaque fiducial markers were placed inside each patients' mask at the exact location of each TLD packet, and the masks were scanned with CT. These scans were registered with the original planning image set. TLD chip packets were represented in the TPS by regions of interest (ROI) with the same dimensions (0.94 cm x 0.44 cm x 0.18 cm). These regions were placed to coincide with the marker positions at three different depths: 1) on the skin surface ("skin surface"), 2) straddling the skin surface ("mid-skin"), and 3) just below the skin surface ("in-skin"). The voxel size was defined by the dose grid dimension of 0.25 cm. As a result, the TLD ROI spanned 6 voxels in the treatment plan. The standard deviation of the average dose across these voxels was recorded for each TLD position.

6.2.4 Relationship between the Standard Deviations and TPS Dose Gradients

To understand the source of the variation in the TLD dose measurements, the standard deviations were compared against their corresponding TPS calculated dose gradients perpendicular and parallel to the skin surface. Since only the relationship between these quantities was investigated, proxy variables were used instead of the exact dose gradients. The dose gradient perpendicular to the skin, referred to here as the depth dose gradient, was approximated by subtracting the skin surface dose from the in-skin dose as follows,

$$\nabla D_{depth} = D_{in\ skin} - D_{surface} \tag{6.1}$$

The standard deviation within each TLD ROI in the TPS patient plan was used to represent the surface dose gradient in the plane of the skin.

6.3 Results

In total, 50 sets of TLD measurements were collected on ten patients (five sites per patient). For each TLD data set, the interquartile range test was used to identify outliers. Thirty-eight individual TLD measurements were removed (less than one from each location). One data set was removed due to the addition of bolus under the patient mask during the course of treatment.

6.3.1 Testing Temporal Independence

For each TLD data set, the Pearson correlation coefficient was used to determine the probability that there existed a correlation between the measurements and week of treatment. Four of the 49 data sets had p-values less than 0.05, indicating that there was very low probability that they were uncorrelated (i.e. that they may be time dependent). These four data sets represent 8% of the total, only slightly higher than would be expected by chance if they were all completely uncorrelated (5%). Therefore, it was concluded that there was no significant relationship between the measured TLD dose and time, thus satisfying the requirements for subsequent analysis of the individual TLD sets by descriptive statistics, and the mean and standard deviation of each TLD data set was calculated.

6.3.2 TLD Dose Variation

In order to test the relationship between the standard deviations and their corresponding means, the Pearson correlation coefficient was calculated and no dose dependence was found ($p = 0.27$). It is usual to express the uncertainty in a TLD measurement as a percent. However, when the standard deviations were expressed as percentages of the corresponding means, there was a dose dependence that would prevent further statistical analysis ($p = 2.3E\text{-}04$). Therefore all subsequent analysis was performed on the standard deviations and the relative standard deviations were not further analyzed. The mean, median, and first and third quartiles of the standard deviations are shown in Table 6.1.

Table 6.1: Descriptive statistics for the standard deviations from each TLD location.

Mean	6.7 cGy
Median	4.8 cGy
First Quartile	3.0 cGy
Third Quartile	8.6 cGy
Range	23.8 cGy

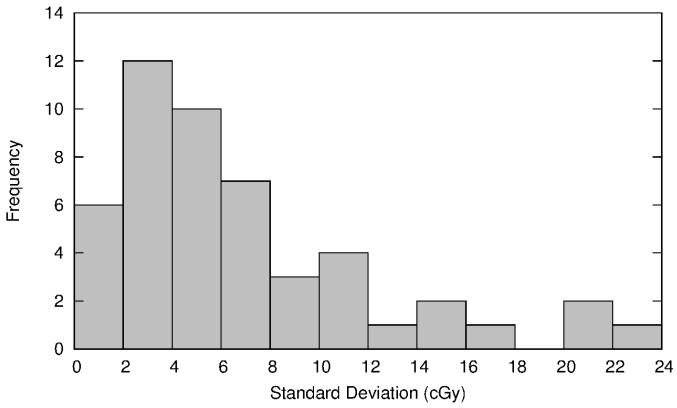

Figure 6.1: A histogram of the standard deviations for the 49 TLD data sets.

Since there is no dose dependence, the standard deviation of each of the data sets can be treated as an independent sample of a greater population and, therefore, can be used to estimate the additional variance due to TLD positioning error. Since they do not follow a normal distribution, the mean of the standard deviations (6.7 cGy) does not represent the population's standard deviation. According to Cochran's theorem,[11] the sample variances should follow a scaled chi-squared distribution. For such a distribution, a better measure of the population variance is the expectation value of the sampled variances, which would be equal to the mean of the square of the sample standard deviations. That is,

$$\sigma^2 \sim E\left(s^2\right) = \frac{\sum_{i=1}^{n}\left(s_i^2\right)}{n} \tag{6.2}$$

The TLD sample standard deviations follow this scaled chi-squared distribution, as shown in Figure 6.1. Therefore, the population standard deviation was approximated from these data as 8.7 cGy using Equation 6.2.

6.3.3 Gradient Dose Dependence

The Pearson correlation coefficient was used to test for a dependence between the sample standard deviations and the corresponding TPS calculated surface and depth dose gradients. No statistically significant relationship was found with any of the three surface dose gradient proxies ($p_{\text{in-skin}} = 0.70$, $p_{\text{skin-surf}} = 0.50$, $p_{\text{mid-skin}} = 0.47$). There was also no relationship found between the sample standard deviations and the depth dose gradient proxy ($p = 0.10$).

6.4 Discussion & Conclusions

The TLD dose data sets at each measurement location were shown to be independent of time and therefore the calculation of the standard deviation was considered valid. Forty-nine samples of TLD standard deviation were obtained. Since no dose dependence was found for these sample standard deviations, it was also valid to infer the population standard deviation from these values. The population standard deviation was approximated to be 8.7 cGy from the expectation value of the sample variance. This corresponds to 4.4% to 74.0% for the range of doses observed in this study. However, if doses below 83.1 cGy are excluded (by the interquartile range outlier test), the uncertainty does not exceed 10.5%. Therefore, the TLD reproducibility, including patient and TLD positioning variation, is 10.5%. This is 7.5% greater than the inherent uncertainty associated with TLDs irradiated in a uniform field.

No relationship was found between each location's standard deviation in dose and TPS calculated depth dose gradient. This can be explained by the fact that the TLD is always positioned on the skin surface. Any motion of the TLD along the depth dose gradient direction would involve movement of the skin surface and a corresponding movement of the depth dose gradient. Similarly, no relationship was found between each location's standard deviation in dose and the surface dose gradient surrogate. This suggests that a single dose calculation in the TPS does not adequately represent the variation in dose within the TLD due to patient setup error. Further investigation would require simulating patient setup error within the TPS through successive displacements of the isocenter.

Aside for the TLD placement and patient positioning uncertainties, it is possible that some of the measured dose variation was due to the mask perforation pattern.

As established by Lee et al.[12], thermoplastic immobilization masks have measurable shielding and build-up effects. This has the potential to contribute to the measured dose variation if the TLDs are positioned near a gap in the mask plastic.

This study investigated the reproducibility of TLD measurements in a clinical setting. The TLD measurement uncertainty was found to be three times larger (10.5%) than the standard calibration uncertainty for TLDs in a uniformly irradiated field. When performing in vivo dosimetry, it is common practice to report and investigate the dose discrepancy when the difference between the measured and planned doses exceeds 5%.[1] However, this study suggests that some of these discrepancies could be attributed to TLD and patient positioning errors that have not been accounted for. The results of this study could be strengthened by an expanded sample size with additional measurements. Instead of weekly measurements that resulted in 5-7 TLD readings, dose measurements could be performed daily, resulting in up to 35 individual samples for each measurement location.

Acknowledgments

This work was financially supported by the Natural Sciences and Engineering Research Council of Canada.

References

[1] M Essers and BJ Mijnheer. "In vivo dosimetry during external photon beam radiotherapy". In: *International Journal of Radiation Oncology*Biology*Physics* 43.2 (1999), pp. 245–259. URL: http://www.sciencedirect.com/science/article/pii/S0360301698003411 (cit. on pp. 121, 127).

[2] Ben Mijnheer, Sam Beddar, Joanna Izewska, and Chester Reft. "In vivo dosimetry in external beam radiotherapy." In: *Medical physics* 40.7 (2013-07), p. 070903. ISSN: 0094-2405. DOI: 10.1118/1.4811216. URL: http://www.ncbi.nlm.nih.gov/pubmed/23822404 (cit. on p. 121).

[3] T. H. Kirby, W. F. Hanson, and D. A. Johnston. "Uncertainty analysis of absorbed dose calculations from thermoluminescence dosimeters". In: *Medical Physics* 19.6 (1992), pp. 1427–1433. ISSN: 00942405. DOI: 10.1118/1.596797. URL: http://scitation.aip.org/content/aapm/journal/medphys/19/6/10.1118/1.596797 (cit. on p. 121).

[4] B.J. Mijnheer, J.J. Battermann, and A. Wambersie. "What degree of accuracy is required and can be achieved in photon and neutron therapy?" In: *Radiotherapy and Oncology* 8.3 (1987-03), pp. 237–252. ISSN: 01678140. DOI: 10.1016/S0167-8140(87)80247-5. URL: http://linkinghub.elsevier.com/retrieve/pii/S0167814087802475 (cit. on p. 121).

[5] PM Ostwald and T Kron. "Clinical use of carbon-loaded thermoluminescent dosimeters for skin dose determination". In: *International Journal of Radiation Oncology*Biology*Physics* 33.4 (1995), pp. 943–950. URL: http://www.sciencedirect.com/science/article/pii/0360301695002744 (cit. on p. 121).

[6] BI Rudén. "Evaluation of the clinical use of TLD". In: *Acta Oncologica* 5.October 1975 (1976). URL: http://informahealthcare.com/doi/pdf/10.3109/02841867609131779 (cit. on p. 121).

[7] G Leunens, J Van Dam, A Dutreix, and E van der Schueren. "Quality assurance in radiotherapy by in vivo dosimetry. 1. Entrance dose measurements, a reliable procedure". In: *Radiotherapy and Oncology* 17 (1990), pp. 141–151. URL: http://www.sciencedirect.com/science/article/pii/0167814090901023 (cit. on p. 121).

[8] C J Tung, H C Wang, S H Lo, J M Wu, and C J Wang. "In vivo dosimetry for external photon treatments of head and neck cancers by diodes and TLDS." In: *Radiation protection dosimetry* 111.1 (2004-01), pp. 45–50. ISSN: 0144-8420. DOI: 10.1093/rpd/nch358. URL: http://www.ncbi.nlm.nih.gov/pubmed/15367767 (cit. on p. 121).

[9] Diana L Glennie, Joseph E Hayward, Orest Z Ostapiak, James Wright, Lilian Doerwald-Munoz, and Thomas J Farrell. "Diffuse Reflectance Spectroscopy for Monitoring Erythema in Head & Neck Intensity Modulated Radiation Therapy". In: *Manuscript submitted for publication* (2014) (cit. on p. 121).

[10] Philip R Bevington and D Keith Robinson. "Testing the Fit". In: *Data Reduction and Error Analysis for the Physical Sciences*. Third. Toronto, 2003. Chap. 11, pp. 194–217. ISBN: 0-07-247227-8 (cit. on p. 123).

[11] Keith Knight. "Random vectors and joint distributions". In: *Mathematical Statistics*. Boca Raton, FL: Chapman & Hall/CRC, 1999. Chap. 2, pp. 55–112. ISBN: 1-58488-178-X (cit. on p. 125).

[12] Nancy Lee, Cynthia Chuang, Jeanne M Quivey, Theodore L Phillips, Pam Akazawa, Lynn J Verhey, and Ping Xia. "Skin toxicity due to intensity-modulated radiotherapy for head-and-neck carcinoma." In: *International journal of radiation oncology, biology, physics* 53.3 (2002-07), pp. 630–7. ISSN: 0360-3016. URL: http://www.ncbi.nlm.nih.gov/pubmed/12062606 (cit. on p. 127).

Chapter 7

Concluding Remarks

7.1 Summary & Thesis Conclusions

Skin redness, arising from an increase in hemoglobin, is an important indicator of patient response to a variety of treatments due to its relation to inflammation and tissue oxygenation. Aside from visual assessment which is subjective and therefore imprecise, diffuse reflectance spectroscopy (DRS) is the most popular approach to monitoring changes in the hemoglobin concentration in skin. Depending of the measurement approach and subsequent analysis, a majority of attempts were only capable of accurately measuring hemoglobin concentration changes in the absence of other chromophore concentration changes. In addition, all of the systems were difficult to use (required extensive training or precise measurement) and/or very expensive. The papers of this thesis present an integrating sphere-based total DRS system and spectrally-constrained model that is not only capable of accounting for concentration changes of non-hemoglobin chromophores, but is also user-friendly and cost effective.

The majority of DRS systems rely on fiber-based reflectance spectroscopy that requires training and an understanding of optics to be correctly used. In contrast, an integrating sphere-based system requires little to no formal training prior to use. However, integrating spheres are rarely used because their measured reflectance spectra are not easily converted into the true reflectance spectra, which is a necessary step if spectrally-constrained analysis is to be performed. Before an integrating sphere-based system can be used in this way, its response must be thoroughly characterized. The system presented in Chapter 2 was tested for wavelength accuracy, light source stability, measurement uncertainty and reproducibility. While the individual measurement uncertainty was intensity dependent, it was found to never exceed 1% across the 500 to 700 nm spectrum. The steps required to correct for the Single Beam Substitution Error (SBSE) were outlined and, once performed, resulted in an accurate recovery of the reflectance spectra (to within the measurement uncertainty) for a set of four colored calibration standards.

In Chapter 3, the hypothesis that a cheaper, more user-friendly system would facilitate clinical research was strengthened when the system outlined in Chapter 2 was immediately used to determine the time to maximal effect of epinephrine (a vasoconstrictor). Prior to this work, the commonly cited time interval between injection and incision was 7 to 10 minutes, as measured in 1987 by Larrabee et al.[1] using laser Doppler flowmetry. In this study, 12 volunteers were injected either with lidocaine (a

vasodilator) or lidocaine with epinephrine. DRS measurements were performed with this system over a two hour time period. The Dawson Erythema Index (EI)[2] was used to measure changes in the hemoglobin concentration in the skin. The results showed that the time required to reach the lowest hemoglobin concentration was 26 minutes ± 5 minutes (95CI) which was significantly longer than the previously stated time.

In Chapter 4, the spectrally-constrained model developed for use with the integrating sphere-based system was based on the diffusion theory equation by Farrell et al.[3] In addition to the SBSE, another correction factor was required to account for scattering losses at the detection port of the integrating sphere. The functional form of this new correction factor was determined with Monte Carlo simulations and confirmed with tissue-simulating liquid phantoms. A fitting algorithm was devised that applied the different corrections at strategic positions along the chain, depending on the information required to compute them. The parameters for the model were the concentrations for the individual chromophores found in the epidermal and dermal layers of human skin. Since the reduced scattering coefficient spectrum of human skin has been well established and its spectral shape varies minimally between healthy individuals, an assumed scattering spectrum was used in the model. For this reason, as well as because of the layered structure of skin, absolute hemoglobin concentrations were not possible and still contained clinically useful information. However, relative increases and decreases in the total hemoglobin concentration were possible. Unlike absorbance-based analysis approaches, this spectrally-constrained model was not affected by changes in the concentrations of the other skin chromophores. The model was tested on the spectra obtained during the epinephrine study (Chapter 3) and was shown to agree with the Dawson EI calculations except immediately following injection. Since the Dawson approach is an absorbance-based model and is not capable of accounting for other concentration changes, it was hypothesized that the difference between the two analysis methods was due to an increase in bleeding or swelling that led to an underestimation in the true hemoglobin concentration with the Dawson approach.

In Chapter 5, erythema in cancer patients undergoing intensity modulated radiation therapy (IMRT) was measured using the fully-tested system and model. DRS measurements were performed prior to each delivered fraction of radiation. In addition, weekly visual assessments (VA) by the attending oncologist and radiation dosimetry measurements with TLDs were performed. Due to differences in their measurement

frequencies, a direct comparison between VA and DRS was not possible, but conclusions regarding the optimum use of the DRS system were clearly illustrated. Since DRS measurements are quantitative, they are able to detect the small daily variations in the hemoglobin concentration in human skin that are not visible to the human eye. From control measurements performed outside of the radiation field, the daily variation in hemoglobin concentration was found to be 15.6% (st.dev.). For this reason, daily measurements are recommended along with a smoothing filter to improve the interpretation of the results. Using the daily control measurements to determine a minimum detectable increase (MDI) threshold, the DRS approach was capable of identifying skin redness anywhere from 1 to 19 days prior to visual detection. The guidelines in this paper will provide researchers with a standard protocol for using a DRS system to monitor skin redness in studies that compare treatment or skin care regimens.

Since TLD measurements were performed once a week on each patient, there was a sufficient amount of data to perform descriptive statistics in order to determine the additional uncertainty of *in vivo* TLD measurements due to patient and TLD positioning errors (see Chapter 6). The data were confirmed to have no temporal relationship and the range of the standard deviations was 24 cGy. The distribution of the standard deviations were also found to have no dose dependence and the population standard deviation was approximated to be 8.7 cGy. For doses greater than 83.1 cGy, this represented a maximum added uncertainty of 7.5% above the inherent reading error. Investigations into the causes of these uncertainties showed no statistically significant relationship between the standard deviations and either the surfrace or depth dose gradients.

7.2 Future Work

This thesis presented a novel approach to measuring changes in the hemoglobin concentration in skin. Its development and use, as presented in the papers of this thesis, raised many questions that would be ideal topics for further research. For example, the system was built with components that were on-hand at the time of construction. This included an older laptop, light source, and spectrometer. All further research should be undertaken with an updated system with newer components.

The integrating sphere size was limited by the dimensions of a block of Spec-

tralon® that had been previously purchased. The final sphere geometry was based on a section of integrating sphere theory that indicates, to a limit, that larger integrating spheres (and, as a consequence, the smaller port fractions) make for better illumination and detection devices. This assumption can and should be tested with Monte Carlo simulations to determine how small of a sphere is still useful in this particular application. It may be that small spheres would fit inside the human mouth, expanding the applications of this to oral mucositis, another common side effect of head and neck IMRT.[4]

Other aspects of the system can also be modified to expand the number of applications. For example, by changing the wavelength range and modifying the model, this system and model can be used to monitor the bilirubin concentrations in the skin of jaundiced neonates.[5] There is also a need in forensic medicine for a quantitative method of dating bruises,[6] the coloring of which is due to the breakdown of hemoglobin into waste products such as bilirubin. Finally, there are also several possibilities relating to breast cancer in both tumour detection[7, 8] and the monitoring of patient response.[9, 10]

When characterizing the system response to convert the detected reflectance spectra into the true reflectance spectra, a scattering losses correction factor (SLCF) was necessary to account for an increase in the fraction of photons that scattered away from the detection port between when the Spectralon® standard and the actual sample were measured. With recent advances in tissue simulating phantoms, it may be possible to create a solid phantom with similar scattering properties as human skin. If this sample was used as the calibration plate, it may eliminate the need for the SLCF, thereby streamlining the system characterization process.

One of the limitations of the erythema study was that the protocol did not include a purposeful daily visual assessment of the erythema region. For this measurement approach to be more readily embraced, it must be shown to be concretely superior to visual assessment. Therefore, another study (possibly with additional objectives such as regimen comparison) should include both daily assessments (visual and DRS). While this may seem time-consuming, it is a necessary step if this system is ever to become the gold standard for skin reaction comparison and monitoring. The visual assessments do not need to be performed by the attending oncologist (as they were in Chapter 5), but the person must be properly trained in the interpretation of the visual assessment scale.

The use of the system and model for both the erythema (Chapter 5 and epinephrine (Chapter 3) studies raised important questions about the minimum increase in the total hemoglobin in skin required for visual identification. Both papers suggested that this threshold was significantly higher than originally thought by the investigators. Therefore, a study should be conducted in which redness is induced to varying degrees in different patches of skin, all in the same region on a single volunteer. Assessment would be done both visually and with the DRS system. Redness could either be induced with varying concentrations of lidocaine (either injected or topically applied), or with different doses of ultraviolet radiation.[11, 12] In addition, volunteers for this study should span the Fitzpatrick scale,[13] as redness will be harder to visually detect when more melanin is present in the skin.

There are many potential uses and applications of this DRS system and analysis model. It is the hope of this author that the work included in this thesis provides a clear base for future research into improving the system and analysis method, and that it creates opportunities for clinical research across the health care spectrum.

References

[1] Wayne F Larrabee, Brent J Lanier, and David Miekle. "Effect of epinephrine on local cutaneous blood flow". In: *Head & Neck Surgery* 9.5 (1987-05), pp. 287–289. ISSN: 01486403. DOI: 10.1002/hed.2890090507. URL: http://doi.wiley.com/10.1002/hed.2890090507 (cit. on p. 132).

[2] J B Dawson, D J Barker, D J Ellis, E Grassam, J A Cotterill, G W Fisher, and J W Feather. "A theoretical and experimental study of light absorption and scattering by in vivo skin". In: *Physics in Medicine and Biology* 25.4 (1980-07), pp. 695–709. ISSN: 0031-9155. DOI: 10.1088/0031-9155/25/4/008. URL: http://www.ncbi.nlm.nih.gov/pubmed/7454759%20http://stacks.iop.org/0031-9155/25/i=4/a=008?key=crossref.3a9c201eba5c1754a3a8963193b6ce29 (cit. on p. 133).

[3] Thomas J Farrell and Michael S Patterson. "A diffusion theory model of spatially resolved, stead-state diffuse reflectance for the noninvasive determination of tissue optical properties in vivo". In: *Medical Physics* 19.4 (1992), pp. 879–888 (cit. on p. 133).

[4] Pamela J Hancock, Joel B Epstein, and Georgia Robins Sadler. "Oral and dental management related to radiation therapy for head and neck cancer". In: *J Can Dent Assoc* 69.9 (2003), pp. 585–590. URL: http://www.cda-adc.ca/JCDA/vol-69/issue-9/585.pdf (cit. on p. 135).

[5] L. Randeberg, E. Roll, L. Nilsen, T. Christensen, and L. Svaasand. "In vivo spectroscopy of jaundiced newborn skin reveals more than a bilirubin index". In: *Acta Paediatrica* 94.1 (2005-01), pp. 65–71. ISSN: 0803-5253. DOI: 10.1080/08035250410023179. URL: http://doi.wiley.com/10.1080/08035250410023179 (cit. on p. 135).

[6] Lise Lyngsnes Randeberg, Olav a Haugen, Rune Haaverstad, and Lars O Svaasand. "A novel approach to age determination of traumatic injuries by reflectance spectroscopy." In: *Lasers in surgery and medicine* 38.4 (2006-04), pp. 277–89. ISSN: 0196-8092. DOI: 10.1002/lsm.20301. URL: http://www.ncbi.nlm.nih.gov/pubmed/16538661 (cit. on p. 135).

[7] V G Peters, D R Wyman, M S Patterson, and G L Frank. "Optical properties of normal and diseased human breast tissues in the visible and near infrared." In: *Physics in medicine and biology* 35.9 (1990-09), pp. 1317–34. ISSN: 0031-9155. URL: http://www.ncbi.nlm.nih.gov/pubmed/2236211 (cit. on p. 135).

[8] Bruce J Tromberg, Albert Cerussi, Natasha Shah, Montana Compton, Amanda Durkin, David Hsiang, John Butler, and Rita Mehta. "Review: Imaging in breast cancer: Diffuse optics in breast cancer: detecting tumors in pre-menopausal women and monitoring neoadjuvant chemotherapy". In: *Breast Cancer Research* 7.6 (2005-01), pp. 279–85. ISSN: 1465-542X. DOI: 10.1186/bcr1358. URL: http://www.pubmedcentral.nih.gov/articlerender.fcgi?artid=1410753%5C&tool=pmcentrez%5C&rendertype=abstract (cit. on p. 135).

[9] D Porock and L Kristjanson. "Skin reactions during radiotherapy for breast cancer: the use and impact of topical agents and dressings". In: *European journal of cancer care* 8.3 (1999-09), pp. 143–53. ISSN: 0961-5423. URL: http://www.ncbi.nlm.nih.gov/pubmed/10763645 (cit. on p. 135).

[10] Bruce J Tromberg and Albert E Cerussi. "Imaging breast cancer chemotherapy response with light. Commentary on Soliman et al., p. 2605." In: *Clinical Cancer Research* 16.9 (2010-05), pp. 2486–8. ISSN: 1078-0432. DOI: 10.1158/1078-0432.CCR-10-0397. URL: http://www.pubmedcentral.nih.gov/articlerender.fcgi?artid=3204881%5C&tool=pmcentrez%5C&rendertype=abstract (cit. on p. 135).

[11] B L Diffey and P M Farr. "Quantitative aspects of ultraviolet erythema." In: *Clinical physics and physiological measurement : an official journal of the Hospital Physicists' Association, Deutsche Gesellschaft für Medizinische Physik and the European Federation of Organisations for Medical Physics* 12.4 (1991-11), pp. 311–25. ISSN: 0143-0815. URL: http://www.ncbi.nlm.nih.gov/pubmed/1778030 (cit. on p. 136).

[12] Graham I Harrison and Antony R Young. "Ultraviolet radiation-induced erythema in human skin." In: *Methods (San Diego, Calif.)* 28.1 (2002-09), pp. 14–19. ISSN: 1046-2023. URL: http://www.ncbi.nlm.nih.gov/pubmed/12231183 (cit. on p. 136).

[13] Thomas B. Fitzpatrick. "The Validity and Practicality of Sun-Reactive Skin Types I Through VI". In: *Archives of Dermatology* 124.6 (1988-06), pp. 869–871. ISSN: 0003-987X. DOI: 10.1001/archderm.1988.01670060015008. URL: http://archderm.jamanetwork.com/article.aspx?articleid=549509 (cit. on p. 136).